

Analysis of the 1/3 E949 pnn2 data

Joss Ives, Benji Lewis, Dmitri Patalakha, Zhe Wang, David E. Jaffe

November 20, 2007

Abstract

This will be the abstract.

Contents

Table of Contents	iii
List of Figures	iv
List of Tables	vi
1 Executive Summary	1
2 Philosophy	1
2.1 Target CCD Fitter	2
3 Photon veto cuts	6
3.1 New photon veto cuts	6
3.2 PV optimization	8
4 TDcuts	8
4.1 Electron Finding (EV5)	8
4.2 TD Neural-Net Cut	10
4.3 Conclusions from TD Optimization	10
5 Kinematic cuts	16
5.1 Expand kinematic box	16
5.2 K_{e4} -phobic box	16
5.3 UTCQUAL	20
5.4 PRRF	23
5.5 RSDEDX	24
6 Delayed-coincidence cuts	24
6.1 K^+ Stop Requirement: Delayed Coincidence (DEL3)	24
6.2 Tight Delayed Coincidence (DEL6)	24
6.3 Delayed Coincidence Function (<i>delc</i>)	24

7	Target cuts	26
7.1	TIMKF	26
7.2	CCDPUL	26
7.3	TGdEdX	30
7.4	CHI567	47
7.5	B4EKZ	47
7.6	TGZFOOL	47
7.7	EPIONK	48
7.8	Discarded Cuts	48
8	Skim Definitions	49
9	$K_{\pi 2}$-Scatter background	49
9.1	$K^+ \rightarrow \pi^+ \pi^0$ Target Scatters	49
9.2	$K^+ \rightarrow \pi^+ \pi^0$ Range Stack Scatters	58
10	$K_{\pi 2 \gamma}$ Background	60
11	Beam Background	62
11.1	Single-Beam Background	64
11.2	Double-Beam Background	65
11.3	Beam Background Summary	67
12	Muon Background	68
13	Charge exchange background	68
14	K_{e4} background	71
15	Acceptance	77
15.1	Acceptance Factors from $K_{\mu 2}$ Events	77
15.2	Acceptance Factors from $\pi_{scatter}$ Events	82
15.3	Range-Stack-Kinematic Acceptance	83
15.4	$\pi^+ \rightarrow \mu^+ \rightarrow e^+$ Identification Acceptance	86
15.5	Acceptance Factors from $K_{\pi 2}$ Events	88
15.6	UMC based acceptance	89
15.7	Acceptance Summary	90
16	Kaon exposure	90
17	Single Cut Failure Study	91
17.1	Events Removed by Safety Cuts	91
18	Sensitivity	93
18.1	Single event sensitivity	93
18.2	E949 pnn2 Cell definition	93
18.3	Junk method	94
18.4	BR measurement	97

19 Measurement of the $K_{\pi 2}$ branching fraction	97
19.1 Introduction and experimental data	97
19.2 Monte Carlo kinematic and trigger acceptances	97
19.3 $K_{\pi 2}$ event selection	100
19.4 Acceptance factors for the $K_{\pi 2}$ branching fraction	100
19.5 The measured $K_{\pi 2}$ branching fraction	103
19.6 UMC cut definitions	108

List of Figures

1	Target fitter low-count error fix	3
2	Effect of first bin error fix on target fitter	5
3	TD Threshold Plots	11
4	TDNN Threshold Plots	12
5	Total Acceptance/Total Background versus TD Cut Threshold	14
6	Total Acceptance/Total Background versus TD Cut Threshold with varied Sigmas	15
7	Momentum distribution of K_{e4} normalization sample before CCDPUL cuts.	17
8	K_{e4} -phobic box lower bound scan	18
9	K_{e4} -phobic box upper bound scan	19
10	π mass distribution of π_{scat} sample.	20
11	pnn1 UTC acceptance vs momentum	21
12	$P_{dc} - P_{exp}$ for 10 UTCQUAL cut failure modes	22
13	$P_{dc} - P_{exp}$ for events that <i>failed</i> the UTCQUAL cut before (green) and after (yellow) tuning. UTCQUAL07 is the cut after tuning. The upper one is in linear scale, the lower one is in log scale.	23
14	TGdEdX Calibration of New Means	34
15	TGdEdX Calibration of New Means	35
16	TGdEdX Calibration of New Means	36
17	Ratios of the E949/E787 Calibrations	37
18	Before and after calibration of $like_{TGdEdX}$	39
19	$like_{TGdEdX}$ Distributions with Different Offsets	40
20	$like_{TGdEdX}$ Distributions for Different Piscat Calibrations	41
21	Ratio of Calibration Means	41
22	TGdEdX Rejection Acceptance versus Likelihood Value	45
23	Acceptance and Rejection versus TGDEDX Cut Value	46
24	ptot distribution of the events remaining in the normalization and rejection branches of the $K_{\pi 2}$ TG scatter study	56
25	π^+ kinetic energy distribution in $K\pi 2\gamma$ events	61
26	Energy vs angle of the radiative γ from $K\pi 2\gamma$	62
27	Inefficiency table for single photons.	63
28	A CEX candidate. The x-y view and target view.	69
29	e^+ and π^- kinetic energy vs π^+ momentum for K_{e4} events	72
30	K_{e4} Candidate	74
31	K_{e4} candidate	75

32	Observable absorption energy of π^- stopped in the RS.	76
33	E_{hide} versus T_{xtg}	76
34	π^+ Mass	84
35	$K_{\pi 2}$ events vs run	98
36	$K_{\pi 2}$ branching fraction and f_S vs run	104
37	$K_{\pi 2}$ branching fraction vs rate	105
38	$K_{\pi 2}$ branching fraction vs rate	107
39	The $K_{\pi 2}$ branching fraction versus run number a) for runs with prescaler 163840 and b) for runs with prescaler 131072	108

List of Tables

1	Total Estimated Background and Acceptance Summary	1
2	Acceptances for various target fitter fixes	4
3	Photon Cut Parameters	7
4	TD Optimization Summary	9
5	Muon-Background Summary	9
6	Muon Background at Different TD Neural-Net Cut Thresholds	13
7	E787 and E949 pnn2 kinematic box definitions.	16
8	TGDEDX Calibration Sample	33
9	Kpi2 TG-kinematic Acceptance	42
10	TGDEDX Rejection	43
11	TGDEDX Acceptance/Rejection	44
12	Definition of Skims	49
13	Definition of the classes of events used to measure the PV rejection in the $\pi\nu\bar{\nu}(2)$ kinematic box for $K_{\pi 2}$ scatter backgrounds.	50
14	The rejection branch for the $K_{\pi 2}$ TG scatter background in the loose box.	51
15	The rejection branch for the $K_{\pi 2}$ TG scatter background in the tight (ke4-phobic) box.	52
16	Rejection of the tight (30%) photon veto for the various classes with different combinations of loose and tight versions of the setup cuts	53
17	Rejection of the loose (60%) photon veto for the various classes with different combinations of loose and tight versions of the setup cuts	54
18	Rejection of the loose (90%) photon veto for the various classes with different combinations of loose and tight versions of the setup cuts	55
19	Categorization of events surviving the loose photon veto in the $K_{\pi 2}$ scatter rejection branch	56
20	The normalization branch for the $K_{\pi 2}$ -TG scatter background	57
21	Rejection branch for $K_{\pi 2}$ -RS scatters	59
22	Normalization branch for $K_{\pi 2}$ -RS scatters	59
23	Detailed information in κ estimation.	62
24	$K\pi 2\gamma$ background number normalized to 3/3 data. The first error of $N_{Kp2\gamma}$ is statistical and the second error is from κ and R_γ	63
25	1-Beam Rejection	64
26	1-Beam Normalization	64

27	2-Beam Rejection	65
28	2-Beam Normalization	65
29	Total Beam-Background	67
30	Muon Rejection and Normalization	68
31	Muon Background	68
32	CEX normalization branch	70
33	CEX background number normalized to 3/3 data.	71
34	The pass2 cuts history of the normalization branch of the 1/3 data for K_{e4} study. R-cut is $\overline{TGPV \cdot OPSVETO}$	73
35	Rejection of $R_{TGPV \cdot OPSVETO}$ as a function of E_{hide} for loose cuts.	77
36	Rejection of $R_{TGPV \cdot OPSVETO}$ as a function of E_{hide} for tight cuts.	77
37	K_{e4} Background	77
38	Setup Cuts for $K_{\mu 2}$ Acceptance Samples	78
39	RS-Reconstruction Acceptance	78
40	TG and UTC Reconstruction Acceptance	79
41	$K_{\mu 2}$ Target and Beam Acceptance	81
42	Photon-Veto Acceptance	81
43	Setup Cuts for $\pi_{scatter}$ Acceptance Samples	82
44	BADSTC Acceptance	82
45	RS-Kinematic Acceptance	83
46	RS-Kinematic Acceptance in Small Box	85
47	RS-Kinematic Acceptance in Large Box	85
48	$\pi^+ \rightarrow \mu^+ \rightarrow e^+$ Identification Acceptance	86
49	$\pi^+ \rightarrow \mu^+ \rightarrow e^+$ Identification Acceptance	87
50	Setup Cuts for $K_{\pi 2}$ Acceptance Samples	88
51	UTC Acceptance	88
52	OPSVETO Acceptance	88
53	TG-Kinematic Acceptance	89
54	UMC based acceptance.	90
55	Acceptance Summary	90
56	Number of Single-Cut Failures	91
57	Acceptance loss and rejection for each background.	93
58	Acceptance and background summary of each cell.	94
59	Detailed background information of each cell.	95
60	UMC $K_{\pi 2}$ acceptance of cuts applied in the $K_{\pi 2}$ branching fraction analysis. NIDIF is on.	99
61	The number of selected $K_{\pi 2}$ candidate events with a comparison to the 2002 PNN1 results.	101
62	$K_{\pi 2}$ -based acceptances of cuts applied in the $K_{\pi 2}$ BR analysis.	102
63	$K_{\pi 2}$ branching fraction results for all runs and broken down by prescale factor.	103
64	Measured rate-dependence of the $K_{\pi 2}$ branching fraction and factors entering in the branching fraction calculation for all data (top) and runs with the prescale factor 163840.	106
65	$K_{\pi 2}$ candidate selection for runs with prescale 131072 and 163840.	110

Background Component	Entire “Loose”	Cleanest cell “Tight”
$K_{\pi 2}$ TT scatter	$0.575 \pm 0.184^{+0.063}_{-0.201}$	$0.115 \pm 0.058^{+0.039}_{-0.022}$
$K_{\pi 2}$ RS scatter	-0.0070 ± 0.0042	-0.0031 ± 0.0018
$K_{\pi 2\gamma}$	$0.050 \pm 0.008^{+0.003}_{-0.003}$	0.005 ± 0.001
K_{e4}	$0.18 \pm 0.10^{+0.23}_{-0.12}$	$0.012 \pm 0.007^{+0.015}_{-0.008}$
CEX	$0.092 \pm 0.053^{+0.070}_{-0.018}$	$0.004 \pm 0.002^{+0.003}_{-0.001}$
Muon	0.00305 ± 0.00305	0.0030 ± 0.0030
Two-beam	0.0438 ± 0.0200	0.00317 ± 0.00317
One-beam	0.00157 ± 0.00157	0.00035 ± 0.00035
Total Background	$0.945 \pm 0.217^{+0.249}_{-0.235}$	$0.143 \pm 0.059^{+0.042}_{-0.023}$
Total Acceptance	$(1.778 \pm 0.063) \times 10^{-3}$	$(0.600 \pm 0.176 \pm 0.0600) \times 10^{-3}$
Single-event sensitivity	??	??

Table 1: The estimated backgrounds for the entire signal region, referred to as “loose” elsewhere in the text, and the cleanest cell, referred to as “tight”, to be used in the analysis. The first error is the statistical uncertainty; the second error (when present) is the estimated systematic uncertainty. The systematic uncertainties for the K_{e4} and CEX backgrounds are assumed to be fully correlated. The cleanest cell corresponds to the tight settings of the KIN, TD, PV and DELCO cuts. The background due to $K_{\pi 2}$ RS scatters is assumed to be negligible and not included in the totals. The bottom rows contains the total acceptance and single event sensitivity of the two regions.

1 Executive Summary

The E949 pnn2 analysis on the 2002 data benefits from the previous successful analyses of the E787 data [1],[11], the upgrades to the E949 detector and improvements to E949 pnn1 analysis. As a consequence, the size of the E949 pnn2 signal region has been increased and the differential signal acceptance and background rejection within the signal region will be utilized in a likelihood analysis. The results for the background, acceptance and single-event sensitivity are summarized in Table 1 for the entire signal region and the cleanest region within the signal region.

2 Philosophy

Many cuts tuned and improved by the E949 pnn1 analysis are used in this analysis. In addition cuts devised for the E787 pnn2 analyses, but not required by pnn1, are also used in this analysis. The general philosophy of this note is to only describe cuts or calculations that have been changed from the E949 pnn1 analysis as described in E949 Technotes K-034 [21] and K-038 [17] or the E787 pnn2 analysis described in E787 TN-385, TN-386 [1] or B.Bhuyan’s thesis [11].

2.1 Target CCD Fitter

The target CCD fitter received some modifications and bug fixes since its implementation in the E787 PNN2 analysis.

The rest of this section describes and discusses the modifications and fixes that were made. The bug fixes were for the following bugs:

- The fitter was using the raw energy of the pulse as opposed to the normalized energy of the pulse calculated within the fitting routine.
- The flag indicating a saturated pulse was not set properly.

The modifications to the way the fitter functions are summarized as follows:

- Bins with zero counts that were adjacent to bins containing greater than zero counts were included in the minimization of the fit where they were previously excluded.
- The errors associated with the first bin and with bins containing less than ten counts were increased to de-weight these bins in the fit.
- Hold and release fitting for the double-pulse fits. The four-parameter double-pulse fit was changed from a one-stage fit to a two-stage fit. In the first stage, the time for the first pulse was fixed at the time found in the single-pulse fit while the other three parameters were allowed to wander. In the second stage, the values from these three parameters were used as initial guesses and all four parameters were allowed to wander.
- The maximum number of target fibers that were fit was increased to 31 from 15.

2.1.1 Optimizing the fitter

A sample of km2 monitors was used for optimizing the target fitter. For the sample, the following cuts were applied as setup cuts: TGQUALT, DELC, NPITG, TARGET, TGCUT, UTC, RD_TRK, TRKTIM, RDUTM. This left approximately 50,000 events to which CCDBADFIT, CCDPUL and EPIONK were applied. The resulting acceptances of these cuts are shown in Table 2 before applying the following fixes:

Low-Count Error Fix

The errors associated with a specific channel in the fitter having a number of counts N from the E787 PNN2 analysis was given as

- High-gain: Error = $0.74 + 0.69 \times \sqrt{N}$
- Low-gain: Error = $1.21 + 0.35 \times \sqrt{N}$

For counts (N) below 10, this function was found to underestimate the error as shown in Figure 1. This was fixed by applying the error corresponding to $N = 10$ counts for all channels having 10 or less counts.

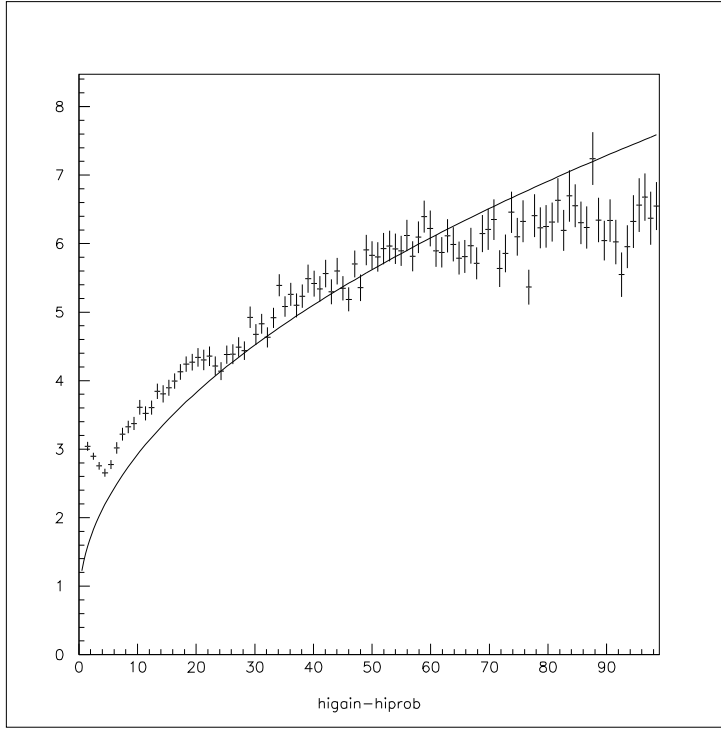


Figure 1: This plot shows the results of leaving the second bin out of the fitter and comparing the actual counts in that bin to those predicted by the fit. The x-axis shows the number of counts in that second bin. The y-axis shows *predicted – counts* for only positive values of this quantity. The line shows the error for each bin from the equation $0.74 + 0.69 \times \sqrt{\text{counts}}$. For different bins, the turn-up occurring in the data below 5 counts typically occurred in the first 5 to 10 bins. Based on these observations, the error applied to all bins having less than 10 counts was fixed at the error associated with 10 counts.

First Bin Error Fix

It was found that for a given pedestal-subtracted pulse that the fit is very sensitive to the first bin. The fitting starts on the first non-zero pulse-height bin and a very low number of counts (such as 1 or 2) counts in this first bin tends to give a very large contribution to the chi-squared of the fit. As shown in Figure 2, a reasonable looking fit can have a large chi-squared contribution due to the first bin. This contribution is reduced by doubling the error associated with the first bin.

Intermediate zero count bins included in the fit

The previous (E787 PNN2) fitter did not include intermediate bins having zero counts in the fit. This was changed so that the fitter first identifies the first and last bins of the pulse are first identified. Then up to the first 30 bins of this pulse are fit with bins having zero counts included. Bins which have been identified as saturated are not included in

Acceptances for Target Fitter Fixes			
Fix to the fitter	CCDBADFIT	CCDPUL	ALL
No fixes	0.797	0.454	0.362
First bin and low-count error fixes	0.876	0.518	0.453
First bin and low-count error fixes + 0-count bins included	0.881	0.504	0.443

Table 2: The sample used to optimize the target fitter was km2 monitors with the following cuts applied as setup cuts: TGQUALT, DELC, NPITG, TARGET, TGCUT, UTC, RD_TRK, TRKTIM, RDUTM. After these setup cuts have been applied, approximately 50,000 events remained to which CCDBADFIT, CCPUL and EPIONK were applied. The ALL column shows the combined acceptance of the set of cuts consisting of CCDBADFIT, CCPUL and EPIONK applied sequentially. The acceptance of the EPIONK cut is 0.999 for all 3 situations so it was not given a column in the table. The row "First bin and low-count error fixes" includes both the first bin error fix (doubling the error for this bin) and the low-count error fix (assigning an error equal to that for 10 counts for all bins having less than 10 counts). The row "First bin and low-count error fixes + 0-count bins included" includes the above fixes in addition to the fix which includes intermediate zero count bins in the fit.

the fit.

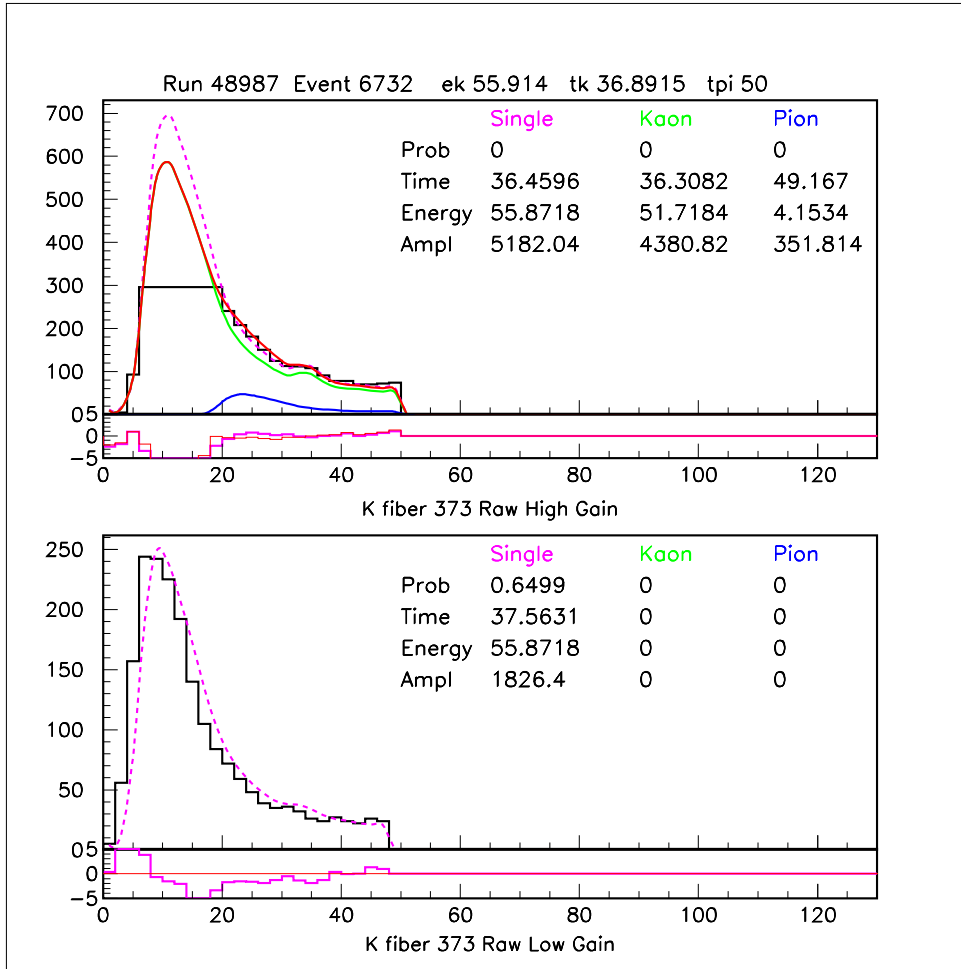


Figure 2: The high-gain single-pulse probability of 0 when the error associated with this bin is treated as usual. This is due to the first bin having only two counts versus the shape of the reference pulse predicting a larger number of counts. Had this bin had a pedestal subtraction that left it with zero counts, the next bin would have been used for the fit and the resulting fit would have been a non-zero probability. To reduce the effect of this sensitivity to the first bin, the errors assigned to the first bin are always doubled. When the fit is performed with this increased first bin error, the single-fit probability for the high-gain is 0.069 instead of the zero probability shown in this figure.

2.1.2 Hold and Release Double-Pulse Fit

The fitter was updated so that the double-pulse fit is a two-stage process. For the first stage of the double-pulse fit process, the first-pulse time is fixed at the time returned from the single-pulse fit. The three other parameters (first-pulse amplitude, second-pulse time and second-pulse time) are allowed to wander in the fit. For the second stage of the double-pulse fit, the values returned from the first stage of the double-pulse fit are used as the guesses.

The sample used to optimize this modification to the fitter was km2 monitors with the following cuts applied: TARGET, TGCUT, UTC, RD_TRK, TRKTIM, RDUTM, TGQUALT, DELC and NPITG. After these cuts were applied, 7021 events remained. With the two-stage fit used instead of the previous one-stage fit the total acceptance of CCDBADFIT and CCDPUL went from 0.402 to 0.451.

3 Photon veto cuts

PVCUTPNN2 removes events with photon activity at track time, t_{RS} , by searching all systems with the ability to detect photons for hits coincident with the track time, but not associated with the charged track. The time window and energy threshold for each category are shown in Table 3. BV, BVL, and RS hits are subdivided based upon the quality of the information from the hit. The acceptance of PVCUTPNN2 is 0.6391 ± 0.0022 as measured by $K_{\mu 2}$ monitor triggers. The tight parameters yield an acceptance of 0.3585 ± 0.0024 . Acceptances of the individual photon-detector cuts are listed in Table 42. Acceptance values of 30% and 60% were chosen during cut optimization to give appropriate levels of signal to background in the tight and loose signal region.

3.1 New photon veto cuts

The pnn2 photon veto differs the E949 pnn1 photon veto in the use of the active degrader (AD), downstream photon veto (DSPV), early BV cut, and the use of TD information to supplement the TDC information for the BVL. In addition, a safety cut, $EARLY_{BVL}$, described in Sec. 17 and designed to remove events where both photons from π^0 decay in $K_{\pi 2}$ events strike a single BVL counter [5] was added. The precise impact of the use of TD information to supplement the TDC information for the BVL was not evaluated, but we note that it has the potential to move single-ended hits to the more reliable double-ended hit category.

3.1.1 AD photon veto

The active degrader (AD) is a cylindrical, copper-scintillator sandwich-style detector divided into 12 azimuthal sectors [6]. Each sector is equipped with a CCD, TDC and multiplexed into ADCs. The CCDs were used for the PV. It was added to improve the PV rejection in the beam region. Extensive studies [4] showed activity coincident with TRS in sectors not traversed by the incident kaon in samples of events enhanced in $K_{\pi 2}$ target scatters identified by “kinks” in the pion trajectory in the target. The cut requires

Category	60% (Loose)			30% (Tight)		
	Timing (ns) offset	Timing (ns) window	Energy (MeV)	Timing (ns) offset	Timing (ns) window	Energy (MeV)
BV	2.25	7.95	0.20	1.35	8.85	0.70
early BV	-20.70	15.0	30.00	-22.5	15.0	30.0
BVL	3.15	7.55	0.30	3.15	7.55	0.30
RS	0.05	4.30	0.30	2.25	5.55	0.60
EC	1.80	6.15	0.40	1.75	7.75	0.20
EC inner-ring	0.99	4.64	0.20	-2.45	11.55	0.20
EC 2 nd pulse	-1.60	4.07	10.60	-1.51	4.19	1.70
TG	-0.25	2.40	2.00	-2.15	4.40	1.40
IC	1.25	3.25	5.00	3.20	6.10	5.00
VC	-2.40	4.15	6.80	-0.20	7.25	6.00
CO	2.90	2.95	0.60	2.15	2.95	1.60
μ CO	-1.60	3.90	3.00	-0.60	3.90	0.60
AD	3.00	5.00	0.60	3.00	5.00	0.60
DSPV	2.50	7.50	0.00	2.50	7.50	0.00
BV _{early}	3.50	1.50	10.00	3.50	1.50	10.00

Single-end hit categories

	hit-ends							
	energy	time						
BV	both	single	3.05	15.95	1.00	0.55	13.05	0.40
BV	single	both	4.80	1.50	1.40	4.00	3.10	0.60
BV	single	single	-8.10	8.50	1.60	-8.30	6.90	1.00
BVL	both	single	-5.65	11.80	8.19	-5.65	11.80	8.19
RS	both	single	-2.85	0.70	5.20	0.01	5.36	0.20
RS	single	both	6.60	1.35	0.00	3.70	6.10	0.00
RS	single	single	-6.80	1.22	3.40	-11.54	4.53	0.60
RS	no	both	-3.00	5.00	0.40	-3.00	5.00	0.40

Table 3: 30% and 60% photon cut parameters. The time window is shown in ns and energy threshold in MeV. The BV, BVL, and RS photon cuts require both ends of the detector obtain a result for time and energy. Additional photon cuts are applied when the both-ends requirement in time and energy are not met. *single* refers to a hit in only one end of the detector observed in either *energy* or *time*. *both* means both ends were hit and *no* means a hit was not observed in either end. $|t - t_{offset}| < t_{window}$ is defined as a coincident hit.

activity within $-2, +8$ ns of TRS and more than 5 ns from TK (to exclude activity from the incident kaon). A rejection in the “kink” sample of 1.95 ± 0.08 was obtained with an acceptance loss of 0.94.

3.1.2 Early BV photon veto cut

The presence of > 30 MeV of energy in the BV due to early accidentals could blind the BV to hits coincident with TRS. Such events were vetoed with little loss of acceptance [4].

3.1.3 Downstream photon veto

The downstream photon veto (DSPV) is a square, lead-scintillator sandwich-style detector with ~ 7.3 radiation lengths at normal incidence located downstream of the target PMTs along the kaon beam direction [8]. Using the classes defined for the evaluating the PV rejection of $K_{\pi 2}$ target scatters (Table 13), a rejection of 1.125 (18/16) was measured based on any DSPV activity within $-5, +10$ ns of TRS with an acceptance of 0.9999 (20881/20883) [7].

3.2 PV optimization

As performed by Ilektra, discussed in [4] and described in Ref. [2].

4 TDcuts

A study was performed to determine possible acceptance gains from removing EV5 (electron finding) and loosening TDNN ($\pi^+ \rightarrow \mu^+ \rightarrow e^+$ neural-net). The effects on the total background and total acceptance was optimized to give the best performance; muon background was measured directly, while other backgrounds were assumed to scale with increased acceptance based upon background values as reported in [4].

Other TD cuts remained unchanged since E949-PNN1 analysis.

4.1 Electron Finding (EV5)

The cut EV5 was scrutinized to determine if it is possible to remove it from the E949 offline cut-list, to gain the observed 17% acceptance loss.

To determine the effect EV5 has on the muon background, the muon background was measured with and without EV5. Table 4 shows the effect of EV5 on the TD rejection. Table 5 shows the effect of EV5 on the muon background. Note that the muon tail for the PNN2 energy-range box is very high due to limited statistics in rejection measurement. The total muon background is the sum of the muon-band plus the muon-tail measurements.

The acceptance of EV5, when applied last, is 0.83. When EV5 is removed, a gain of 17% acceptance with an increase of the muon background by a factor of 2.0 is observed. The total background will be 0.0260 ± 0.0260 (band+tail) when EV5 is not applied which

Rej & Norm Measurement	with EV5	without EV5
Band All Rejection	357.89 ± 119.13	140.04 ± 29.10
Band ERbox Rejection	423.00 ± 422.50	211.50 ± 149.20
Tail All Rejection	679.00 ± 678.50	679.00 ± 678.50
Tail ERbox Rejection	9.00 ± 8.49	9.00 ± 8.49
Muon Normalization	1.0 ± 1.0	1.0 ± 1.0

Table 4: Rejection and Normalization Summary. Band refers to applying \overline{RNGMOM} to the sample and Tail refers to applying $ptot > 229.$, which will tag the muon-band and muon-tail sample respectively. All (ERbox) refer to applying all setup cuts (all setup cuts plus the PNN2 energy range cut).

Background	with EV5	without EV5
Band All	0.00841 ± 0.00841	0.0216 ± 0.0216
Band ERbox	0.00711 ± 0.00711	0.0143 ± 0.0143
Tail All	0.00442 ± 0.00442	0.00442 ± 0.00442
Tail ERbox	0.37500 ± 0.37500	0.3750 ± 0.3750

Table 5: Muon background summary, scaled to the 3/3 sample. Band refers to applying \overline{RNGMOM} to the sample and Tail refers to applying $ptot > 229$ MeV/c, which will tag the muon-band and muon-tail sample, respectively. All (ERbox) refer to applying all setup cuts (all setup cuts plus the PNN2 energy range cut).

is much less than the expected background from TG-scatters of 0.5 events (at the time of this optimization study).

4.2 TD Neural-Net Cut

TD neural-net cut (TDNN), cuts on one parameter. Therefore, loosening was very easily accomplished. The initial cut parameter is 0.76, set in E949-PNN1 analysis. This parameter was varied from 0.05 to 0.8 in 0.05 increments (16 total values) in an attempt to determine the optimal value for PNN2 analysis. The effects of including and excluding EV5 was done in tandem when optimizing TDNN. In Figures 3-6 black (red) points included (omitted) EV5 in the measurement. Figure 3 shows muon background as a function of the TDNN cut value. Figure 4 shows muon background as a function of *acceptance*.

The acceptances were measured in the Piscat TD acceptance measurement as in Section 15.2 applying TDNN last in the measurement order. The muon-band background was measured by inverting RINGMOM and the muon-tail background was measured by requiring $ptot > 229MeV$. At the time this study was performed it was not known if the muon-tail background would be negligible. Therefore, the muon background in this optimization study included band and tail measurements. There was one event remaining in the normalization branch using the nominal TDNN(0.76) cut; the normalization branch was not measured for the TDNN parameter variations to prevent determining possible location of events within the box. Table 6 lists the background and acceptance values for all TD cut parameter values that were analyzed.

The optimal level for the TDNN's cut parameter can be determined by finding the maximum for the ratio of total acceptance to total background. We assume that all other backgrounds will increase with increased acceptance. All backgrounds (except muon) were measured with EV5 and TDNN(0.76) applied. These backgrounds were scaled with the expected acceptance gain when EV5 and TDNN are loosened. Total background is $N_{bkg}^* + N_{muon}$, such that N_{bkg} scales directly with acceptance gain.

Acceptance is normalized to 1.0 when defined as the total acceptance with the TDNN cut parameter being 0.76 and EV5 cut applied (along with all other cuts). The results are plotted in Figure 5. The maximum for the ratio of total acceptance to total background occurs at the maximum tightness for TDNN. As the cuts were loosen, the gains acceptance occurred. However, the other backgrounds increased with increased acceptance. Sensitivity is lost at a greater rate starting at TDNN value of 0.3. The muon background at 0.3 is 0.0857 (a factor of 3.3 increase) and the TDNN acceptance increases to 0.9415 (9.6%).

4.3 Conclusions from TD Optimization

The increase in acceptance from loosening TDNN and EV5 was measured to be $\sim 23\%$ with a muon background at a value much smaller than other backgrounds. Therefore, EV5 should not be applied and TDNN should be loosened to a cut parameter of 0.3. EV5 and the TDNN set at the original 0.76 were used to define a much cleaner PNN2 signal region.

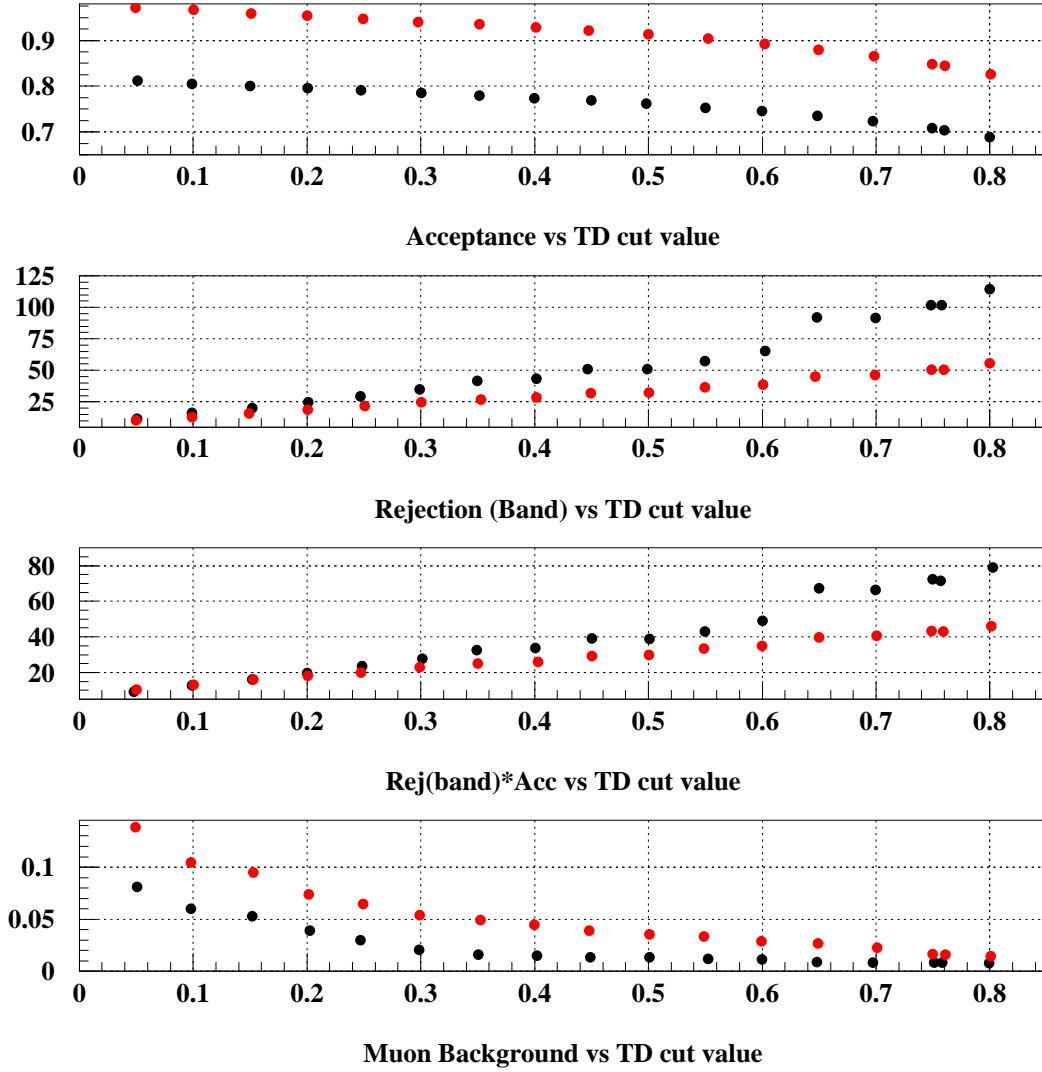
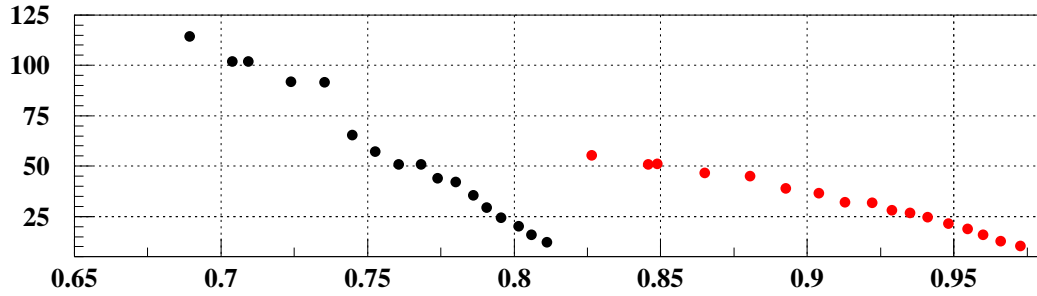
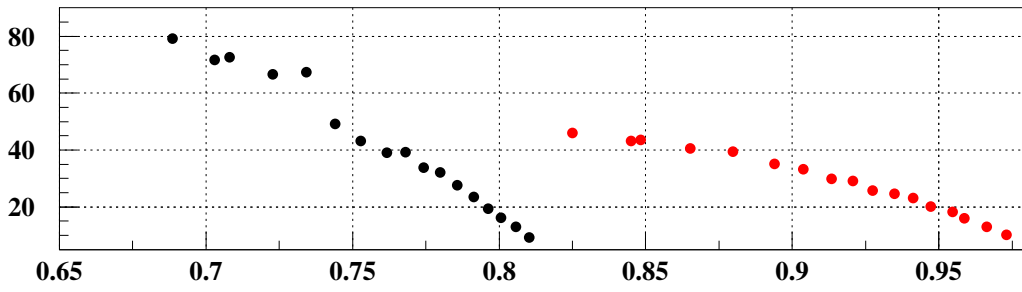


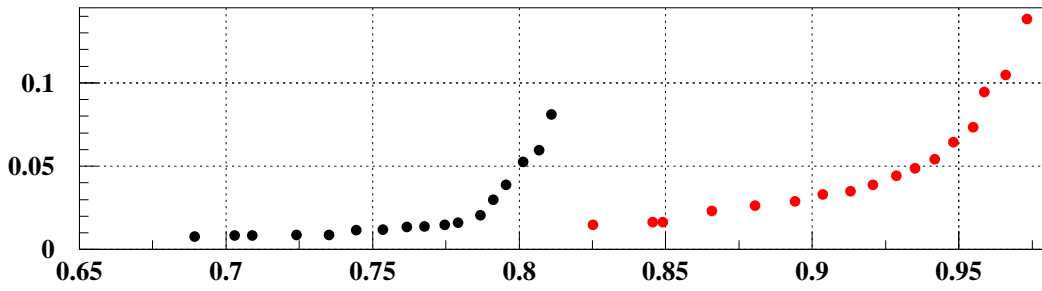
Figure 3: Acceptance, Rejection, and Rejection \times Rejection versus TD cut parameter. Black points include EV5 in the calculation, red points have excluded EV5 from the analysis.



Rejection (Band) vs Acceptance



Rej(band)*Acc vs Acceptance



Muon: Background vs Acceptance

Figure 4: Rejection vs Acceptance with different TDNN cut parameter. Black points include EV5 in the calculation, red points have excluded EV5 from the analysis.

TD cut	with EV5			without EV5		
value	Accept	Band All	Tail All	Accept	Band All	Tail All
0.05	0.9740	0.0470	0.03409	0.9732	0.0689	0.0694
0.10	0.9675	0.0341	0.02545	0.9664	0.0532	0.0516
0.15	0.9612	0.0268	0.02545	0.9602	0.0433	0.0516
0.20	0.9549	0.0220	0.01689	0.9537	0.0366	0.0370
0.25	0.9490	0.0184	0.01123	0.9477	0.0329	0.0312
0.30	0.9428	0.0154	0.00560	0.9415	0.0287	0.0255
0.35	0.9366	0.0130	0.00279	0.9353	0.0262	0.0226
0.40	0.9300	0.0124	0.00279	0.9286	0.0250	0.0197
0.45	0.9224	0.0106	0.00279	0.9211	0.0220	0.0169
0.50	0.9144	0.0106	0.00279	0.9131	0.0214	0.0141
0.55	0.9050	0.00945	0.00279	0.9036	0.0190	0.0141
0.60	0.8939	0.00827	0.00279	0.8928	0.0178	0.0112
0.65	0.8820	0.00590	0.00279	0.8809	0.0154	0.0112
0.70	0.8676	0.00590	0.00279	0.8661	0.0148	0.0084
0.75	0.8511	0.00531	0.00279	0.8495	0.0136	0.00280
0.76	0.8454	0.00531	0.00279	—	0.0136	0.00280
0.80	0.8270	0.00472	0.00279	0.8253	0.0124	0.00280

Table 6: Muon background at different TD Neural-Net cut parameters. Value is using the 'All' Setup cuts, i.e. ERBox not applied. The bold 0.76 line is the TD cut parameter set at the PNN1 level. Error is 100% on all values, the normalization branch is 1 ± 1 with one event remaining. Any loosening of the TDNN will only reduce the normalization branch to zero, which for us will be the same as the nominal cut value. Scaled to the 3/3 sample.

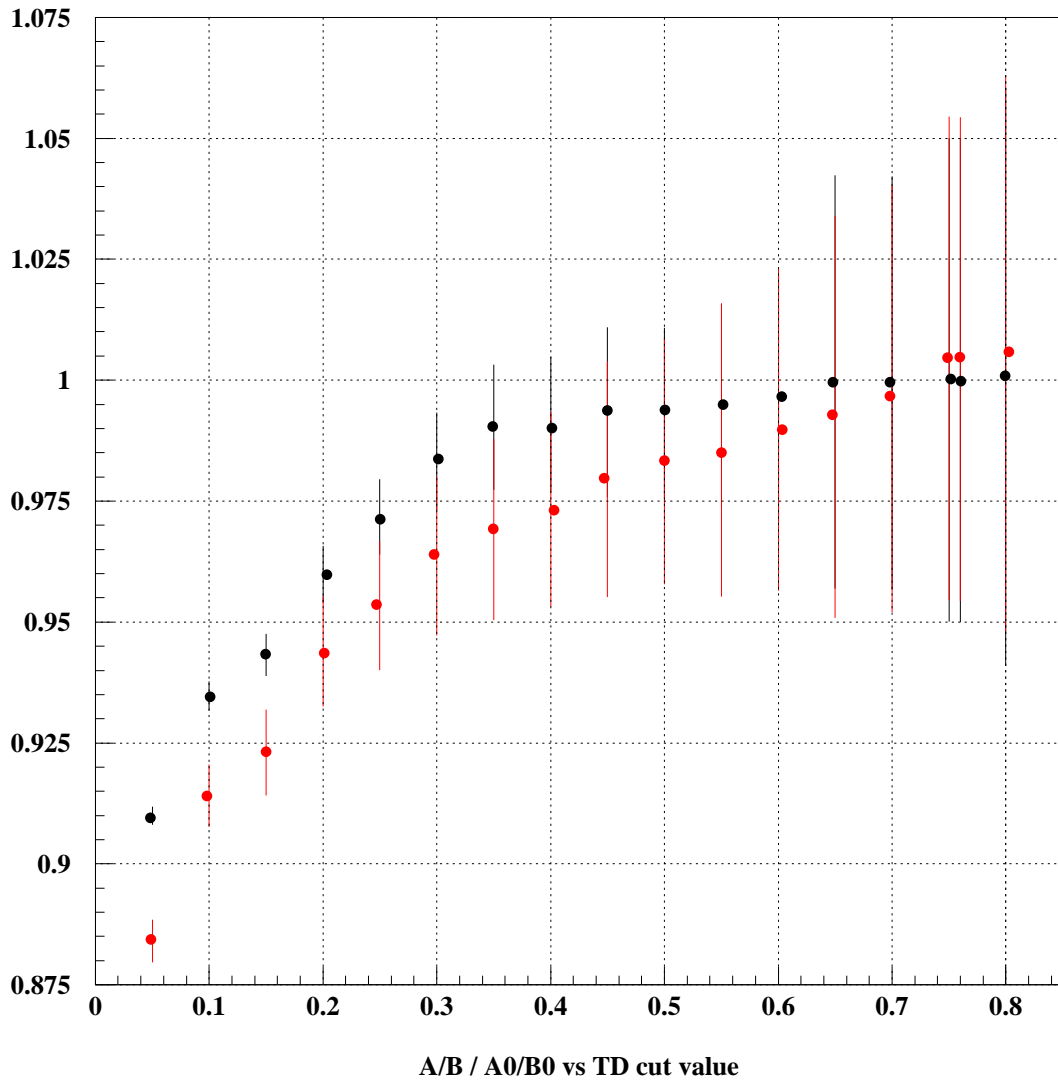
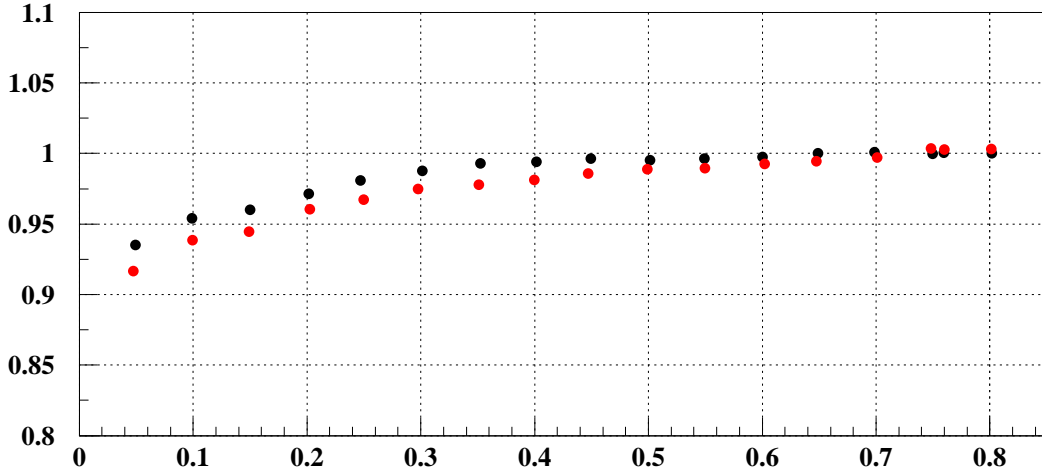
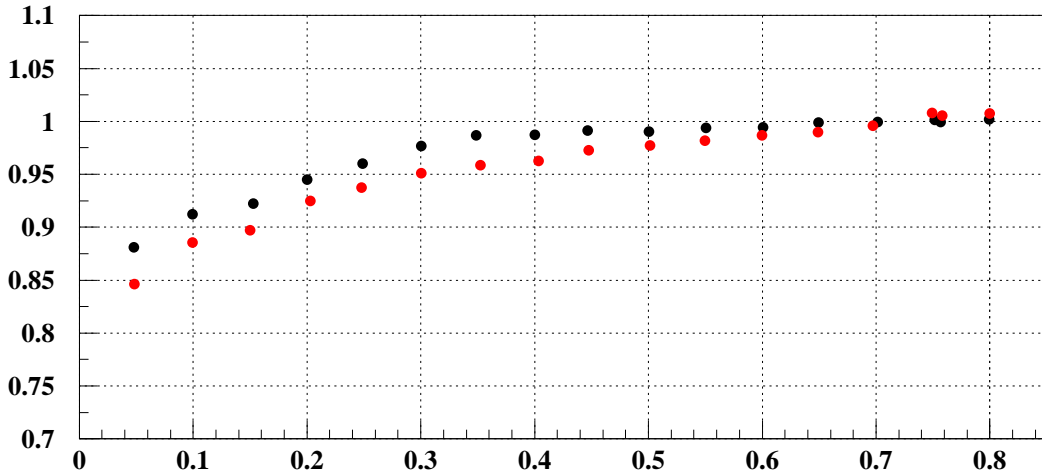


Figure 5: Total Acceptance/Total Background normalized by A_0/B_0 versus TD cut parameter. Black points include EV5 in the calculation, red points have excluded EV5 from the analysis. Acceptance is normalized to the total acceptance at the tight TD cuts (TDNN(pnn1) and EV5 applied). The total background is approximated from other background + muon background.



$A/(B+1\text{sig}) / A0/(B0+1\text{sig})$ vs TD cut value



$A/(B-1\text{sig}) / A0/(B0-1\text{sig})$ vs TD cut value

Figure 6: Same as Figure 5 except the background value has been varied by 1 sigma. Black points include EV5 in the calculation, red points have excluded EV5 from the analysis. Acceptance is normalized to the total acceptance at the tight TD cuts (TDNN(pnn1) and EV5 applied). The total background is approximated from [4] + Muon Background. This assumes no dependence of the TD cuts on other background or acceptances.

Table 7: E787 and E949 pnn2 kinematic box definitions. The K_{e4} -phobic box is described in Sec. 5.2.

	E787	E949	K_{e4} -phobic box
PTOT (MeV/c)	(140, 195)	(140, 199)	(165, 197)
ETOT (MeV)	(60, 95)	(60, 100.5)	(72,100)
RTOT (cm)	(12, 27)	(12, 28)	(17,28)

5 Kinematic cuts

5.1 Expand kinematic box

Pions from $K_{\pi 2}$ produce a monochromatic peak in momentum, energy and range. The nominal upper bounds of pnn2 signal box are $2.5 \times \sigma_p$ below the $K_{\pi 2}$ momentum peak, ($2.5 \times \sigma_e$ below the energy peak and $2.75 \times \sigma_r$ below the range peak. We exploit the improvements in resolution in momentum, energy and range for E949 [2] to increase the size of the signal region. The definition of the kinematic box is tabulated in Tab. 7. More detail information can be found in [15].

5.2 K_{e4} -phobic box

Additional kinematic cuts were created to define a low background region inside the “loose” kinematic box (Table 7). This kinematic is dubbed the “ K_{e4} -phobic box” because the lower limits are specifically designed to kinematically exclude K_{e4} events. The details of the K_{e4} background study are in Sec. 14.

The momentum of π^+ of K_{e4} events peaks around 160 MeV/c. It is the second largest background of whole pnn2 analysis. Suppression of this background mainly relies on the CCDPUL and TGPV cuts. The CCDPUL cut is a very complicated cut, and the pulse fitting algorithm is not simulated in UMC. The existence of the π^- in the final state also complicates this background estimation. Both these factors contribute to the relative large systematic uncertainty assigned to the K_{e4} background estimate.

Fig. 7 presents the momentum distribution of K_{e4} normalization sample before CCDPUL cuts. It agrees pretty well with the analogous spectrum from the UMC sample (Fig. 8, the middle plot of the first row). A visual scan of the target fibers for the events in Fig. 7 confirms that is composed almost entirely of K_{e4} events. The K_{e4} -phobic box is designed to kinematically suppress K_{e4} background and also reduce the relative systematic uncertainty, so that the likelihood-based pnn2 analysis will contain cells with small and relatively well-determined background.

The $K_{\pi 2}$ scattering background is the largest background for pnn2. The upper bound of the loose pnn2 box is very close to $K_{\pi 2}$ peak. Obviously tightening the upper bound of kinematic box will also enhance the S/N. Suppression of $K_{\pi 2}$ background guides the upper kinematic limits of the K_{e4} -phobic box.

Three samples are prepared to determine the kinematic limits of the K_{e4} -phobic box. One is UMC pnn2 sample which represents the acceptance sample. The UMC pnn2 sample is required to pass all requirements except the box cuts.

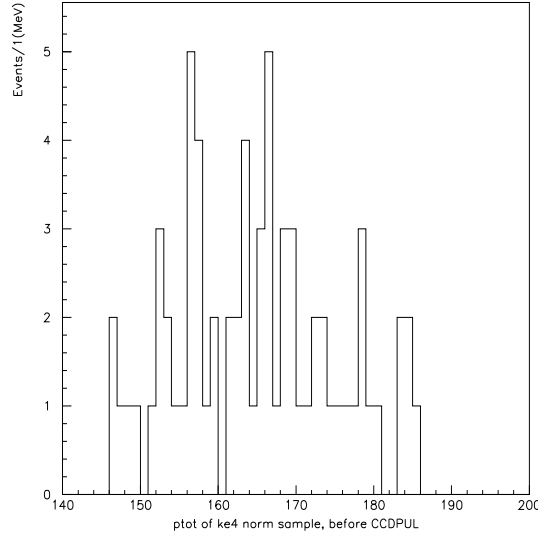


Figure 7: Momentum distribution of K_{e4} normalization sample before CCDPUL cuts.

The second sample is a K_{e4} sample. The sample from data has low statistics, Fig. 7, so a UMC sample that passes all possible pass2 cuts except CCDPUL cuts is used. The rejection of CCDPUL cut is assumed to be insensitive to box cuts. The total area is normalized to the K_{e4} background estimate using the loose cuts.

The third sample is for $K_{\pi2}$. The $K_{\pi2}$ normalization branch is exploited with the assumption that the rejection of the PVCUTS is insensitive to the kinematic box cuts. Its area is normalized to the actual background measurement for loose cuts. As the other background sources are small and are roughly independent of momentum, their contribution is ignored in this study.

The ptot distribution of these three samples is shown in the first row of Fig. 8. The first step is to find the lower bound of the phobic box by computing the signal acceptance and background contribution of the ptot cut. As shown in the second row of Fig. 8, the acceptance decreases slowly before 170 MeV/c and $K_{\pi2}$ background is not affected too much. However the K_{e4} background will drop rapidly above after 160 MeV/c. When K_{e4} and $K_{\pi2}$ are normalized, the acceptance/background has a rather wide maximum at 175 MeV/c (Bottom row of Fig. 8). To keep a higher sensitivity, the lower bound in ptot is set to 165 MeV/c. The etot and rtot lower limits are set to the corresponding values for pions in scintillator.

The second scan is performed for the upper bound with ptot $>$ 170 MeV/c as a setup cut (First row of Fig. 9). The second row of Fig. 9 shows how acceptance and background decrease as the upper ptot cut is tightened. The plot in the third row of Fig. 9 gives the Acc/Bkg as a function of the ptot upper bound cut. The Acc/Bkg ratio is maximize at \sim 195 MeV/c. So the upper bound of ptot is set to 197 MeV/c with corresponding etot and rtot cuts.

The procedure was reversed with the upper limit set first and the lower limit second and consistent results were obtained. The kinematic limits of the K_{e4} -phobic box are given in Table 7.

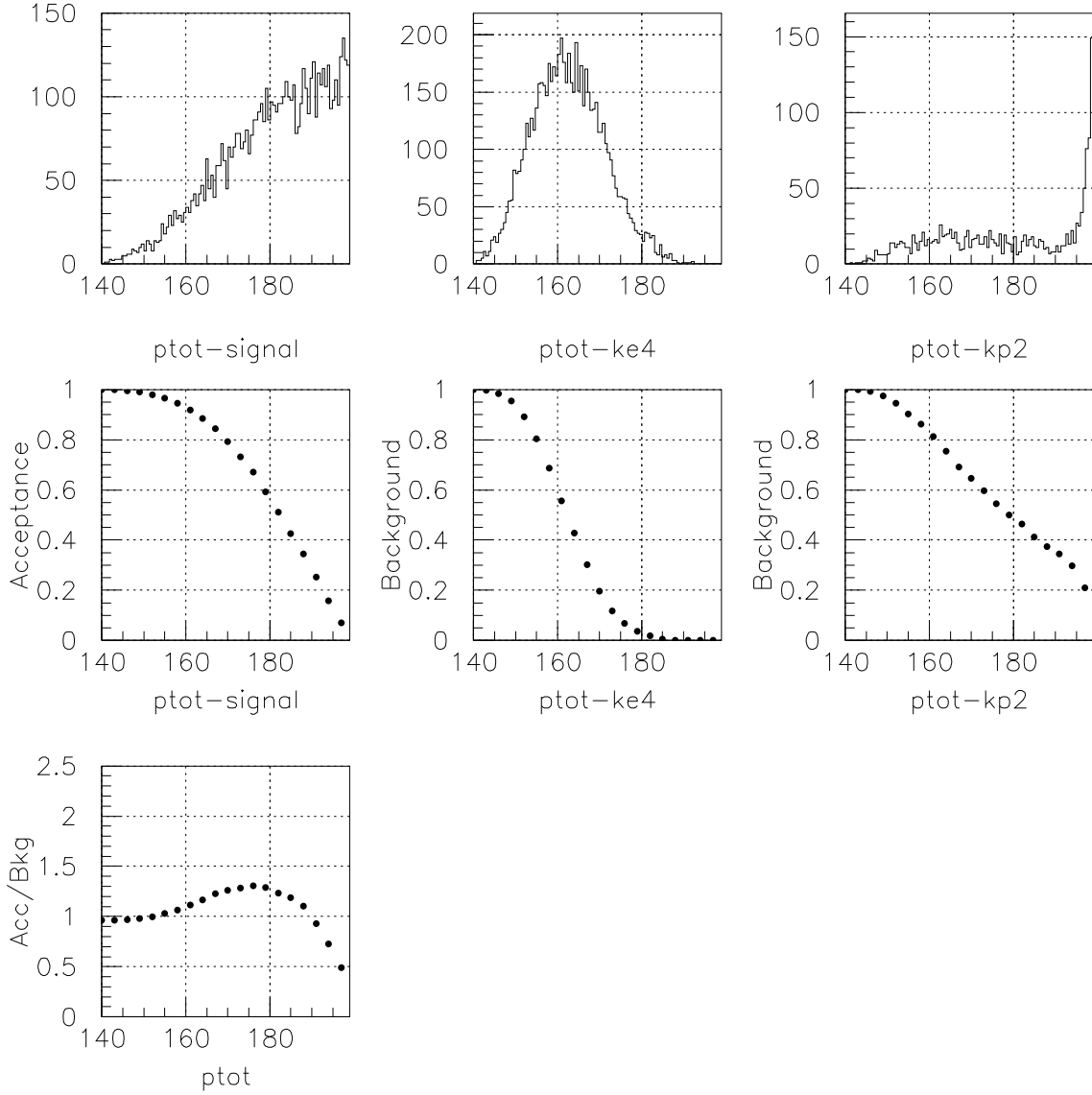


Figure 8: K_{e4} -phobic box lower bound scan. The first row: $ptot$ of UMC acceptance sample, K_{e4} UMC sample and $K_{\pi 2}$ normalization sample. The second row: acceptance loss or background decrease as a function of a $ptot$ lower bound cut for these three samples (normalized to 1.0 for no cut applied). Bottom row: acceptance/background as a function of $ptot$ lower bound cut. Background is the sum of K_{e4} and $K_{\pi 2}$ background, and they are normalized to actual background measurement with loose cuts.

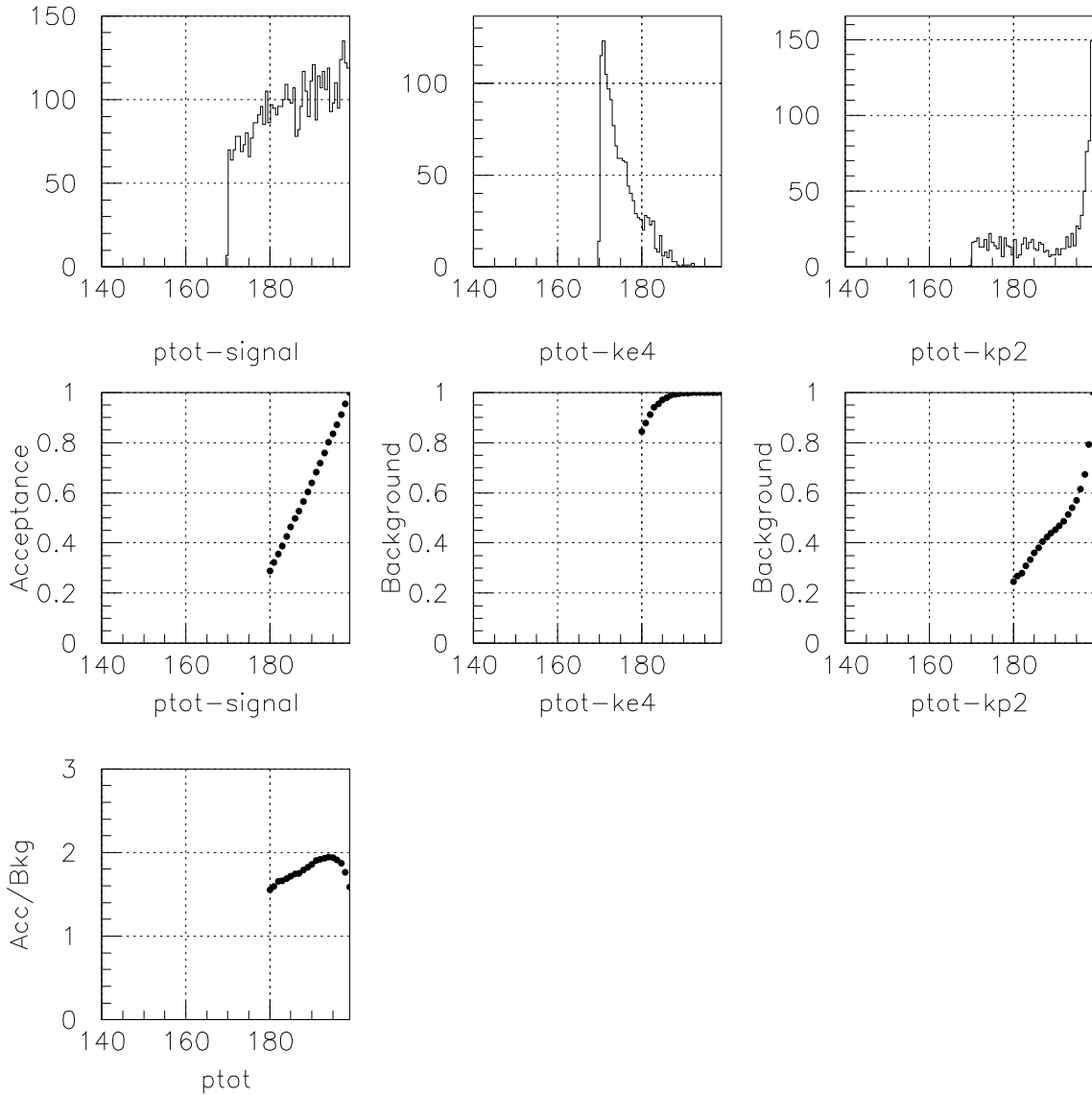


Figure 9: K_{e4} -phobic box upper bound scan. The first row: $ptot$ of UMC acceptance sample, K_{e4} UMC sample and $K_{\pi 2}$ normalization sample where $ptot > 170$ MeV is a setup cut. The second row: acceptance loss or background decrease as a function of a $ptot$ upper bound cut for these three samples (normalized to 1.0 for no cut applied). Bottom row: acceptance/background as a function of $ptot$ upper bound cut. Background is the sum of K_{e4} and $K_{\pi 2}$ background, and they are normalized to actual background measurement with loose cuts.

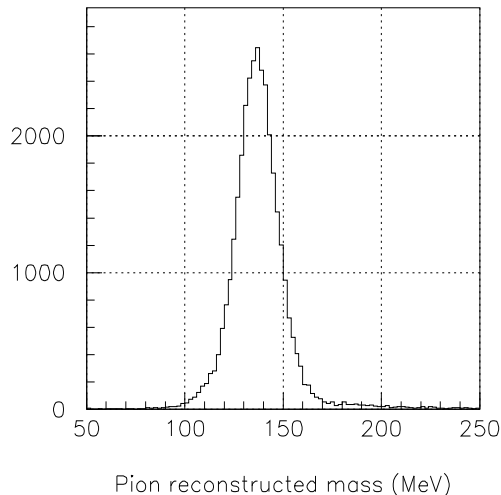


Figure 10: π mass distribution of π_{scat} sample.

5.3 UTCQUAL

The UTCQUAL cut [2] for the E949 pnn1 analysis was designed to suppress tails in the $K_{\pi 2}$ momentum distribution by rejecting events in which the charged track has a poor UTC fit. Poor UTC fitting is associated with fewer x-y hits, fewer z hits, some overlapping hits, etc. and is generally accompanied by worse momentum resolution.

The acceptance of the pnn1 UTCQUAL cut was found to decrease from $\sim 94\%$ [3] at the $K_{\pi 2}$ peak and dropt to $\sim 87\%$ [4] in the pnn2 region. The momentum dependence was examined and it is found that many good track were unnecessarily removed the the pnn1 UTCQUAL cut.

To clearly see this phenomenon, a π_{scat} sample is selected. The setup cuts are quite like to that used in π_{scat} -based acceptance study. A clean π mass plot from this sample is shown in Fig. 10. The gradually dropping acceptance with momentum is shown in Fig.11.

With this sample some further study is done with UTCQUAL cut. For charged tracks, the E949 detector provides range and energy measurements almost independent of the momentum measurement. With energy and range information, the momentum of a track can be estimated. Fortunately this method yields a very good momentum resolution of $\sigma(P_{dc} - P_{exp}) \approx 3.01$ MeV where P_{dc} is the momentum measured directly by the UTC and P_{exp} is momentum estimated from energy and range.) This gives an opportunity to tune UTCQUAL cut independent of momentum.

There are 10 failure modes identified as part of UTCQUAL cut. Some of them are based on probabilities of χ^2 of components of the fit and the others cut on specific cases such as number of hits, etc. If a failure mode removes mainly good tracks, based on the agreement of P_{dc} and P_{exp} , then the component of the cut based on this failure mode is loosened. For instance, as shown in Fig. 12, the cuts for modes 4 and 7 are loosened, whilst obviously a mode 10 cut is very effective at reducing tails. Fig.13 shows the result before and after the tuning for UTCQUAL. A lot of good tracks were recovered. with an

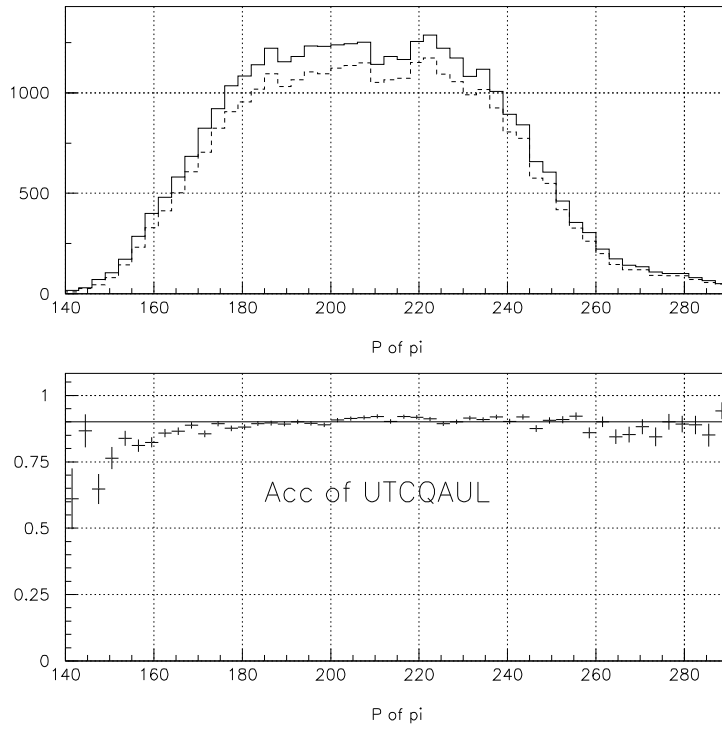


Figure 11: Upper:momentum of pion, the solid line represents all events and the daashed line represents the events pass pnn1 UTCQUAL; Lower: acceptance of UTCQUAL with momentum, the horizontal solid line is at 90%, and the error are statistical only.

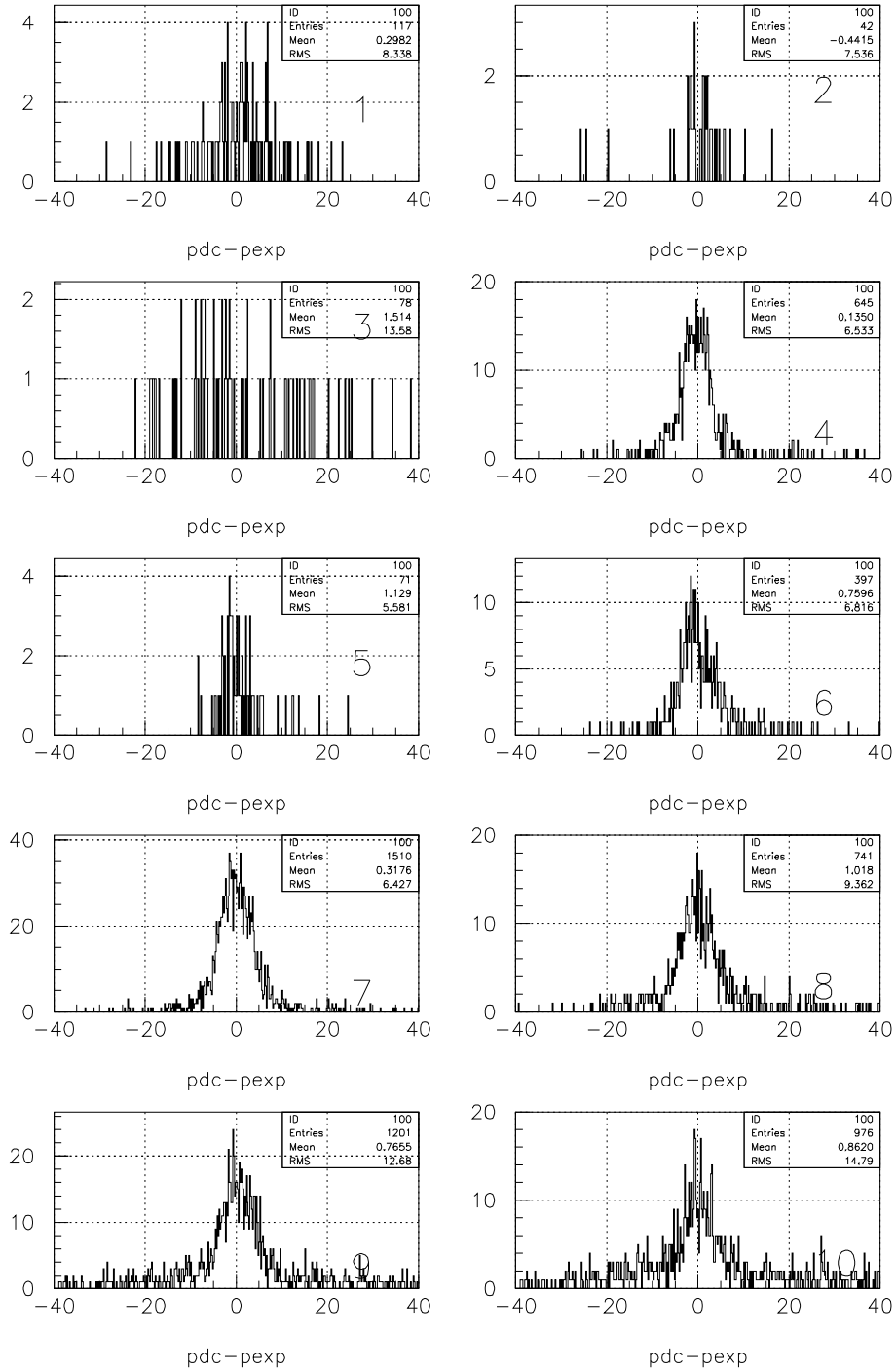


Figure 12: $P_{dc} - P_{exp}$ for events failing pnn1 UTCQUAL for the 10 ten failure modes.

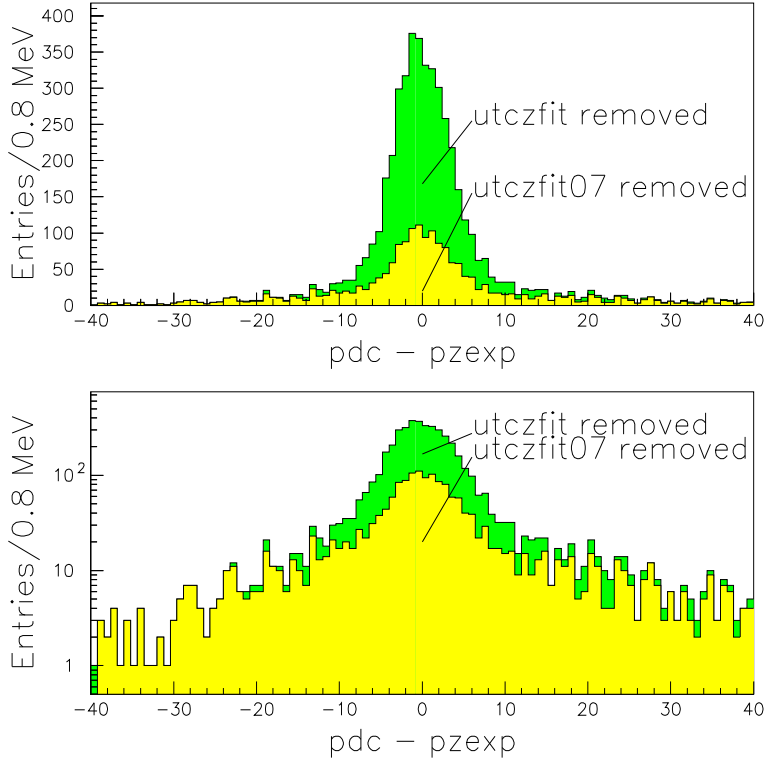


Figure 13: $P_{dc} - P_{exp}$ for events that *failed* the UTCQUAL cut before (green) and after (yellow) tuning. UTCQUAL07 is the cut after tuning. The upper one is in linear scale, the lower one is in log scale.

acceptance improvement from 87% to 95%.

5.4 PRRF

The PRRF cut as used in the pnn1 analysis [2] had 4 components:

1. $PRRF$ = the probability of χ^2 of the RS track (TRKRNG) fit ¹
2. $PRRFZ1$ = probability of χ^2 of the match of the UTC track extrapolation to the z position determined from the RSSC information,
3. $PRRFZ2$ = probability of χ^2 of the match of the UTC track extrapolation to the z position determined from the RS timing, and
4. $PRRFXY$ = probability of χ^2 for the match between the UTC track extrapolation and the RSSC and RS (sector-crossings) xy position measurements.

Use of the pnn1 version of the PRRF cut had a $\sim 30\%$ acceptance loss in tracks that stopped before the first RSSC layer. Since pnn2 accepts shorter range tracks by definition, changes in the PRRF cut were made. The $PRRFXY$ requirement of the PRRF cut

¹In this section we denote the probability cut as $PRRF$ and the composite cut with all components as PRRF.

was removed for pnn2 because a significant fraction of pnn2 signal events have no RSSC hits or RS sector-crossings. Tracks with no RSSC information or sector-crossings are accepted, otherwise $PRRF$ is required to be greater than 0.01. The PRRFZ1 or PRRFZ2 requirements are imposed only when RSSC information or RS timing information is available. The resulting rejection of the PRRF cut is ~ 1.15 with the PRRFZ2 contributing a rejection of ~ 1.11 .

5.5 RSDEDX

In the E949 pnn1 analysis [2], the cut on the probability of χ^2 of the RS counter energy measurements was dependent upon whether the largest deviation in the (expected-measured) energy in a RS counter was positive or negative. This innovation of an asymmetric cut lead to a $\sim 10\%$ increase in muon rejection and a $\sim 2\%$ increase in acceptance of pnn1. It was found that the calibration for the expected energy deposit for the shorter range tracks of pnn2 was not sufficiently robust for the asymmetric cut to be exploited. In addition since the muon background is much less troublesome for pnn2, we reverted to a cut on the probability of χ^2 of > 0.04 independent of the largest deviation.

6 Delayed-coincidence cuts

6.1 K^+ Stop Requirement: Delayed Coincidence (DEL3)

Determining that the incoming K^+ stops within the TG is accomplished by observing a delay in the outgoing charged track which is presumed to be a K^+ -decay product. This requirement will remove beam- π^+ scattering events and K^+ decay-in-flight events. DELC3 requires a delay of at least 3.0 ns between the target π^+ time, t_π , and the target K^+ time, t_K , ($t_{pi} - t_k \geq 3.0$ ns). Additionally, DELC3 requires the constraints defined in the conditional delco function, $delc$, described below. $K_{\mu 2}$ monitors are used to measure an acceptance of 0.8569 ± 0.00020 and an acceptance of 0.9669 ± 0.00023 after all correlated cuts are applied.

6.2 Tight Delayed Coincidence (DEL6)

A tighter delayed coincidence cut is employed for the use in a signal region with reduced background. This is accomplished by a 6.0 ns delayed coincidence requirement ($t_{pi} - t_k \geq 6.0$ ns). $K_{\mu 2}$ monitors are used to measure an acceptance of 0.7044 ± 0.00026 and an acceptance of 0.8804 ± 0.00043 after all correlated cuts are applied.

6.3 Delayed Coincidence Function ($delc$)

This function tightens the delay coincidence when the timing consistency between detectors are degraded. Events are rejected if $t_\pi - t_K < delc_{thres}$. The cut threshold, $delc_{thres}$ is the maximum of the following conditions ($delc_{thres}$ minimum is 2.0 ns).

- $delc_{thres} = 5.0$ ns if the discrepancy between the TG K^+ time and B4 hit time is greater than 1.0 ns.

- $delc_{thres} = 6.0$ ns if the discrepancy between the TG π^+ time and track time is greater than 1.5 ns.
- $delc_{thres} = 5.0$ ns if t_π is obtained from the time of the I-Counter hit, not from the TG π^+ fiber hits.
- $delc_{thres} = 4.0$ ns if the energy deposit of a K^+ in the TG is less than or equal to 50MeV.
- $delc_{thres} = 3.0$ ns if there are less than four TG π^+ fibers found.
- $delc_{thres} = 3.0$ ns if the beam likelihood value is less than 200 (to be explained in the Pathology Cuts section).
- $delc_{thres} = 4.0$ ns if the discrepancy between any of the individual K^+ fiber times and the average K^+ time is greater than 2.0 ns.
- $delc_{thres} = 4.0$ ns if the discrepancy between any of the individual π^+ fiber times and the average π^+ time is greater than 3.5 ns.

7 Target cuts

7.1 TIMKF

The fixes to TIMKF are as follows:

- It was found that a small fraction of the events (5 of 16000 in the study) were passing identical values to linfit for the y-array. This resulted in an infinite slope being determined by linfit. The code was modified so that this type of information was flagged, the fit never performed, and the event automatically failing the TIMKF cut.
- The ccd rise times associated with the variable ccdrk have changed from the E787 to the E949 analyses. One of the fail conditions for TIMKF is when either of the probability distributions xprob1 or xprob2 have a value of less than 0.05. The change in ccd rise times resulted in non-flat probability distributions for these two probability variables. To flatten these probability distributions, the errors in the y-array passed to linfit (the variable tres) was multiplied by 0.8.
- It was found that approximately 1% of the events passing the target cut study setup cuts retained their initialization values (equal to -8) in the variables xin, yin, x_b4sw and y_b4sw. As TIMKF uses these distances in some of its calculations, events with variables still containing this initialization data are now rejected.

7.2 CCDPUL

The former CCDPUL pull cut as it was used in the E787 PNN2 analysis was actually two cuts in one. An event could fail the cut if any of the target fibers failed either the "Pion energy" or the "Bad pulse fit" conditions. This cut has since been split into two cuts. The first is a safety cut called CCDBADFIT to deal with the "Bad pulse fit" condition. The second keeps the name CCDPUL and deals with the "Pion energy" condition.

7.2.1 Description of CCDPUL

The CCDPUL cut removes events that have kaon fibers with second pulse energies above a certain threshold (1.25 MeV) at a time that is consistent with the global pion time, t_{pi} . As each fiber has two gain channels (low-gain and high-gain), before checking for the time and energy conditions for a target fiber the CCDPUL algorithm needs to determine which CCD data is used: the low-gain, the high-gain. This cut is a three stage process.

CCDPUL - The First Stage

Separately the results of the fits from the low-gain and high-gain target CCDs are considered. The high-gain channel data is not passed onto the second stage if any of the following conditions are met:

- The single fit probability is greater than 0.25 as the double-pulse fit is only performed if the single fit probability is less than or equal to 0.25.

- The number of bins in the second pulse with non-zero amplitude less than 3.
- The double fit probability is equal to 0.

The same conditions as above were applied to the low-gain channels with one additional condition. If the fiber is found to be multiplexed with other fibers having activity within ± 5 ns of the global pion time t_{pi} , the energy within that time window from those other fibers is subtracted from the second pulse energy of the fiber being examined.

CCDPUL - The Second Stage

During the second stage of CCDPUL, an algorithm decides which CCD data is used: the low-gain, the high-gain, or a weighted average of the two. If only the high-gain or low-gain CCD data for this fiber has been passed on from the first stage, that is what will be used. If the first stage passed on both the high-gain and the low-gain CCD data the decision of how to use these data was based on the following conditions which are checked **in sequence**:

- An average of the the high-gain and low-gain will be used if the fiber energy as determined by ADC is between 10 MeV and 30 MeV and the fractional error in the second-pulse amplitude for both the low-gain and high-gain CCD channels is greater than 0.05. A typical pulse will start to saturate at around 25 MeV so the fiber energy condition includes high-gain fibers that show small amounts of saturation. The second-pulse energy and relative time between the first and second pulses are the quantities which are determined via the weighted average. For the rest of the quantities passed onto the third stage, the information from the high-gain channel is used. The following equations show how the weighed average is determined for a quantity x :

$$w_{hi} = \frac{dA_{hi}^2}{dA_{hi}^2 + dA_{lo}^2}$$

$$w_{lo} = \frac{dA_{lo}^2}{dA_{hi}^2 + dA_{lo}^2}$$

$$x = x_{hi}w_{hi} + x_{lo}w_{lo}$$

where dA_{lo} and dA_{hi} are the errors on the second-pulse amplitudes of the low-gain and high-gain double pulse fits respectively.

- Use high-gain if it has not saturated.
- Use low-gain if high-gain has saturated and the energy in the fiber as determined by ADC is greater than 40 MeV. The low-gain channel will typically start to saturate at around 40 MeV.
- Choose the better fit based on the fiber energy E_k (from ADC) and the time difference between the global pion time t_{pi} and the global kaon time t_k . High gain is used if either of these conditions are met:

$$15 < E_k < 25 \text{ .AND. } t_{pi} - t_k > 12$$

$$25 < E_k < 40 \text{ .AND. } t_{pi} - t_k > 20$$

Low gain is used if either of these conditions are met:

$$15 < E_k < 25 \text{ .AND. } t_{pi} - t_k < 12$$

$$25 < E_k < 40 \text{ .AND. } t_{pi} - t_k < 20$$

This information is then passed onto the third stage.

CCDPUL - The Third Stage

All fibers passed onto stage 3 are checked for second-pulse energy above a certain threshold where the timing of the second pulse is consistent with the global pion time t_{pi} . The event fails if any fiber in stage 3 meets both of the following conditions:

- The second-pulse energy is above 1.25 MeV
- The quantity $deltat$ falls between -7.5 and 10 ns inclusive. The quantity $deltat$ is a measure of consistency between the global pion (t_{pi}) and kaon (t_k) times and the first (t_1) and second (t_2) pulse times from the fit for that kaon fiber:

$$deltat = (t_2 - t_1) - (t_{pi} - t_k)$$

7.2.2 Description of CCDBADFIT

The CCDBADFIT safety cut removes events that have kaon fibers where it can be concluded that the fitter was unable to make a successful fit on that fiber. This occurs when the probabilities for both the single and double-pulse fits are equal to zero. As with CCDPUL, the two gain channels (low-gain and high-gain) for each fiber are considered when determining that the fitter was unable to make a successful fit. As with CCDPUL, this cut is a three-stage process.

CCDBADFIT - The First Stage

Separately the results of the fits from the low-gain and high-gain target CCDs are considered. The high-gain channel data is not passed onto the second stage if any of the following conditions are met:

- The single fit probability is greater than 0.25 as the double-pulse fit is only performed if the single fit probability is less than or equal to 0.25.
- The number of bins in the second pulse with non-zero amplitude less than 3.

- The double fit probability is equal to 0 when the single fit probability is greater than 0.

The same conditions as above were applied to the low-gain channels.

CCDBADFIT - The Second Stage

During the second stage of CCDBADFIT, a similar decision making process is used as CCDPUL to determine which CCD data is used: the low-gain or the high-gain. The difference is that a weighted average of the low-gain and high-gain is never used, but the rest of the decision making sequence is the same.

CCDBADFIT - The Third Stage

All fibers passed onto stage 3 are checked for probabilities equal to zero for both the single and double-pulse fits. If this condition is met and the fiber energy as determined by the ADC is greater than 1.25 MeV, the event fails the CCDBADFIT cut.

7.2.3 CCDBADFIT and CCDPUL Coding Changes

As was discussed previously in this section, the CCDPUL cut was split into two cuts: CCDBADFIT which deals with unfitable pulses and CCDPUL which deals with rejecting events showing appropriate second pulse activity.

From a combination of optimization and observation of many pulse fits, the classification for unfitable pulses (CCDBADFIT) was changed from pulses having both single and double-fit probabilities lower than 0.01 to both these fits having probabilities equal to 0. Due to the ntuple granularity, target fitting probabilities equal to 0 in the ntuple correspond to probabilities less than 10^{-5} . Additionally, the condition that CCDBADFIT could only cut a fiber having more ADC energy than the CCDPUL energy threshold was added. It doesn't matter if the fitter couldn't find a solution if there isn't enough energy in the fiber that it could possibly fail CCDPUL.

Due to the method in which fibers are passed from the second to third stages of CCDPUL or CCDBADFIT, it is possible for up to 62 fibers to be passed onto the third stage of CCDPUL or CCDBADFIT. The target fitter treats the low-gain and high-gain CCD data separately and makes no correspondance between the low-gain and high-gain data of a given channel. There is a maximum of 31 low-gain and 31 high-gain channels which can be fit, but it is entirely possible that due to some fibers missing data in either the high-gain or low-gain channels, there could be more than 31 different fibers which have been fit. This possibility was not accounted for in CCDPUL (or CCDBADFIT) and we saw a few events where the number of fibers being passed from the second to third stages of CCDPUL and CCDBADFIT exceeded 31 and caused an "array out of bounds" error. This was corrected by changing the maximum number of fibers which could be passed on from stage two to stage three of these cuts from 31 to 62.

The condition that only target fibers identified as kaon fibers was added.

7.2.4 CCDBADFIT and CCDPUL Optimization

For the E787 pnn2 analyses [11], the energy threshold above which second pulses would cause an event to be rejected by CCDPUL was set to 1.5 MeV for the 1997 data set and 1.0 MeV for the 1996 data set. The second pulse needed to be within ± 10 ns of pion time.

From the optimization, the second-pulse threshold energy was set to 1.25 MeV. The timing window was made asymmetric and the the quantity $deltat$ had to fall between -7.5 and 10 ns inclusive for a second pulse above the energy threshold to fail the cut. The quantity $deltat$ is a measure of consistency between the global pion (t_{pi}) and kaon (tk) times and the first (t_1) and second (t_2) pulse times from the fit for that kaon fiber given by $deltat = (t_2 - t_1) - (t_{pi} - tk)$.

7.3 TGdEdX

We observed a 9% acceptance loss in TGDEDX compared to what Bipul measured in E787-PNN2. I describe how the cut works, changes made to the cut, and the how I re-calibrated this cut with current data.

7.3.1 Description

The dEdx of pions in the PNN2 box 140 MeV/c to 199.5 MeV/c changes from 3.08 MeV/cm to 2.47 MeV/cm in scintillator Therefore the target dEdx cut has to be performed as a function of momentum for PNN2. The TGDEDX cut calculates the target dEdX "likelihood" using the total measured momentum ($ptot$) target range (rtg), and target energy (etg). PISCAT monitors are used to determine the expected rtg based upon the observed $ptot$, etg . The data was chosen to be in the pion band. The total momentum was quantified in 5 momentum bins ($< 170 MeV/c$, $170 - 180$, $180 - 188$, $188 - 199.53$, > 199.53 and 14 target energy bins (0-2MeV, 2-4MeV,..., 26-28MeV); The value of a 15th bin is equal to the 14th bin. For each bin we store the fitted mean and sigma of the measured target range. A Gaussian distribution is assumed during the calibration. Signal events are cut by TGDEDX if $like_{tgdedx} < 0.05$.

$$like_{tgdedx} = \frac{1}{2} \cdot \left(1 + erf \left(\frac{rtg - rtg_{exp}(etg, ptot)}{\sigma_{exp}(etg, ptot)} \right) \right) \quad (1)$$

TGDEDX cuts events when the target range is smaller than expected for a given etg , $ptot$.

7.3.2 TGdEdX Coding Changes

In E787-PNN2, *swathccd* does not allow pion hits that occur in kaon flagged fiber; E949 allows this possibility. These K/Pi fibers only exist when $t_{pi} - tk > 15ns$ and so we will not observe these type of hits in Piscat monitors which is used in the calibration. Therefore, we must not include pions hits occurring in a kaon fiber when cutting an event because it is not considered in the calibration sample. TGDEDX modifies a local etg variable to exclude these hits. All results reported in this note uses this modified version of TGDEDX.

7.3.3 TGdEdX Calibration

The calibration uses Piscat Monitors. The cuts used to determine the final sample are shown in Tables 8. The last cut, $Kpiang > 35^\circ$, was not used in the final determination of the sample due to lack of statistics.

The kumacs used to produce the calibration values and plots seen in this note are stored at `~benjil/bkg/studies/tgdedx/calib/`. The calibration histograms were created from histograms embedded in the piscat acceptance study, see `~/bkg/src/piscatacc.f` and `~/bkg/src/special_plots.f`. The acceptance measurement on TGDEDX was done using Kpi2 monitors, see `~/bkg/src/kp2acc.f`.

Figure 19, created by `~benjil/bkg/studies/tgdedx/calib/error_function.kumac`, shows the shape of the distribution for different offsets in the mean and sigma of the gaussian fit. If we plot Lik_{TGdEdX} for piscats using the updated calibration parameters then we would see a flat distribution. When we measure Lik_{TGdEdX} on Kpi2's, Figure 18, we observe a symmetric distribution with a slight offset to larger values. This implies that our calibration sample has worse resolution than our acceptance sample. This is most likely due to a better determination of the decay vertex in Kpi2's.; Measurement of the decay vertex is the key determination of the target range (rtg).

To determine if the calibration removes the energy (etg) dependence, I plotted the ratio of the E949 calibration means to the E787 calibration means. Figure 17, indicates that we are calibrating out any energy (etg) dependence.

A Piscat sample with a better determination of the decay vertex was obtained by making a cut a $kpiang$, the angle made from the Kaon entering position, decay vertex, and the exiting value of the Pion. An angle of 55° was required in this sample. An additional sample was created by applying the 30% acceptance PV cut, instead of the 60%. The calibration parameters, for TGDEDX, were determined and we measured the effect on the Kpi2 monitor sample. Figure 20 shows that there is no difference between the E949 calibration and the tighter PV sample. A small difference is observed between the E949 and the calibration with $kpiang > 55^\circ$ required. Figure 21 show that there is no noticeable dependence on etg for the different calibration sets (most relevant points in Figure 21 are *ptot bin 5*).

Cut name	Events remaining (Acc)
<i>BADRUN</i>	5859925 (-)
<i>DUPEV</i>	5859925 (-)
<i>RD_TRK</i>	5859442 (-)
<i>TRKTIM</i>	5856748 (-)
<i>TARGET</i>	5856748 (-)
<i>STLAY</i>	4949979 (-)
<i>UTC</i>	4593392 (-)
<i>RDUTM</i>	4497125 (-)
<i>PDC</i>	2833580 (-)
<i>ICbit</i>	2833580 (-)
<i>b4abm2</i>	1986916 (-)
$ t_{pi} - trs \geq 5$	1881543 (-)
$ i_{ctime} - trs \geq 5$	1847951 (-)
<i>BAD_sTC</i>	1845076 (-)
<i>TGCUT</i>	1508139 (0.817386)
<i>tgqualt</i>	1435572 (0.951883)
<i>npitg</i>	1435572 (1)
<i>timcon</i>	1430524 (0.996484)
<i>tgtcon</i>	1390018 (0.971685)
<i>b4etcon</i>	1360826 (0.978999)
<i>targf</i>	1278186 (0.939272)
<i>dtgttp</i>	1278117 (0.999946)
<i>rtdif</i>	1181683 (0.92455)
<i>eiccon</i>	1149627 (0.972873)
<i>ticcon</i>	1149616 (0.99999)
<i>pigap</i>	1034138 (0.899551)
<i>tgdb4</i>	886404 (0.857143)
<i>tgdb4tip</i>	561715 (0.633701)
<i>tgdvxtip</i>	466019 (0.829636)
<i>tgdvxpi</i>	427166 (0.916628)
TGB4	427166 (1)
<i>phivtx1</i>	315481 (0.738544)
<i>pv(not tg) Loose60</i>	87063 (0.275969)
<i>cos3d</i>	76823 (0.882384)
<i>utcqual Loose</i>	72564 (0.944561)
<i>rngmom</i>	65767 (0.906331)
<i>rsdedxmax</i>	46384 (0.705278)
<i>rsdedxcl</i>	41896 (0.903242)
<i>rslike</i>	41429 (0.988853)
RSDEDX	41429 (1)
<i>tgz > -10.</i>	41244 (0.995535)
<i>Kpiang > 35°</i>	23662 (0.573708)
<i>continued on next page</i>	

Cut name	Events remaining (Acc)
<i>Kpiang</i> > 55°	14323 (0.605317)

Table 8: Cuts Used in TGDEDX calibration. E949 calibration used the events in red.

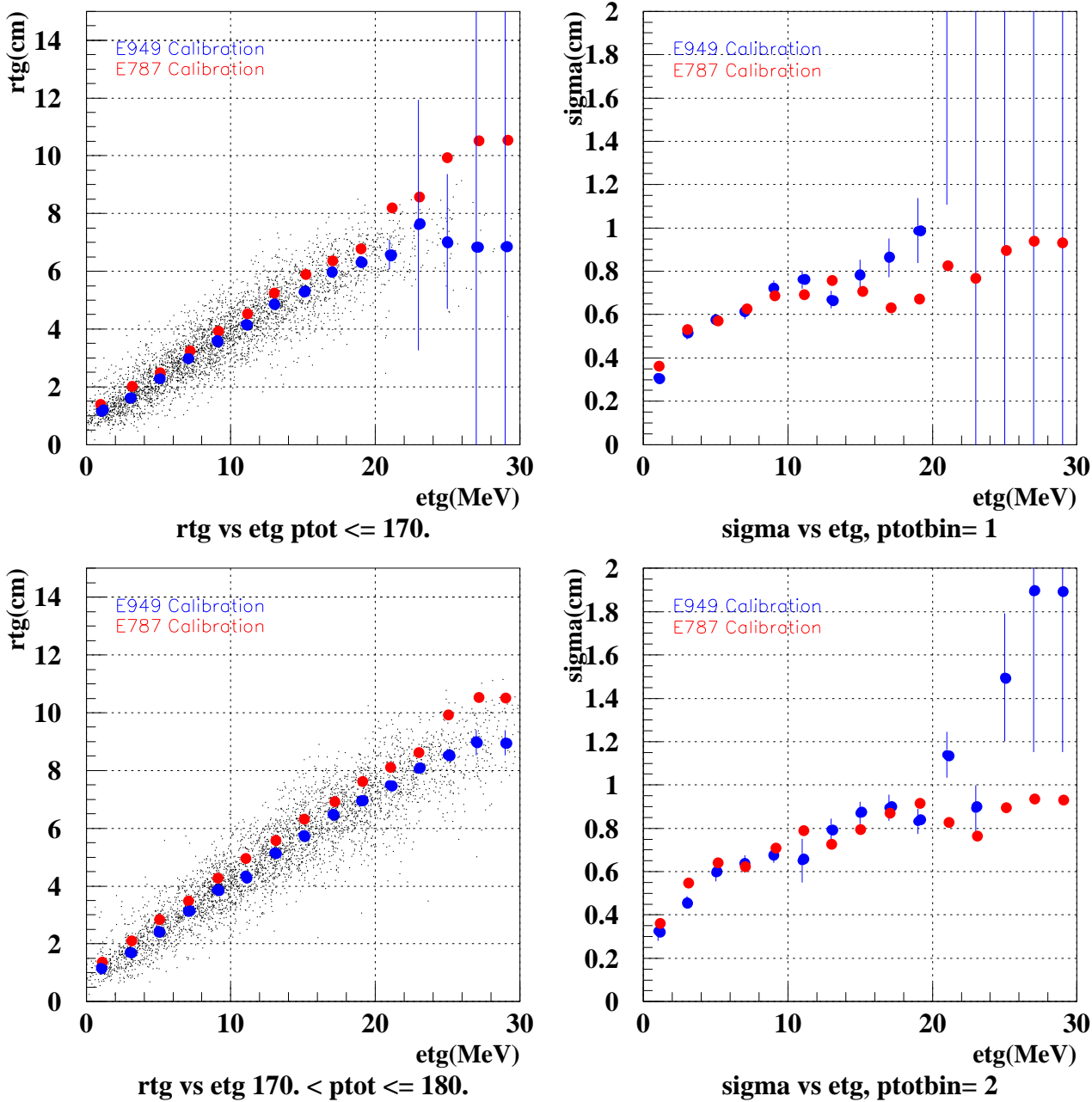


Figure 14: Calibration of new means. Red points are the original means. Blue points are the new means with error bars being the uncertainty on the mean from a gaussian fit

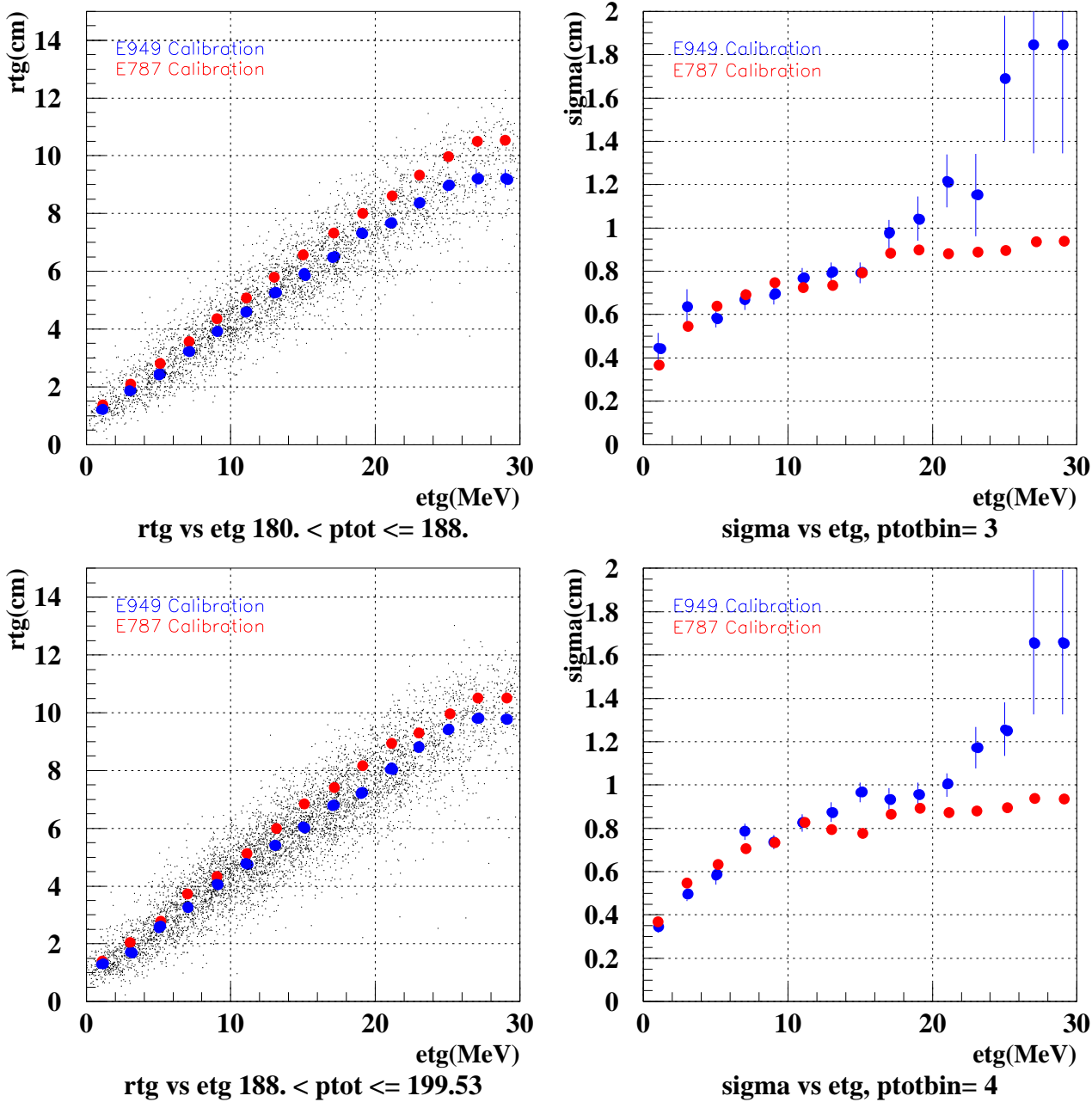


Figure 15: Calibration of new means. Red points are the original means. Blue points are the new means with error bars being the uncertainty on the mean from a gaussian fit

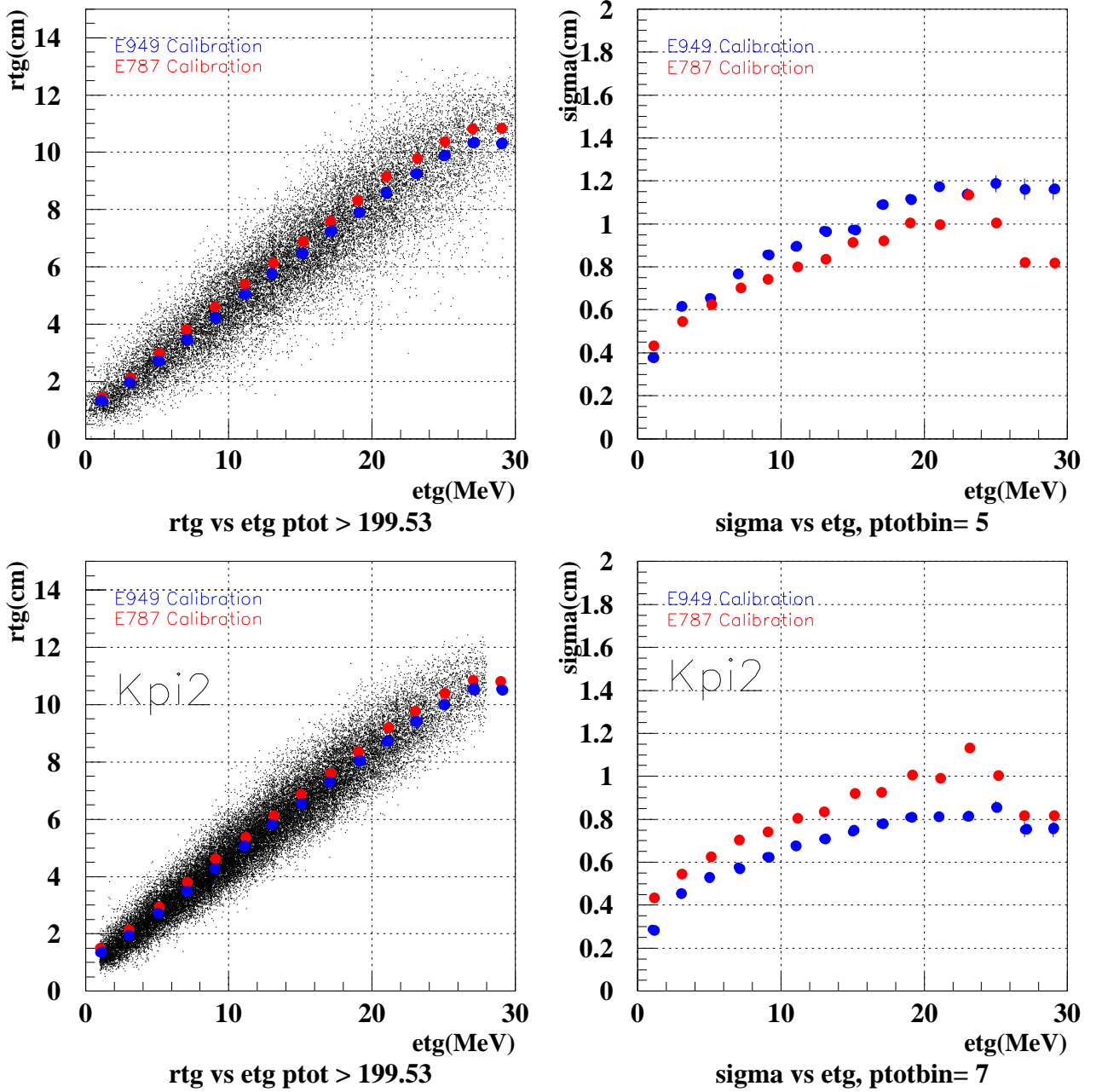


Figure 16: Calibration of new means. The bottom plot is doing the calibration process on Kpi2 monitors. Red points are the original means. Blue points are the new means with error bars being the uncertainty on the mean from a gaussian fit

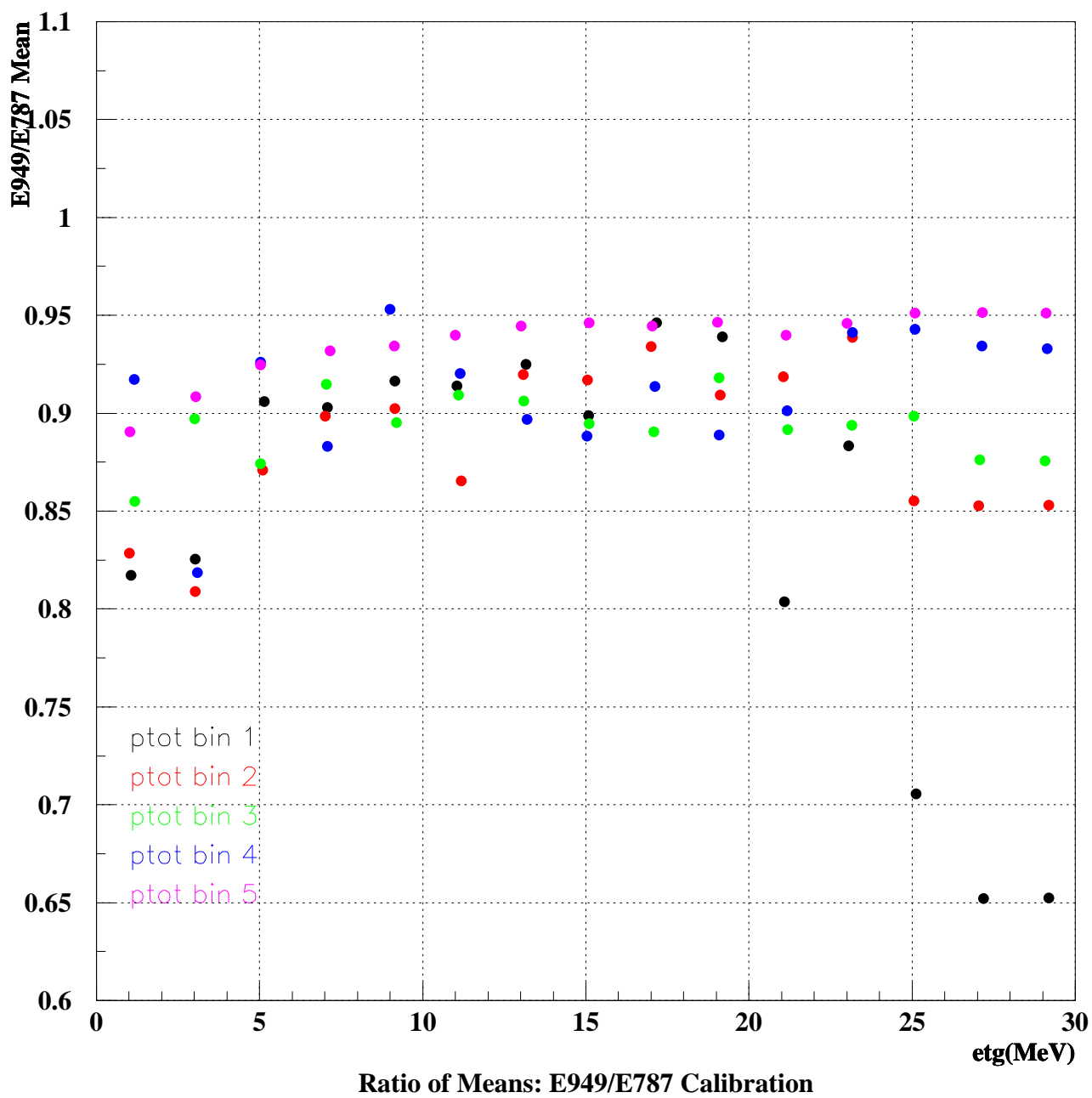


Figure 17: Ratios of the E949/E787 Calibrations.

7.3.4 Original Parameters

The means and sigmas are listed below in the 5 $ptot$ bins, mean N such that $N = 1 : ptot < 170MeV/c$, $N = 2 : 170 < ptot \leq 180$, $N = 3 : 180 < ptot \leq 188$, $N = 4 : 188 < ptot \leq 199.53$, $N = 5 : ptot > 199.53$; Same notation for sigmas. The 15 numbers in each row are for $etg = 1MeV, 3MeV, \dots, 29MeV$.

```

data mean1/1.41,1.99,2.51,3.28,3.92,4.56,5.23,5.88,6.30,6.77,8.2,8.6,9.95,10.5,10.5/
data sigm1/0.36,0.53,0.57,0.62,0.69,0.70,0.76,0.71,0.64,0.67,0.83,0.77,0.90,0.93,0.93/
data mean2/1.41,2.09,2.82,3.50,4.29,5.02,5.62,6.31,6.96,7.60,8.17,8.58,9.95,10.5,10.5/
data sigm2/0.36,0.54,0.64,0.62,0.71,0.79,0.72,0.79,0.88,0.91,0.83,0.77,0.90,0.93,0.93/
data mean3/1.41,2.09,2.82,3.53,4.36,5.05,5.83,6.60,7.29,7.99,8.61,9.33,9.95,10.5,10.5/
data sigm3/0.36,0.54,0.64,0.70,0.74,0.72,0.73,0.79,0.89,0.90,0.87,0.89,0.90,0.93,0.93/
data mean4/1.41,2.09,2.82,3.72,4.28,5.17,6.06,6.83,7.39,8.17,8.93,9.33,9.95,10.5,10.5/
data sigm4/0.36,0.54,0.64,0.71,0.73,0.83,0.79,0.78,0.86,0.90,0.87,0.89,0.90,0.93,0.93/
data mean5/1.48,2.15,2.97,3.75,4.58,5.37,6.10,6.84,7.64,8.36,9.16,9.77,10.38,10.83,10.83/
data sigm5/0.44,0.54,0.62,0.71,0.74,0.80,0.84,0.91,0.92,1.0,0.99,1.14,1.0,0.81,0.81/

```

7.3.5 New Parameters

```

data mean1/1.15,1.64,2.27,2.96,3.59,4.16,4.83,5.29,5.95,6.35,6.58,7.,7.5,8.0,8.0/
data sigm1/0.31,0.52,0.57,0.61,0.72,0.76,0.67,0.79,0.86,0.99,1.04,1.28,1.28,1.28,1.28/
data mean2/1.17,1.69,2.45,3.15,3.86,4.35,5.17,5.77,6.49,6.91,7.50,8.05,8.53,8.96,8.96/
data sigm2/0.33,0.46,0.60,0.64,0.68,0.65,0.79,0.87,0.90,0.83,1.14,0.89,1.50,1.89,1.89/
data mean3/1.20,1.87,2.46,3.23,3.91,4.59,5.29,5.91,6.50,7.34,7.67,8.35,8.95,9.21,9.21/
data sigm3/0.45,0.64,0.59,0.67,0.69,0.77,0.79,0.79,0.97,1.04,1.22,1.15,1.69,1.85,1.85/
data mean4/1.29,1.71,2.61,3.29,4.08,4.77,5.43,6.07,6.76,7.27,8.04,8.78,9.40,9.80,9.80/
data sigm4/0.35,0.49,0.58,0.78,0.74,0.82,0.87,0.97,0.94,0.96,1.00,1.17,1.26,1.66,1.66/
data mean5/1.32,1.96,2.74,3.50,4.27,5.04,5.76,6.47,7.21,7.91,8.59,9.25,9.88,10.30,10.30/
data sigm5/0.38,0.61,0.66,0.77,0.86,0.89,0.97,0.97,1.09,1.12,1.17,1.14,1.19,1.16,1.16/

```

7.3.6 Manual changes

The fit in the $ptot$ range of $< 170MeV/c$ and $etg > 20MeV$ was very poor due to lack of statistics. I modified the last 5 values. The means were determine by constraining the values below the values observed in mean2(11-15) and doing a linear extrapolation from the previous set of points. This was done by "eye". The last 4 sigmas were determine by doing a fit on rtg values with a slice of $20 < etg < 30$ and performing a gaussian fit. I determined the sigma for the $etg = 19MeV$ by extending the etg -slice to $17 < etg < 21$.

- From fits

```

data mean1/1.15,1.64,2.27,2.96,3.59,4.16,4.83,5.29,5.95,6.35,6.58,7.60,7.03,6.84,6.84/
data sigm1/0.31,0.52,0.57,0.61,0.72,0.76,0.67,0.79,0.86,0.99,2.02,3.64,3.84,12.70,12.70/

```

- By hand

```

data mean1/1.15,1.64,2.27,2.96,3.59,4.16,4.83,5.29,5.95,6.35,6.58,7.,7.5,8.0,8.0/

```

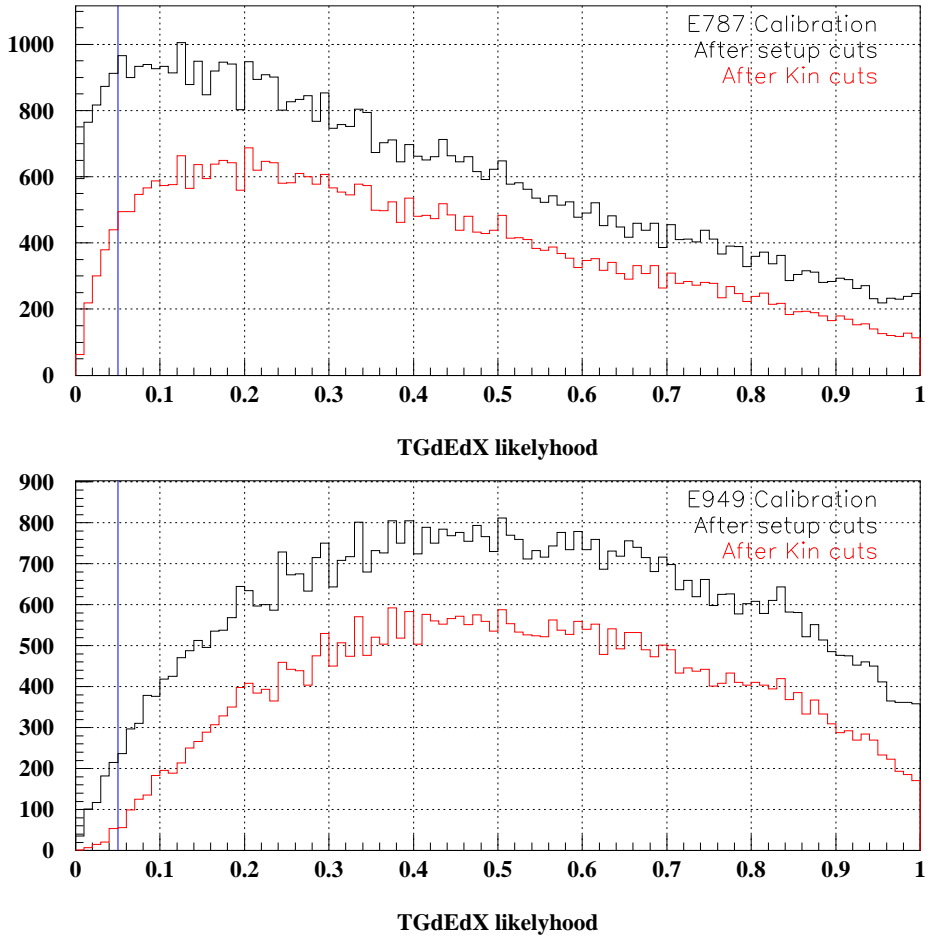


Figure 18: Before and after calibration of $like_{TGdEdX}$. The plots are done in the Kpi2-TG Kinematic acceptance study. The setup cuts are all cuts applied before TGDEDX cut is applied. The Kin cuts are all cuts in the acceptance study except for TGDEDX. TGDEDX cuts events less than 0.05, shown as the blue line.

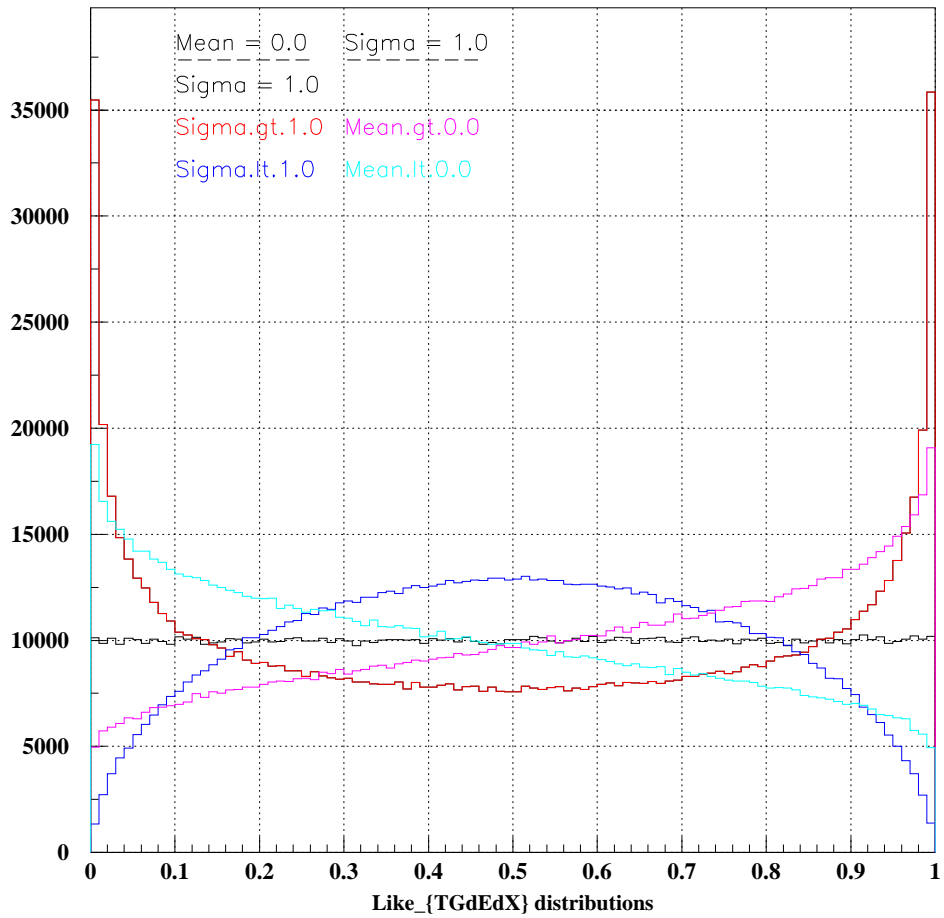
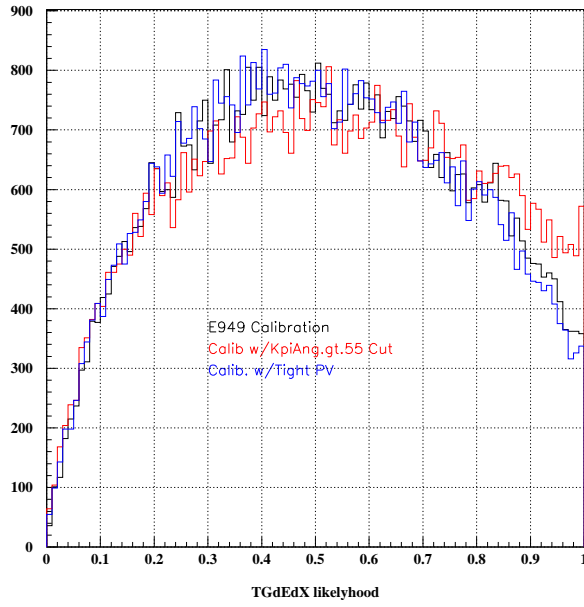
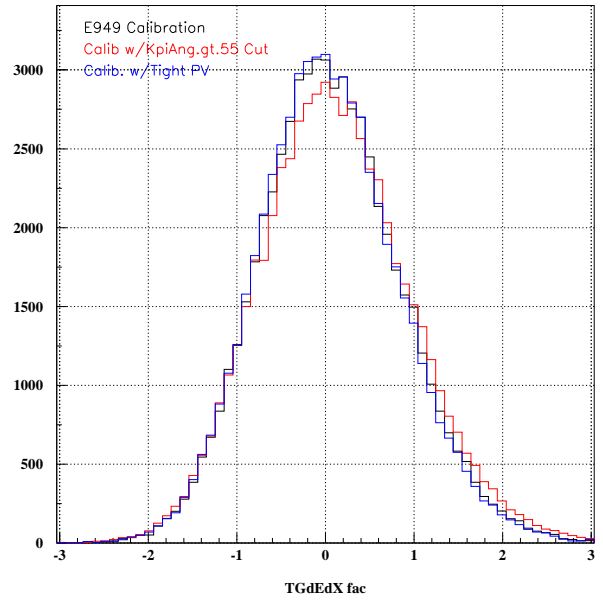


Figure 19: $like_{TGdEdX}$ distributions for different offsets in the calibration.



(a) $like_{TGdEdX}$



(b) $\frac{rtg - rtg_{exp}(etg, ptot)}{\sigma_{exp}(etg, ptot)}$

Figure 20: Distributions for different piscat calibrations.

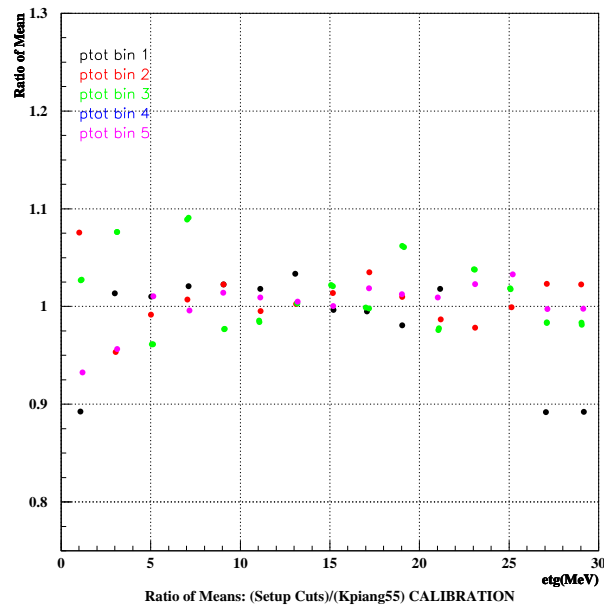


Figure 21: Ratio of calibration means used in Figure 20.

7.3.7 TGdEdX Acceptance Sample

E787-PNN2 measured an acceptance of 0.9858. Using the E787-PNN2 calibration, I measure an acceptance of 0.9339. With the new parameters the acceptance of TGDEDX increases to 0.989; An increase of 5.2%. The overall acceptance increase in the Kpi2 TG-Kinematic study is 2.0%. The correlation of *epitg* and *chi567* mitigates the increase observed in TGDEDX.

Cut Applied	Events remaining (Acc)
<i>SetupOPS</i>	62149 (-)
<i>opsveto</i>	60535 (-)
<i>TGPVCUT</i>	59882 (-)
TGDEDX	59231 (0.989129)
<i>tger</i>	59215 (0.99973)
<i>tgenr</i>	57283 (0.967373)
<i>tglike1</i>	56252 (0.982002)
<i>tglike2</i>	55351 (0.983983)
TGLIKE	55351 (1)
<i>epitg</i>	49614 (0.896352)
<i>epimaxk</i>	49614 (1)
<i>tgedge</i>	49348 (0.994639)
<i>drp</i>	49263 (0.998278)
<i>chi567 Loose</i>	42369 (0.860057)
<i>chi5max</i>	39447 (0.931034)
Total Acc.	0.658746 ± 0.00269197

Table 9: Kpi2 TG-kinematic Acceptance

7.3.8 TGdEdX Rejection Sample

E787 tuned the cut to a $Rej_{TGDEDX} = 1.44$, but TGDEDX had no rejection after all cuts. This is due to high correlation with *chi567*.

Cut Applied	Events remaining (Rej)
<i>BADRUN</i>	30408052 (0.00)
<i>DUPEV</i>	30408048 (1.00)
<i>TRIGGER</i>	15232707 (2.00)
<i>ICbit</i>	15232564 (1.00)
<i>lhex</i>	15232564 (1.00)
<i>DC</i>	15232516 (1.00)
<i>Lev11</i>	15232516 (1.00)
<i>RD_TRK</i>	15232515 (1.00)
<i>TRKTIM</i>	15232515 (1.00)
<i>TARGET</i>	15232515 (1.00)
<i>STLAY</i>	15232515 (1.00)
<i>UTC</i>	15232515 (1.00)
<i>RDUTM</i>	15232515 (1.00)
<i>BAD_STC</i>	15232515 (1.00)
<i>PDC</i>	15232515 (1.00)
<i>pv(not tg) Loose60</i>	12954315 (1.18)
<i>TGCUT</i>	7142934 (1.81)
<i>tgqualt</i>	6765533 (1.06)
<i>npitg</i>	6765533 (1.00)
<i>timcon</i>	6685429 (1.01)
<i>tgtcon</i>	6316877 (1.06)
<i>b4etcon</i>	6184009 (1.02)
<i>DCBIT</i>	6184009 (1.00)

continued on next page

Cut Applied	Events remaining (Rej)
<i>DELCO</i>	4280023 (1.44)
<i>Delc Loose</i>	3595811 (1.19)
<i>PSCUT</i>	2185154 (1.65)
<i>b4dedx</i>	2169877 (1.01)
<i>bwtrs</i>	1799849 (1.21)
<i>cpitrs</i>	1797020 (1.00)
<i>cpitail</i>	1796540 (1.00)
<i>cktrs</i>	1781679 (1.01)
<i>cktail</i>	1762093 (1.01)
<i>b4trs</i>	1674587 (1.05)
<i>b4ccd</i>	1650344 (1.01)
<i>upvtrs</i>	1623531 (1.02)
<i>rvtrs</i>	1615563 (1.00)
<i>tqgeo</i>	1060126 (1.52)
<i>b4ekz</i>	886102 (1.20)
<i>tgzfool</i>	870567 (1.02)
<i>targf</i>	826789 (1.05)
<i>dtgttp</i>	826779 (1.00)
<i>rtdif</i>	819240 (1.01)
<i>tgktim</i>	811136 (1.01)
<i>iccon</i>	792084 (1.02)
<i>ticcon</i>	792075 (1.00)
<i>pigap</i>	774063 (1.02)
<i>tgdb4</i>	760772 (1.02)
<i>tgdb4tip</i>	752741 (1.01)
<i>tgdvxtip</i>	746892 (1.01)
<i>tgdvxpi</i>	729199 (1.02)
TGB4	729199 (1.00)
<i>phivtx1</i>	672405 (1.08)
<i>ccdpul</i>	166933 (4.03)
<i>timkf</i>	149649 (1.12)
<i>verrng</i>	135863 (1.10)
<i>anglt</i>	135717 (1.00)
<i>ALLKfit</i>	133136 (1.02)
<i>tpics</i>	133047 (1.00)
<i>kic</i>	133004 (1.00)
<i>epionk</i>	132901 (1.00)
<i>BOX Loose</i>	12503 (10.63)
<i>icodel14</i>	12503 (1.00)
<i>cos3d</i>	12181 (1.03)
<i>layv4</i>	12181 (1.00)
<i>zfrf</i>	12158 (1.00)
<i>zutout</i>	12134 (1.00)
FIDUCIAL	12134 (1.00)
<i>utccual Loose</i>	11226 (1.08)
<i>prrf1</i>	10855 (1.03)
<i>prrfz</i>	9906 (1.10)
PRRF	9906 (1.00)
<i>rsdedxmax</i>	9406 (1.05)
<i>rsdedxcl</i>	6725 (1.40)
<i>rslike</i>	6725 (1.00)
RSDEDX	6725 (1.00)
<i>rngmom</i>	1016 (6.62)
<i>tgdb4</i>	1016 (1.00)
<i>tgdb4tip</i>	1016 (1.00)
<i>tgdvxtip</i>	1016 (1.00)
<i>tgdvxpi</i>	1016 (1.00)
TGB4	1016 (1.00)
<i>piflg</i>	990 (1.03)
<i>elveto</i>	924 (1.07)
<i>tdfool</i>	920 (1.00)
<i>tdvarnn02 Loose</i>	849 (1.08)
TD Loose	849 (1.00)
TGDEDX	629 (1.35)
<i>epitg</i>	551 (1.54)
<i>epimaxk</i>	551 (1.00)
<i>chi567 Loose</i>	415 (1.33)
<i>chi5max</i>	389 (1.07)
TGDEDX	365 (1.07)

Table 10: TGDEDX Rejection Table. The red TGDEDX is the measured value at this point in the table, but TGDEDX is not applied on the events for remain cuts in this table.

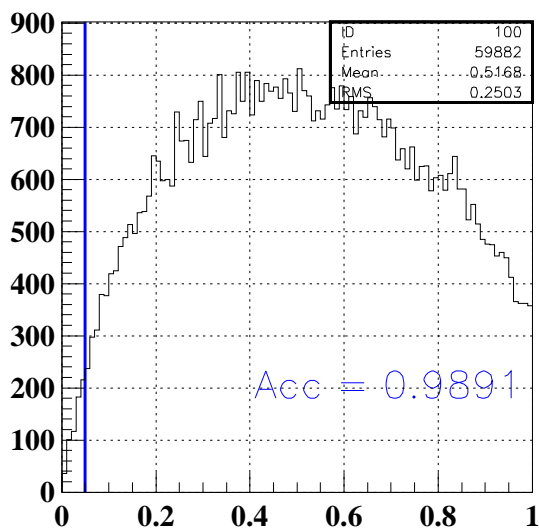
7.3.9 TGdEdX Results

I decided to use the cut parameters as outlined in the *New Parameter* section. These numbers were based upon the piscat sample with the largest statistics. The other samples ($k_{\text{piang}} > 55^\circ$, tight PV) did not show any improvement in making the sample more signal like. In addition, the statistics of these samples were lacking in the lower momentum bins. Also, the acceptance after calibration being the same as was measured in E787 is a convincing argument that I implemented the calibration study correctly and these parameters are acceptable.

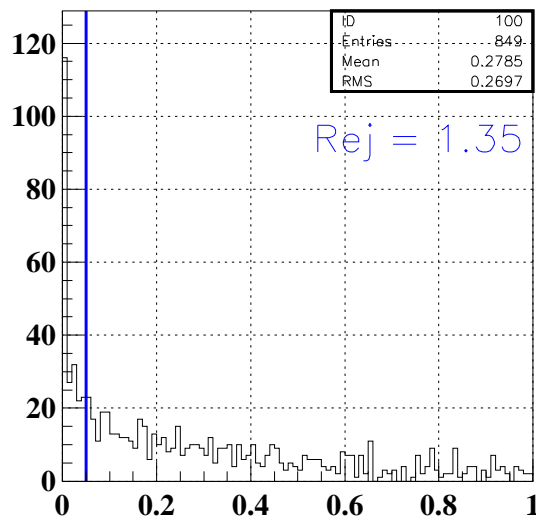
Determining TGDEDX's cut value (nominal value of 0.05) is shown in Figure 23. The *acceptance*, *rejection*, and *acceptance* \times *rejection* is plotted as a function of the cut value. The *acceptance* \times *rejection* indicates that we can improve our signal to background by tightening this cut. However, I recommend that we keep this current cut value of 0.05 to maximize our acceptance.

cut value	<i>Acc</i>	<i>Rej</i>	<i>Acc</i> \times <i>Rej</i>
E787 0.05	0.9858	1.44	1.42
E949 0.05	0.989	1.35	1.34

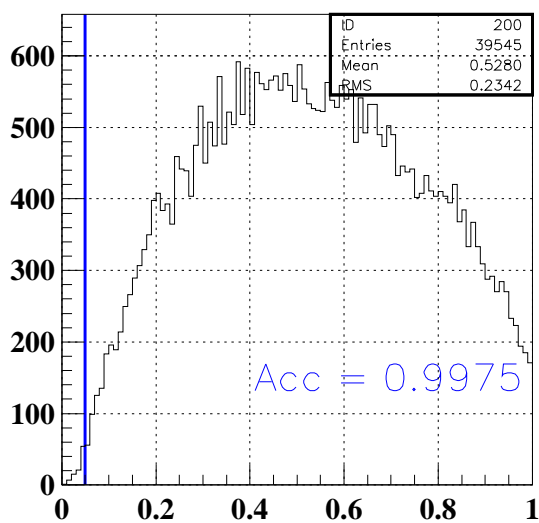
Table 11: TGDEDX Acceptance Rejection Table. The TGDEDX cut is $like_{TGdEdX} < cut\ value$.



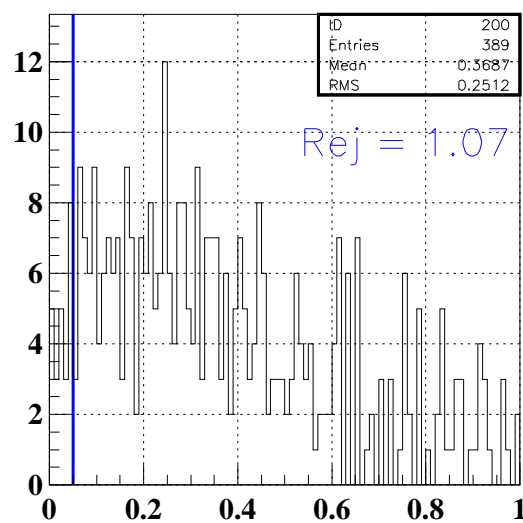
TGdEdX likelihood



TGdEdX likelihood



TGdEdX likelihood



TGdEdX likelihood

Figure 22: Bipul had a rejection of 1.44. No rejection after all cuts.

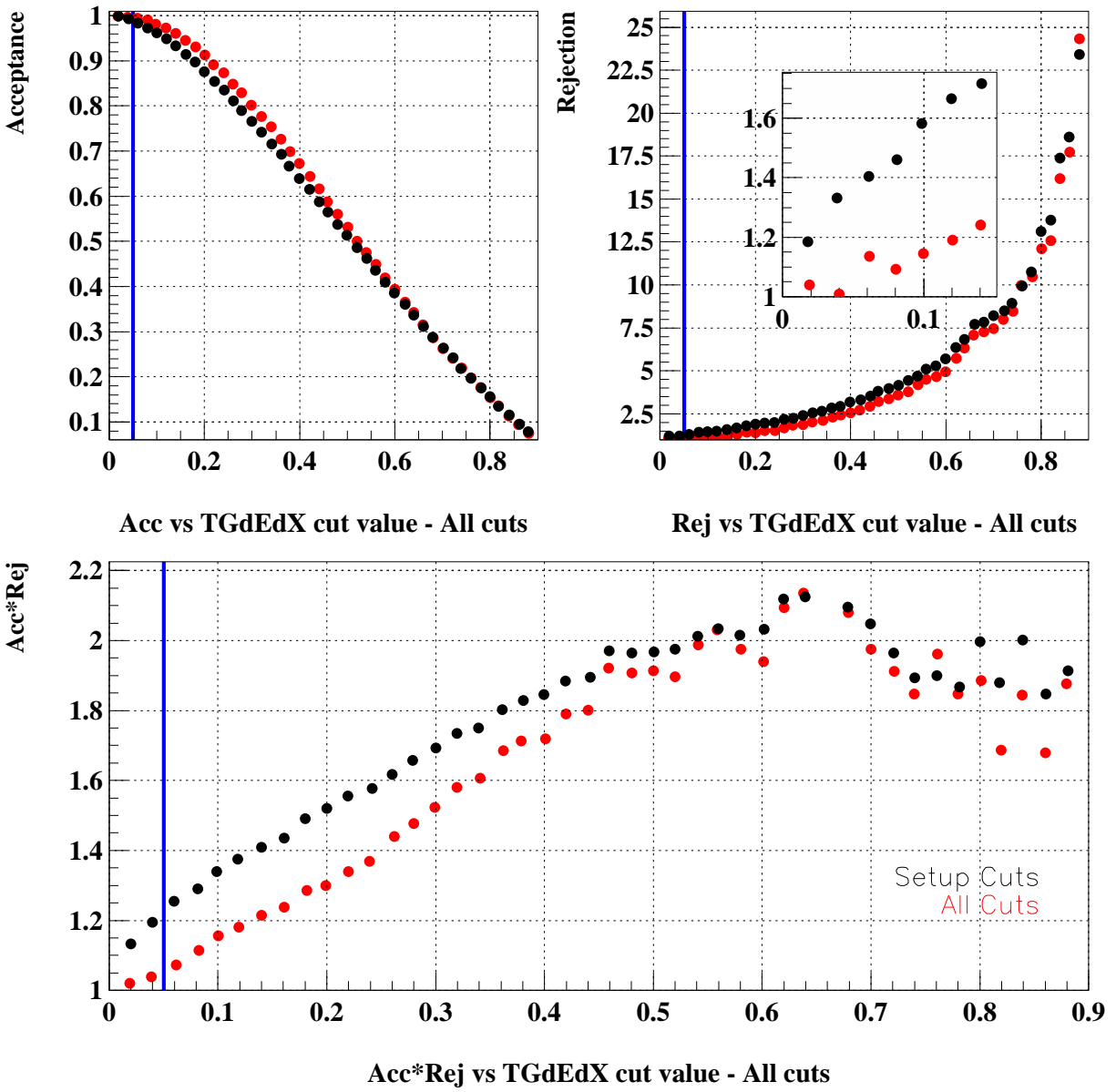


Figure 23: Acceptance and Rejection versus TGDEDX cut value. The TGDEDX cut is $like_{TGdEdX} < cut\ value$. The blue line is at the nominal cut value of 0.05. The red points are after all other cuts in the

7.4 CHI567

The track fitter of charged pion in the target gathers the energy deposit and position information of all possible pion fibers considers whether they agree with the UTC track curvature and momentum. A detailed description can be found in [11]. CHI567 is one of output this fitter. A cut on CHI567 may remove target scattering background. (CHI567 is the sum of the 5th, 6th and 7th terms in the χ^2 of the fitter.) CHI5 tells whether the energy deposit in each fiber agrees with that expected from dE/dx for the energy resolution of the target fiber. CHI6 and CHI7 are penalty terms in the fitter corresponding to the case of a fiber without energy but the track is projected to traverse the fiber and the case of a fiber with energy, but the track is not projected to traverse it, respectively.

Just like the rest of us, target fibers have to face an aging problem. This is thought to induce a dramatic lowering of the acceptance of the CHI567 cut. From an independent calibration for target fibers done by Benji and from a direct tuning of the probability of CHI567, a degradation of more than 20% in energy resolution is found with respect to E787. A correction factor, 1.621, is introduced to redefine the CHI5 contribution to CHI567,

$$CHI567 = CHI5/1.621 + CHI6 + CHI7 .$$

After this redefinition and optimization, the cut on the probability of CHI567 is set at 0.015.

A bug in this target fitter was also rectified for the E949 pnn2 analysis. MINUIT is used in this fitter. The last action it takes is to vary the fitted parameters and find out the errors on these parameters. The best estimation of these parameters are kept by MINUIT. However, if some quantities are extracted from these parameters, one must remember to use the final fitted result, and not those still in fitting process. In principle it is supposed to affect every event and also affect all CHI567 related cuts, such as CHI5MAX, ANGLI, etc. But only for some events this correction will show significant changes. Correction of this bug did not have a significant effect on either the global acceptance and rejection.

7.5 B4EKZ

B4EKZ is a likelihood based on the consistency of the the B4 energy, EK and TGZ. As this cut was found to have some rejection as $K_{\pi 2}$ scatters in the target, we use the tighter cut of $B4EKZ > 10$ as recommended by previous pnn2 analysis [1] instead of the the pnn1 level of $B4EKZ > 2$.

7.6 TGZFOOL

The TGZFOOL cut requires the reconstructed z of the kaon decay (TGZ) to be in the fiducial volume of the target, $TGZ > -5$ cm. This cut eliminates $K_{\pi 2}$ scatters in the target as well as beam pions that scatter in B4 [1]. In E949 pnn1, this requirement had been loosened to > -15 cm.

7.7 EPIONK

The target reconstruction by SWATHCCD is capable of finding a second pulse from a pion in kaon fiber for large decay times and/or a small kaon energy deposit in the fiber. The EPIONK cut is a requirement that the energy of the second pulse be less than a certain value (1.5 MeV for E787 pnn2 [11]). Modifications to the CCDPUL fitter for E949 moved some events that had been subjected to the CCDPUL cut to be subjected to the EPIONK cut instead. To ensure consistency, the EPIONK cut was set to the same value as the CCDPUL cut of 1.25 MeV.

7.8 Discarded Cuts

We briefly explain why target cuts used the E787 pnn2 or E949 pnn1 analysis were discarded for this analysis.

7.8.1 B4TIM

The B4TIM cut rejects events when the B4 strobe time differs from the kaon time in the target by more than 2 ns [11]. This cut was required to enable the CCDPUL fit algorithm to be reliable for the E787 pnn2 analyses. With the modifications described in this note, the B4TIM cut was no longer needed for CCDPUL reliability. Since B4TIM has a $\sim 3\%$ acceptance loss and does not suppress background, it was discarded for E949. Extensive studies showed that background rejection on the “late kaons” admitted by removing this cut was consistent with the overall background rejection.

7.8.2 PBG

Since the lead glass detector in the beam was replaced by the active degrader, we discarded PBG, the cut based on the lead glass detector.

8 Skim Definitions

List of setup cuts, PASS1, which were applied before processing of the event continued.

- PRESCALE (1/3 or 2/3), DUPEV, PASS1, TRBIT 1.0 2.0 ,LEV11 ,LEV12 ,RD_TRK ,STLAY ,BAD_STC ,RSHEX ,TRKTIM ,FITPI/OFF ,UTC ,RDUTM ,PDC ,LAY14 ,UTC1 ,RANGE1 ,RSHEX2.

Table 12 lists the cuts which compose the eight skims employed by the analysis. Skims 5-7 (1/3 sample) were used for optimization of cuts and initial background evaluation. Skims 1-3 (2/3 sample) will be used for background evaluation. Skim 4 and 8 (3/3 kink sample) were used in PV optimization.

skim	Data Sample	Cuts
1 (5)	1/3 (2/3) $K_{\pi 2}$	TGCUT, PSCUT, TDCUT, TGPVCUT
2 (6)	1/3 (2/3) $K_{\mu 2}$	TGCUT, PSCUT, PVCUT, TGPVCUT, DELCO
3 (7)	1/3 (2/3) $\pi_{scatter}$	TGCUT, TDCUT, PVCUT
4 (8)	1/3 (2/3) kinks	GOODKINK

Table 12: Definition of skims. Each skim is an enhanced background sample, as denoted in the *Data Sample* column. The union of skim 1-3 (5-7) comprise the 1/3 (2/3) signal sample. “kinks” are TG-scatters in the x - y plane.

9 $K_{\pi 2}$ -Scatter background

9.1 $K^+ \rightarrow \pi^+ \pi^0$ Target Scatters

The $K_{\pi 2}$ decay, where the π^+ scatters in the target, is the dominant background for the $\pi\nu\bar{\nu}(2)$ analysis. As it has been shown with Monte Carlo simulations, the photon distribution from the π^0 decay is more uniform in polar angle for events where the π^+ has scattered in the target, than for unscattered ones. Therefore, the PV rejection for TG scatter events is expected to be different than that for $K_{\pi 2}$ events in the peak. The π^+ kinematics cannot be used in the bifurcation study, since the PV rejection has to be measured inside the $\pi\nu\bar{\nu}(2)$ kinematic box.

9.1.1 Rejection Branch

The other set of cuts used to suppress this background are the target quality cuts (TG-CUT06). These eliminate events with evidence of a scattered pion in the target, either the scatter occurred outside the Kaon fibers (scatters visible in xy , or “ xy -scatters”) or inside them (events where the π^+ started in the beam direction and then scattered into the detector acceptance, or “ z -scatters”). The two categories are not mutually exclusive. By inverting some of these cuts and applying others, samples with varying mixtures of xy - and z -scatters can be created for the rejection branch. These samples will be contaminated

CLASS	TGCUTS
1	All cuts, KP2BOX
2	$\overline{CCDPUL}, \overline{EPIONK}$
3	$\overline{CCDPUL}, \overline{EPIONK}$, all others
4	CCDPUL, EPIONK, TGZFOOL, EIC, OPSVETO, \overline{OTHERS}
5	$\overline{CCDPUL}, \overline{EPIONK}, \overline{CHI567}, \overline{VERRNG}$
6	$\overline{CCDPUL}, \overline{EPIONK}, \overline{CHI567}, \overline{VERRNG}$, all others
7	$\overline{CHI567}, \overline{VERRNG}$
8	$\overline{CHI567}, \overline{VERRNG}$, all others
9	$\overline{CCDPUL}, \overline{EPIONK}, \overline{CHI567}, \overline{VERRNG}$, KIC, PIGAP, TARGF, TPICS
10	$\overline{B4EKZ}$
11	$\overline{B4EKZ}$, all others
12	$\overline{CCDPUL}, \overline{EPIONK}, \overline{B4EKZ}$
13	$\overline{CCDPUL}, \overline{EPIONK}, \overline{B4EKZ}$, all others

Table 13: Definition of the classes of events (2-13) used to measure the PV rejection in the $\pi\nu\bar{\nu}(2)$ kinematic box. Class 1 events have passed all the TG quality cuts, therefore they are required to be in the $K_{\pi 2}$ kinematic box as to not look in the signal region. All Classes that have either CCDPUL applied or CCDPUL inverted have the three associated safety cuts (CCDBADFIT, CCDBADTIM and CCD31FIB) applied.

to an extent with K_{e4} , $K_{\pi 2\gamma}$ and Charge Exchange background, but the contamination is shown to be small. Thirteen such “classes” were used, described in Table 13, and the PV rejection was measured on them in the $\pi\nu\bar{\nu}(2)$ kinematic box (Table 14) . The rejection in the $K_{\pi 2}$ peak is also given for comparison. The PV rejections measured for different classes are consistent with each other within statistical uncertainties.

For the final PV rejection, class 12 was used, because it had adequate statistics and it is expected to be the richest in z-scatters, since the cuts that majorly attack them are inverted: CCDPUL and EPIONK cut events with large pulses in the kaon fibers at trs, and B4EKZ rejects events in which the z position of the decay vertex found by the UTC does not agree with the kaon energy deposit (and thus path length) in the target. Both these signatures are characteristic of a decay pion that started in the beam direction in the kaon fiber, and then scattered into the detector. The difference in PV rejection between different classes with adequate statistics was used as an estimate for the systematic uncertainty.

Due to the loss of statistics in the rejection branch for the tight box, the rejection of the tight (30%) photon veto is measured on a rejection branch that uses the loose versions of the kinematic box, the TD cuts and DELCO. In doing this it is assumed that the rejection of the (30%) photon on these classes is the same for the loose and tight cuts. Table 16 shows that the rejection does not change within statistical error when applying the tight versions of these cuts. Since these statistical errors are so large, this comparison of rejections using different tight cuts was repeated using the loose (60%) and super-loose (90%) photon vetos. Tables 17 verify that within statistical error the photon

Rejection Branch - Loose Box							
CLASS	PNN2BOX (PV60)				KP2BOX (PV60)		
	bef. PV	af. PV	rejection	bg (3/3)	bef. PV	af. PV	rejection
1	N/A	N/A	N/A	N/A	60670	35	1733.4±292.9
2	24672	9	2741.3±913.6	0.558±0.188	147607	121	1219.9±110.9
3	2692	3	897.3±517.8	1.707±0.989	59429	54	1100.5±149.7
4	4220	3	1406.7±811.9	1.088±0.631	61703	38	1623.8±263.3
5	30209	12	2517.4±726.6	0.608±0.178	183128	147	1245.8±102.7
6	4069	3	1356.3±782.8	1.129±0.654	86702	72	1204.2±141.9
7	24574	6	4095.7±1671.8	0.374±0.153	89458	57	1569.4±207.8
8	356	1	356.0±355.5	4.310±4.320	13635	11	1239.5±373.6
9	23976	10	2397.6±758.0	0.638±0.204	172316	141	1222.1±102.9
10	11037	4	2759.2±1379.4	0.555±0.278	29962	28	1070.1±202.1
11	48	1	48.0±47.5	32.553±32.931	3009	2	1504.5±1063.5
12	26613	10	2661.3±841.4	0.575±0.184	159607	129	1237.3±108.9
13	3215	3	1071.7±618.4	1.429±0.828	65626	58	1131.5±148.5

Table 14: The rejection branch for the $K_{\pi 2}$ TG scatter background in the loose box: PV rejection using the loose photon veto (PV60) for the $\pi\nu\bar{\nu}(2)$ and $K_{\pi 2}$ boxes, and respective background, for the 12 classes. The classes that are skipped do not have enough statistics for a meaningful measurement. The same setup cuts as in the normalization branch (Table 20) are applied.

veto rejection is the same for the loose and tight sets of cuts.

The purity of the rejection sample can be examined with respect to the setup cuts used. In class 12 of the rejection branch (see 14) there are 10 events surviving the loose (60%) PV. The fractions of total events remaining that are $K_{\pi 2}$ scatters for various combinations of loose and tight versions of the setup cuts are found in Table 19. This table shows that the sample purity does not change significantly for the various combinations of loose and tight setup cuts.

9.1.2 Normalization Branch

In the normalization branch (see Table 20), all the cuts in TGCUT06 were applied, and the PV was inverted. Some contamination from $K_{\pi 2}$ -RS scatters and $K_{\pi 2\gamma}$ is expected, but these backgrounds are small compared to $K_{\pi 2}$ -TG scatters. The ptot distribution of the events remaining in the normalization branch after the inversion of PVCUTPNN2, after the application of all the TGCUT06 except CCDPUL, and after the application of CCDPUL is shown in (another ilektra fig). In the same figure, the ptot distribution of the events in class 12 of the rejection branch is also shown before and after PVCUTPNN2. Both of those distributions look adequately $K_{\pi 2}$ -scatter-like.

Rejection Branch - Tight Box							
CLASS	PNN2BOX loose (PV30)				KP2BOX loose (PV30)		
	bef. PV	af. PV	rejection	bg (3/3)	bef. PV	af. PV	rejection
1	N/A	N/A	N/A	N/A	60670	35	1733.4±292.9
2	24672	3	8224.0±4747.8	0.093±0.054	147607	121	1219.9±110.9
3	2692	1	2692.0±2691.5	0.285±0.286	59429	54	1100.5±149.7
4	4220	1	4220.0±4219.5	0.182±0.182	61703	38	1623.8±263.3
5	30209	4	7552.2±3775.9	0.102±0.051	183128	147	1245.8±102.7
6	4069	1	4069.0±4068.5	0.189±0.189	86702	72	1204.2±141.9
7	24574	1	24574.0±24573.5	0.031±0.031	89458	57	1569.4±207.8
8	356	1	356.0±355.5	2.163±2.171	13635	11	1239.5±373.6
9	23976	3	7992.0±4613.9	0.096±0.056	172316	141	1222.1±102.9
10	11037	1	11037.0±11036.5	0.070±0.070	29962	28	1070.1±202.1
11	48	1	48.0±47.5	16.340±16.546	3009	2	1504.5±1063.5
12	26613	4	6653.2±3326.4	0.115±0.058	159607	129	1237.3±108.9
13	3215	1	3215.0±3214.5	0.239±0.239	65626	58	1131.5±148.5

Table 15: The rejection branch for the $K_{\pi 2}$ TG scatter background in the tight (ke4-phobic) box: PV rejection using the tight photon veto (PV30) for the $\pi\nu\bar{\nu}(2)$ and $K_{\pi 2}$ boxes, and respective background, for the 12 classes. The rejection of the tight photon veto was measured on the loose versions of DELCO, TDCUTS and the kinematic box as there were not enough statistics when using the tight versions of these cuts. The classes that are skipped do not have enough statistics for a meaningful measurement. The same setup cuts as in the normalization branch (Table 20) are applied.

PV30 Rejection					
CLASS	All Loose	Ke4 Box	DELCO6	TDTIGHT	All Tight
2	24672/3 = 8224±4747.8	18528/3 = 6176±3565.4	21272/1 = 21272±21271.5	18419/1 = 18419±18418.5	11921/0 = 11921±11920.5
3	2692/1 = 2692±2691.5	2065/1 = 2065±2064.5	2163/1 = 2163±2162.5	2033/0 = 2033±2032.5	1250/0 = 1250±1249.5
4	4220/0 = 4220±4219.5	3262/0 = 3262±3261.5	3734/0 = 3734±3733.5	3135/0 = 3135±3134.5	2123/0 = 2123±2122.5
5	30209/4 = 7552.25±3775.9	22778/4 = 5694.5±2847	26345/2 = 13172.5±9314	22520/2 = 11260±7961.7	14795/1 = 14795±14794.5
6	4069/1 = 4069±4068.5	3164/1 = 3164±3163.5	3296/1 = 3296±3295.5	3066/0 = 3066±3065.5	1926/0 = 1926±1925.5
7	24574/1 = 24574±24573.5	18632/1 = 18632±18631.5	21929/1 = 21929±21928.5	18317/1 = 18317±18316.5	12376/1 = 12376±12375.5
8	356/0 = 356±355.5	297/0 = 297±296.5	305/0 = 305±304.5	253/0 = 253±252.5	186/0 = 186±185.5
9	23976/3 = 7992±4613.9	18018/3 = 6006±3467.3	20549/1 = 20549±20548.5	17838/1 = 17838±17837.5	11486/0 = 11486±11485.5
10	11037/1 = 11037±11036.5	7981/1 = 7981±7980.5	9876/1 = 9876±9875.5	8211/1 = 8211±8210.5	5292/1 = 5292±5291.5
11	48/0 = 48±47.5	43/0 = 43±42.5	39/0 = 39±38.5	33/0 = 33±32.5	24/0 = 24±23.5
12	26613/4 = 6653.25±3326.4	19957/4 = 4989.25±2494.4	23061/2 = 11530.5±8152.9	19847/2 = 9923.5±7016.6	12881/1 = 12881±12880.5
13	3215/1 = 3215±3214.5	2430/1 = 2430±2429.5	2572/1 = 2572±2571.5	2410/0 = 2410±2409.5	1451/0 = 1451±1450.5

Table 16: Rejection of the tight (30%) photon veto for the various classes with different combinations of loose and tight versions of the setup cuts: kinematic box cut, TD cuts and DELCO. The 'All Loose' and 'All Tight' columns mean that those three sets of cuts were all loose or all tight. For the other three columns, all the cuts are loose except the one listed, which is tight. The numbers shown are the number of events before the photon veto is applied divided by the number of events remaining after the photon veto is applied and the resulting rejection with statistical error. If there are zero events remaining after the photon veto is applied, the rejection is determined assuming 1 event remained.

PV60 Rejection					
CLASS	All Loose	Ke4 Box	DELCO6	TDTIGHT	All Tight
2	24672/9 = 2741.33±913.6	18528/7 = 2646.86±1000.2	21272/3 = 7090.67±4093.5	18419/4 = 4604.75±2302.1	11921/1 = 11921±11920.5
3	2692/3 = 897.333±517.8	2065/3 = 688.333±397.1	2163/2 = 1081.5±764.4	2033/1 = 2033±2032.5	1250/1 = 1250±1249.5
4	4220/3 = 1406.67±811.9	3262/1 = 3262±3261.5	3734/3 = 1244.67±718.3	3135/3 = 1045±603	2123/1 = 2123±2122.5
5	30209/12 = 2517.42±726.6	22778/8 = 2847.25±1006.5	26345/6 = 4390.83±1792.3	22520/7 = 3217.14±1215.8	14795/2 = 7397.5±5230.5
6	4069/3 = 1356.33±782.8	3164/3 = 1054.67±608.6	3296/2 = 1648±1165	3066/1 = 3066±3065.5	1926/1 = 1926±1925.5
7	24574/6 = 4095.67±1671.8	18632/2 = 9316±6587.1	21929/4 = 5482.25±2740.9	18317/5 = 3663.4±1638.1	12376/2 = 6188±4375.2
8	356/0 = 356±355.5	297/0 = 297±296.5	305/0 = 305±304.5	253/0 = 253±252.5	186/0 = 186±185.5
9	23976/10 = 2397.6±758	18018/7 = 2574±972.7	20549/4 = 5137.25±2568.4	17838/5 = 3567.6±1595.3	11486/1 = 11486±11485.5
10	11037/4 = 2759.25±1379.4	7981/3 = 2660.33±1535.7	9876/2 = 4938±3491.3	8211/3 = 2737±1579.9	5292/2 = 2646±1870.7
11	48/0 = 48±47.5	43/0 = 43±42.5	39/0 = 39±38.5	33/0 = 33±32.5	24/0 = 24±23.5
12	26613/10 = 2661.3±841.4	19957/8 = 2494.63±881.8	23061/4 = 5765.25±2882.4	19847/5 = 3969.4±1774.9	12881/2 = 6440.5±4553.8
13	3215/3 = 1071.67±618.4	2430/3 = 810±467.4	2572/2 = 1286±909	2410/1 = 2410±2409.5	1451/1 = 1451±1450.5

Table 17: Rejection of the loose (60%) photon veto for the various classes with different combinations of loose and tight versions of the setup cuts: kinematic box cut, TD cuts and DELCO. The 'All Loose' and 'All Tight' columns mean that those three sets of cuts were all loose or all tight. For the other three columns, all the cuts are loose except the one listed, which is tight. The numbers shown are the number of events before the photon veto is applied divided by the number of events remaining after the photon veto is applied and the resulting rejection with statistical error. If there are zero events remaining after the photon veto is applied, the rejection is determined assuming 1 event remained.

PV90 Rejection					
CLASS	All Loose	Ke4 Box	DELCO6	TDTIGHT	All Tight
2	24672/141 = 174.979±14.7	18528/102 = 181.647±17.9	21272/106 = 200.679±19.4	18419/111 = 165.937±15.7	11921/63 = 189.222±23.8
3	2692/13 = 207.077±57.3	2065/13 = 158.846±43.9	2163/9 = 240.333±79.9	2033/9 = 225.889±75.1	1250/7 = 178.571±67.3
4	4220/31 = 136.129±24.4	3262/23 = 141.826±29.5	3734/27 = 138.296±26.5	3135/23 = 136.304±28.3	2123/13 = 163.308±45.2
5	30209/178 = 169.713±12.7	22778/129 = 176.574±15.5	26345/138 = 190.906±16.2	22520/139 = 162.014±13.7	14795/80 = 184.938±20.6
6	4069/14 = 290.643±77.5	3164/14 = 226±60.3	3296/10 = 329.6±104.1	3066/10 = 306.6±96.8	1926/8 = 240.75±84.9
7	24574/130 = 189.031±16.5	18632/97 = 192.082±19.5	21929/103 = 212.903±20.9	18317/102 = 179.578±17.7	12376/62 = 199.613±25.3
8	356/0 = 356±355.5	297/0 = 297±296.5	305/0 = 305±304.5	253/0 = 253±252.5	186/0 = 186±185.5
9	23976/139 = 172.489±14.6	18018/103 = 174.932±17.2	20549/105 = 195.705±19.1	17838/105 = 169.886±16.5	11486/60 = 191.433±24.6
10	11037/88 = 125.42±13.3	7981/59 = 135.271±17.5	9876/68 = 145.235±17.6	8211/71 = 115.648±13.7	5292/40 = 132.3±20.8
11	48/0 = 48±47.5	43/0 = 43±42.5	39/0 = 39±38.5	33/0 = 33±32.5	24/0 = 24±23.5
12	26613/156 = 170.596±13.6	19957/114 = 175.061±16.3	23061/119 = 193.79±17.7	19847/121 = 164.025±14.9	12881/71 = 181.423±21.5
13	3215/17 = 189.118±45.7	2430/17 = 142.941±34.5	2572/12 = 214.333±61.7	2410/13 = 185.385±51.3	1451/10 = 145.1±45.7

Table 18: Rejection of the loose (90%) photon veto for the various classes with different combinations of loose and tight versions of the setup cuts: kinematic box cut, TD cuts and DELCO. The 'All Loose' and 'All Tight' columns mean that those three sets of cuts were all loose or all tight. For the other three columns, all the cuts are loose except the one listed, which is tight. The numbers shown are the number of events before the photon veto is applied divided by the number of events remaining after the photon veto is applied and the resulting rejection with statistical error. If there are zero events remaining after the photon veto is applied, the rejection is determined assuming 1 event remained.

Setup Cuts	Total Events	$K_{\pi 2}$ TG-Scatter		Other		
		Events	Fraction	Ke4	Possible Ke4	2-Beam
All Loose	10	7	0.70 ± 0.15	1	1	1
Ke4-phobic Kinematic Box	8	6	0.75 ± 0.15	1	0	1
DELCO6	4	3	0.75 ± 0.22	0	0	1
TDTIGHT	5	2	0.40 ± 0.22	1	1	1
All Tight	2	1	0.50 ± 0.35	0	0	1

Table 19: Categorization of events surviving the loose photon veto in the $K_{\pi 2}$ scatter rejection branch Class 12. The combinations of loose and tight setup cuts are described in Table 17.

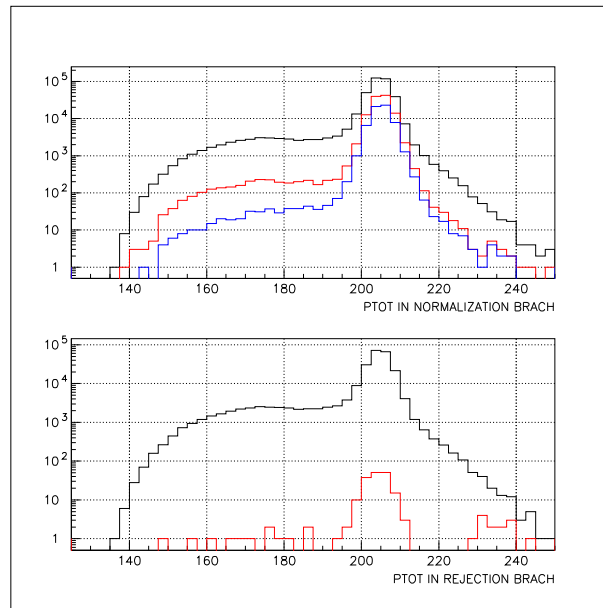


Figure 24: Top: ptot distribution of the events remaining in the normalization branch of the $K_{\pi 2}$ TG scatter study after the inversion of PVCUT (black), after the application of all the TGCUT06 except CCDPUL (red), and after the application of CCDPUL (blue). Bottom: ptot distribution of the events in CLASS12 of the rejection branch of the $K_{\pi 2}$ TG scatter study before (black) and after (red) PVCUT.

CUT	PNN2BOX loose	PNN2BOX tight	KP2BOX
ALL_EVENTS	92709440	92709440	92709440
BAD_RUN,KERROR	90192880	90192880	90192880
SKIM5,RECON	2635077	2635077	2635077
PSCUT06	952180	952180	952180
DELCO3	945357	778661	945357
TDCUT02	711847	428074	711847
KINCUT06	417199	257607	417199
BOX	38835 (10.7429)	18911 (13.6221)	337622 (1.2357)
\overline{PVCUT}	38820 (1.00039)	18907 (1.00021)	337377 (1.00073)
B4EKZ(IC)	27787 (1.39706)	13617 (1.38848)	307443 (1.09736)
TGZFOOL	27396 (1.01427)	13437 (1.0134)	302502 (1.01633)
EPITG	17250 (1.58817)	8228 (1.63308)	265780 (1.13817)
EPIMAXK	17250 (1)	8228 (1)	265780 (1)
TARGF	14700 (1.17347)	6914 (1.19005)	256810 (1.03493)
DTGTTP	14700 (1)	6914 (1)	256803 (1.00003)
RTDIF	14590 (1.00754)	6870 (1.0064)	254618 (1.00858)
DRP	14388 (1.01404)	6791 (1.01163)	253746 (1.00344)
TGKTIM	14144 (1.01725)	6761 (1.00444)	251265 (1.00987)
EIC	13847 (1.02145)	6623 (1.02084)	247096 (1.01687)
TIC	13847 (1)	6623 (1)	247095 (1)
TGEDGE	13621 (1.01659)	6535 (1.01347)	244792 (1.00941)
TGDEDX	12809 (1.06339)	6120 (1.06781)	243294 (1.00616)
TGENR	12533 (1.02202)	5988 (1.02204)	236833 (1.02728)
PIGAP	12342 (1.01548)	5883 (1.01785)	235171 (1.00707)
TGB4	11082 (1.1137)	5251 (1.12036)	221207 (1.06313)
KIC	11076 (1.00054)	5248 (1.00057)	221103 (1.00047)
PHIVTX	8289 (1.33623)	3826 (1.37167)	213725 (1.03452)
OPSVETO	7238 (1.14521)	3374 (1.13397)	204252 (1.04638)
TGLIKE	6812 (1.06254)	3176 (1.06234)	197703 (1.03313)
TIMKF	5542 (1.22916)	2621 (1.21175)	175933 (1.12374)
NPITG	5542 (1)	2621 (1)	175933 (1)
ALLKFIT	5295 (1.04665)	2507 (1.04547)	169905 (1.03548)
TPICS	5291 (1.00076)	2504 (1.0012)	169877 (1.00016)
EPIONK	4970 (1.06459)	2321 (1.07885)	159031 (1.0682)
CHI567	4143 (1.19961)	1898 (1.22287)	138310 (1.14982)
VERRNG	3455 (1.19913)	1592 (1.19221)	129595 (1.06725)
CHI5MAX	3454 (1.00029)	1591 (1.00063)	129595 (1)
ANGLI	3445 (1.00261)	1588 (1.00189)	129524 (1.00055)
CCDBADFIT	3083 (1.11742)	1426 (1.1136)	114548 (1.13074)
CCDBADTIM	2999 (1.02801)	1386 (1.02886)	112173 (1.02117)
CCD31FIB	2999 (1)	1386 (1)	112171 (1.00002)
CCDPUL	510 (5.88039)	256 (5.41406)	60635 (1.84994)

Table 20: The normalization branch for the K_{π_2} -TG scatter background: events after setup cuts and TGCUTS and their rejection (in brackets), for $\pi\nu\bar{\nu}(2)$ loose, $\pi\nu\bar{\nu}(2)$ ke4-phobic, and K_{π_2} boxes. For the tight box, tight versions of the cuts marked with '*' were applied. Note that the loose 60% photon veto is inverted for both the loose and tight normalization branches.

9.1.3 Background

Using the numbers from Tables 14 and 20, the $K_{\pi 2}$ target scatter background for the loose box is

$$\begin{aligned}
 n_{K_{\pi 2}-TGscat} &= 3 \times \frac{N}{R_{PVclass12} - 1} \\
 &= 3 \times \frac{510}{(2661.3 \pm 841.4) - 1} \\
 &= 0.575 \pm 0.184(\text{stat.})_{-0.201}^{+0.063}(\text{sys.})
 \end{aligned} \tag{2}$$

The systematic error comes from the difference in background predicted by the class with the highest (CLASS7) and lowest (CLASS9) PV rejection, with respect to the central value from CLASS12. Only classes with adequate statistics are considered.

Using the numbers from Tables 15 and 20, the $K_{\pi 2}$ target scatter background for the tight box is

$$\begin{aligned}
 n_{K_{\pi 2}-TGscat} &= 3 \times \frac{N}{R_{PVclass12} - 1} \\
 &= 3 \times \frac{256}{(6653.2 \pm 3326.4) - 1} \\
 &= 0.115 \pm 0.058(\text{stat.})_{-0.022}^{+0.039}(\text{sys.})
 \end{aligned} \tag{3}$$

The lower bound on the systematic error comes from the difference in background predicted by the class with the highest (CLASS2) PV rejection, with respect to CLASS12. Only classes with adequate statistics are considered. The upper bound on the systematic error comes from the difference in background for CLASS12 between the "All Loose" and "Ke4-phobic kinematic box" setups cuts as shown in Table 16.

9.2 $K^+ \rightarrow \pi^+ \pi^0$ Range Stack Scatters

Pions from the $K_{\pi 2}$ decay can also undergo inelastic scattering in the Range Stack and fall into the $\pi\nu\bar{\nu}(2)$ kinematic box by losing energy in the scattering process. However, for these events to be a background for this analysis, the pion momentum also has to be mis-measured and the photons from the π^0 decay have to be missed. Therefore, this background is expected to be smaller compared to the $K_{\pi 2}$ target scattered background. It should be noted that these background events are already included in the normalization branch in Table 20², but they are not included in the rejection branch in Table 14 because the target cuts were reversed to measure this PV rejection. The $K_{\pi 2}$ events which scattered in the RS should be assigned the same Photon Veto rejection as the $K_{\pi 2}$ peak events, since the pion did not scatter in the target. The most effective cuts against this background are the Range Stack track quality cuts RSDIDX and PRRF (collectively referred to as RSCT), the BOX cut on $ptot$ and the Photon Veto cut. Tables 21 and 22 summarize this

²Correcting the normalization of $K_{\pi 2}$ -TG scatters for $K_{\pi 2}$ -RS scatters does not make a significant difference in the background, given the statistical uncertainty.

Rejection				
CUT	Loose Box		Tight Box	
	KP2BOX	PNN2 LOOSE RE BOX	KP2BOX	PNN2 TIGHT RE BOX
SETUP				
PBOX from KP2BOX	92680	720	61653	345
LAYER14	92627	720	61619	345
FIDUCIAL	85452	650	56897	308
UTCQUAL	82761	637	55098	303
RNGMOM	82060	637	54628	303
RSDEDX	71644	114	47810	63
PRRF	60670	82	40647	44
PVCUT	35	0	11	0

Table 21: Rejection branch for $K_{\pi 2}$ -RS scatters. PBOX is the momentum cut and RE BOX the range and energy cut.

Normalization				
CUT	Loose Box		Tight Box	
	KP2BOX	PNN2BOX	KP2BOX	PNN2BOX
SETUP				
<u>RSDEDX.or.PRRF</u>	25001	218	16360	82
LAYER14	24981	218	16348	82
FIDUCIAL	22516	203	14744	76
UTCQUAL	21611	180	14135	69
RNGMOM	21390	154	13981	67
<u>PVCUT60</u>	21381	154	13974	67

Table 22: Normalization branch for $K_{\pi 2}$ -RS scatters.

background study. The SETUP cuts are the same as the $K_{\pi 2}$ target scatter normalization branch. Table 21 contain events in the $K_{\pi 2}$ momentum peak. Events with the momentum of the $K_{\pi 2}$ peak events, but lowered in range and energy are assumed to have scattered in the Range Stack.

The efficiency ϵ_{RSCT} and the rejection R_{RRSCT} of these cuts can be measured as

$$\begin{aligned}
\epsilon_{RSCT}(\text{loose}) &= 60670/82060 = 0.739 \pm 0.002 \\
R_{RSCT}(\text{loose}) &= 637/82 = 7.768 \pm 0.801
\end{aligned}
\tag{4}$$

$$\begin{aligned}
\epsilon_{RSCT}(\text{tight}) &= 40647/54628 = 0.744 \pm 0.002 \\
R_{RSCT}(\text{tight}) &= 303/44 = 6.886 \pm 0.960
\end{aligned}
\tag{5}$$

Table 22 shows the normalization branch. The RSCT cut is reversed and all other cuts are applied. The various contributions to the total 154 events left at the the end of

the branch have to be considered in order to calculate the background of interest. The largest component of this sample comes from scattering in the target that contaminated the RSCT reversed sample because of the inefficiency of the RSCT cuts. On the other hand, the total 510 events in the loose box for the $K_{\pi 2}$ target scatter normalization branch (Table 20) have a target scattered (N_{tg}) and a RS scattered (N_{rs}) component. Therefore

$$\begin{aligned} N_{tg} + N_{rs} &= 510 \\ \frac{1 - \epsilon_{RSCT}}{\epsilon_{RSCT}} \times N_{tg} + (R_{RSCT} - 1) \times N_{rs} &= 154 \end{aligned} \quad (6)$$

Solving this system of equations gives a negative solution for the range stack scattered component N_{rs} for both the loose and tight boxes:

$$N_{rs}(\text{loose}) = -4.022 \pm 2.352$$

and using the tight box values

$$N_{rs}(\text{tight}) = -3.799 \pm 1.897$$

The final background from the RS scattered events can be measured by applying the $K_{\pi 2}$ peak Photon Veto rejection (CLASS1):

$$R_{PV-K_{\pi 2}peak}(\text{loose}) = 60670/35 = 1733.4 \pm 292.9 \quad (7)$$

$$R_{PV-K_{\pi 2}peak}(\text{tight}) = 40647/11 = 3695.2 \pm 1114.0 \quad (8)$$

to N_{rs} which gives

$$n_{K_{\pi 2}-RSscat}(\text{loose}) = 3 \times \frac{N_{rs}}{R_{PV-K_{\pi 2}peak} - 1} = -0.0070 \pm 0.0042 \quad (9)$$

$$n_{K_{\pi 2}-RSscat}(\text{tight}) = -0.0031 \pm 0.0018. \quad (10)$$

Since both of these values are negative, but consistent with zero, both the loose and tight backgrounds from the pion scattering (from the $K^+ \rightarrow \pi^+\pi^0$ decay) in the range stack are negligible for the 1/3 sample.

10 $K_{\pi 2\gamma}$ Background

The $K_{\pi 2\gamma}$ ($K \rightarrow \pi^+\pi^0\gamma$) background is expected to be small as compared to the $K_{\pi 2}$ scattering background in pnn2 analysis because of the presence of the extra photon and the small branching ratio. For $K \rightarrow \pi^+\pi^0\gamma$ decay, the γ can be emitted by direct emission (DE) or inner bremsstrahlung (IB). The partial branching fraction for T_{π^+} in the range of 55-90 MeV is $(4.4 \pm 0.7) \times 10^{-6}$ for DE and $(2.75 \pm 0.15) \times 10^{-4}$ [10] for IB. Since it is difficult to isolate this background from the $K_{\pi 2}$ scattering background, both Monte Carlo and data are used. The method can be summarized with the following formula [11]:

$$N_{K_{\pi 2\gamma}} = \frac{N_{K_{\pi 2-peak}}}{\kappa \cdot R_{\gamma}} .$$

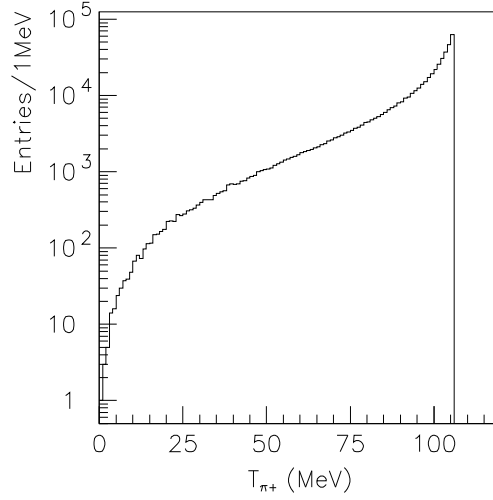


Figure 25: π^+ kinetic energy distribution in $K\pi 2\gamma$ events

$N_{Kp2-peak}$ is the number of $K\pi 2$ peak events which passed all pass2 cuts and $K\pi 2$ box cuts instead of pnn2 box cuts, and is estimated by data. The factor κ , estimated from UMC, is the relative acceptance of the charged track between $K\pi 2$ ($K\pi 2$ box) and $K\pi 2\gamma$ (pnn2 box) events. The extra PV rejection from the radiative γ is contained in R_γ .

$N_{Kp2-peak}$ is measured to be 11 and 35 for tight and loose cuts respectively. (Loose refers to loose PV, TD, KIN and DELCO3, while tight to tight PV, TD, KIN(ke4-phobic) and DELCO6.)

To study the relative acceptance κ for the charged track 2×10^5 $K\pi 2$ events and 5×10^5 $K\pi 2\gamma$ events are generated by UMC. The branching ratio of $K\pi 2$ is 0.2092 ± 0.0012 [10]. Fig. 25 shows the true kinematic energy distribution for $K\pi 2\gamma$ events. Note that the DE process is ignored due to its low branching ratio. With this information, the effective branching ratio for the range of 0-106 MeV can be calculated as:

$$Br(K\pi 2\gamma) = \frac{\int_0^{106} dN}{\int_{55}^{90} dN} \times (2.75 \pm 0.15) \times 10^{-4} = (1.11 \pm 0.06) \times 10^{-3} .$$

The generated UMC events are required to pass pnn1 or pnn2 trigger simulation without the online photon veto, L1.N or L0rr2 triggers. Then these events are required to pass all possible offline cuts for UMC. The photon veto cuts are not applied, and the $K\pi 2$ and pnn2 box cuts are applied for the $K\pi 2$ and $K\pi 2\gamma$ events, respectively. κ is calculated as:

$$\kappa = \frac{Br(K\pi 2) \times \frac{N_{K\pi 2 \text{ offline cuts}}}{N_{K\pi 2 \text{ KT}}}}{Br(K\pi 2\gamma) \times \frac{N_{K\pi 2\gamma \text{ offline cuts}}}{N_{K\pi 2\gamma \text{ KT}}}} .$$

The result and detailed information in κ calculated are listed in Tab. 23. The value of κ is mainly determined by the relative branching ratio and kinematic box cuts, and is very

Table 23: Detailed information in κ estimation.

	$K\pi 2$	$K\pi 2\gamma$
N_{KT}	199986	499973
Passed pnn1 or pnn2 trigger	30625	64217
Passed Tight offline cuts	7608	7409
Passed Loose offline cuts	9776	11035

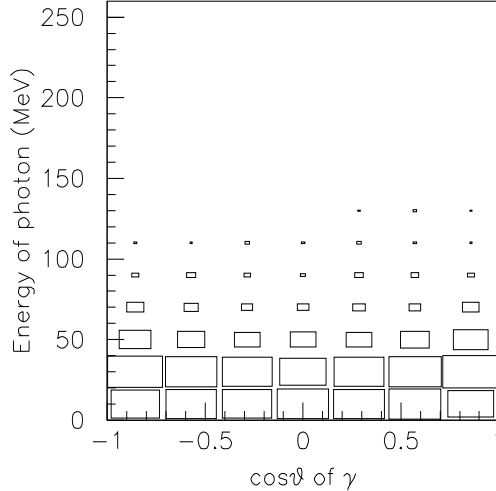


Figure 26: The UMC truth spatial and energy distribution of the third photon of $K\pi 2\gamma$ events after it passed all offline cuts. (Use loose offline cuts for example here.)

insensitive to the other cuts.

The photon veto rejection due to the photons from π^0 decay for both $K\pi 2$ and $K\pi 2\gamma$ event is expected to be roughly equal. However the existence of the radiative γ in $K\pi 2\gamma$ background will give higher total rejection. The UMC truth spatial and energy distribution of the third photon, after the $K\pi 2\gamma$ events passed all offline cuts, is shown in Fig. 26 (Loose offline cuts). A single photon inefficiency A table [12] was built with conservative photon veto cuts with data [5] and is shown in Fig. 27. R_γ is calculated by convolving these two tables. All of the results and estimated backgrounds are summarized in Tab. 24. The tighter kinematic box also suppresses $K\pi 2\gamma$.

11 Beam Background

The PV is applied at the same level as PNN1 for the beam backgrounds. Therefore, we must scale by $\frac{A_{PV_{pnn2}}}{A_{PV_{pnn1}}}$ where $A_{PV_{pnn1}} = 0.95$ and $A_{PV_{pnn2}} = 0.619$ for the loose signal region and $A_{PV_{pnn2}} = 0.330$ for the tight region. Scaling by the PV acceptance-loss is justified by these backgrounds not being dependent upon the PV cuts. Also, there is no expectation of additional rejection against these background for the PV cuts (except for the ADPV cut in the 2-beam background which is discussed in Section 11.2). Since the

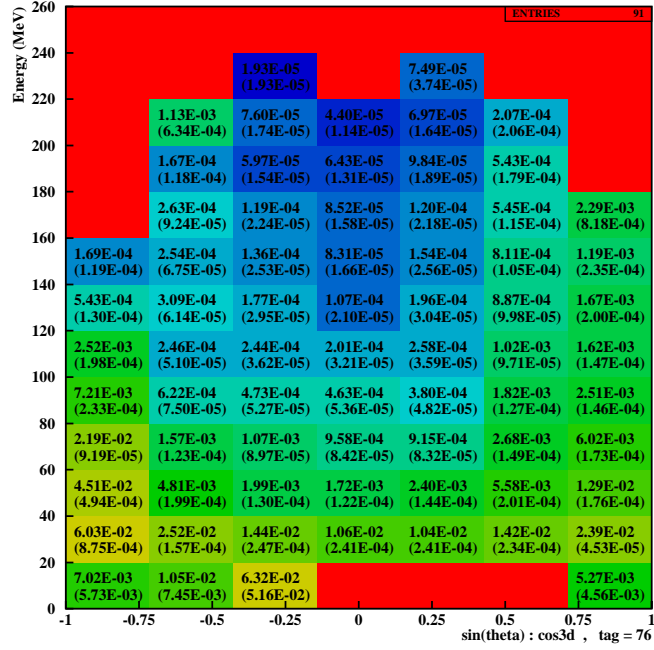


Figure 27: Inefficiency table for single photon. Missing entries are assumed to have 100% inefficiency.

Table 24: $K\pi 2\gamma$ background number normalized to 3/3 data. The first error of $N_{Kp2\gamma}$ is statistical and the second error is from κ and R_γ .

	Tight cuts	Loose cuts
$N_{Kp2\text{-peak}}$	11	35
κ	483 ± 28	417 ± 24
R_γ	5.11 ± 0.11	5.04 ± 0.10
$N_{Kp2\gamma}$	$0.013 \pm 0.004 \pm 0.001$	$0.0500 \pm 0.0084 \pm 0.0030$

beam backgrounds involve very limited statistics, including the PV_{pnn2} cut will remove all events from the normalization branch well before all cuts are applied.

11.1 Single-Beam Background

<i>Setup Brach (n)</i>	beam loose	beam tight
<i>Loose Setup</i>	10327.5 ± 7302.3 (2)	17371.0 ± 17370.5 (1)
<i>TD</i>	17192.0 ± 17191.5 (1)	10480.0 ± 10479.5 (1)
<i>TD · KIN</i>	6239.0 ± 6238.5 (1)	3755.0 ± 3754.5 (1)

Table 25: **1-Beam Rejection Summary** of Tables 6-8. Each row is a different branch to measure the DELCO rejection. First number is the rejection. The number in parenthesis is the number of events remaining that the rejection is based upon. The minimum rejection is used in calculation of the 1-BM background for a conservative estimate.

<i>Norm. branches</i>	beam loose	beam tight
<i>DELCO · PV_{pnn1}</i>	5.0 ± 2.2	2.0 ± 1.4

Table 26: **1-Beam Normalization Summary**

$$N_{1bm} = 3 \times \frac{A_{PV_{pnn2}}}{A_{PV_{pnn1}}} \times \frac{N_{1bm}}{R_{delco} - 1} \quad (11)$$

$$\begin{aligned} N_{1bm_{loose}} &= 3 \times \frac{0.619}{0.95} \times \frac{5.0 \pm 1.0}{(6239.0 \pm 6238.5) - 1} \\ &= (1.57 \pm 1.57) \times 10^{-3} \end{aligned} \quad (12)$$

$$\begin{aligned} N_{1bm_{tight}} &= 3 \times \frac{0.330}{0.95} \times \frac{2.0 \pm 1.0}{(3755 \pm 3754.5) - 1} \\ &= (0.55 \pm 0.55) \times 10^{-3} \end{aligned} \quad (13)$$

If we “measure” the tight value from scaling from 1-beam loose value, we obtain the following: Note that the factor of 3 is included in the value of $N_{1bm_{loose}}$.

$$N_{1bm_{tight}}^{scaled} = \frac{A_{PV_{tight}}}{A_{PV_{loose}}} \times \frac{A_{TD_{tight}}}{A_{TD_{loose}}} \times \frac{A_{BOX_{tight}}}{A_{BOX_{loose}}} \times \frac{A_{DELCO_{tight}}}{A_{DELCO_{loose}}} \times N_{1bm_{loose}} \quad (14)$$

$$\begin{aligned} N_{1bm_{tight}}^{scaled} &= \frac{0.330}{0.619} \times \frac{0.704}{0.942} \times (0.68) \times \frac{0.7129}{0.8671} \times 0.00157 \\ &= (0.35 \pm 0.35) \times 10^{-3} \end{aligned} \quad (15)$$

$N_{1bm_{tight}}^{scaled}$ is consistent with $N_{1bm_{tight}}$. If we use the $Rej_{delco} = 6239$ from the loose region (which has more statistics) for the tight region then $N_{1bm_{tight}} = 0.33 \times 10^{-3}$.

11.2 Double-Beam Background

11.2.1 2-beam results

<i>rejection (n)</i>	beam loose	beam tight
$R_{KK} : BWTRS \cdot CkTRS \cdot CkTail$	61.9 ± 9.8 (39)	59.9 ± 12.7 (22)
$R_{Kpi} : BWTRS \cdot CpiTRS \cdot CpiTail$	352.5 ± 124.5 (8)	274.3 ± 111.8 (6)

Table 27: **2-Beam Rejection Summary** of Tables 14-15. First number is the rejection. The number in parenthesis is the number of events remaining that the rejection is based upon. K-K is the case where two Kaons are entering the beam. K-pi is the case where we have a Kaon and a Pion entering. $\overline{B4TRS \cdot B4CCD}$ is applied.

<i>Norm. branches</i>	beam loose	beam tight
$n_{KK} : ADPV \cdot B4TRS \cdot B4CCD$	8.0 ± 2.8	1.0 ± 1.0
$r_{KK} : TG \cdot TGKIN \cdot TGPV$	7.3 ± 2.6	7.3 ± 3.9
N_{KK}	1.1 ± 0.55	0.136 ± 0.136
$n_{Kpi} : B4TRS \cdot B4CCD$	10.0 ± 3.2	3.0 ± 1.7
$r_{Kpi} : TG \cdot TGKIN \cdot TGPV$	21.0 ± 10.2	45.0 ± 44.5
N_{Kpi}	0.5 ± 0.3	0.1 ± 0.1

Table 28: **2-Beam Normalization Summary** of Tables 16-19. The 2-BM Normalization has 2 branches that are further bifurcated. $K-K_{r,n}$, $K-pi_{r,n}$ are the results of the bifurcations, r=rejection, n=normalization, which we used to determine the last two rows. N_{K-K} and N_{K-pi} are the 2-BM normalization values which are used in combination with Table 3 to give the final background in Table 5. For KK (Kpi), $\overline{CkTRS \cdot CkTAIL \cdot BWTRS}$ ($\overline{CpiTRS \cdot CpiTAIL \cdot BWTRS}$) is applied

11.2.2 KK-beam background

- Scale by acceptance by PV_{noAD} due to applying ADPV in the normalization branch.

$$N_{KK} = 3 \times \frac{A_{PV_{noAD}}}{A_{PV_{pnn1}}} \times \frac{\left(\frac{n_{KK}}{r_{KK}}\right)}{R_{KK} - 1} \quad (16)$$

$$\begin{aligned} N_{KK_{loose}} &= 3 \times \frac{0.652}{0.95} \times \frac{\left(\frac{8}{51/7}\right)}{61.9 - 1} \\ &= (37.1 \pm 19.5) \times 10^{-3} \end{aligned} \quad (17)$$

$$\begin{aligned}
N_{KK_{tight}} &= 3 \times \frac{0.3455}{0.95} \times \frac{\left(\frac{1}{22/3.}\right)}{59.9 - 1} \\
&= (2.53 \pm 2.53) \times 10^{-3}
\end{aligned} \tag{18}$$

11.2.3 $K\pi$ -beam background

- Only measure the background in the data before the $\pi\nu\nu(2)$ C_π trigger change. This entails scaling by 2.54 to extrapolate to the full running period.
- Scale by the acceptance for the PV_{pnn1} cut.
- Do not apply ADPV due to lack of statistics (lower statistics compared to KK due to C_π trigger change).

$$N_{K\pi} = 3 \times 2.54 \times \frac{A_{PV_{pnn2}}}{A_{PV_{pnn1}}} \times \frac{\left(\frac{n_{K\pi}}{r_{K\pi}}\right)}{R_{K\pi} - 1} \tag{19}$$

$$\begin{aligned}
N_{K\pi_{loose}} &= 3 \times 2.54 \times \frac{0.619}{0.95} \times \frac{\left(\frac{10}{84/4.}\right)}{352.5 - 1} \\
&= (6.73 \pm 6.73) \times 10^{-3}
\end{aligned} \tag{20}$$

$$\begin{aligned}
N_{K\pi_{tight}} &= 3 \times 2.54 \times \frac{0.330}{0.95} \times \frac{\left(\frac{3}{45/1.}\right)}{274.3 - 1} \\
&= (0.646 \pm 0.646) \times 10^{-3}
\end{aligned} \tag{21}$$

The beam background was scaled by the ratio of PV_{pnn1} acceptance to PV_{pnn2} acceptance; PV_{pnn1} was applied to increase statistics. The acceptance values used are 0.95 for pnn1, 0.619 for loose pnn2, 0.330 for tight pnn2. For the K-K background, ADPV is used in the normalization branch. The acceptance of PV_{pnn2} without ADPV is 0.652 (0.3455) for loose (tight). The addition of ADPV was used in the K-K background due to ADPV having additional rejection against 2-beam background and the K-K branch has sufficient statistics to be applied. K- π does not have sufficient statistics due to only using the "1st half of the data because of the C_π trigger change.

11.3 Beam Background Summary

$Bkgrnd (\times 10^{-3})$	k034	e787	beam loose	beam tight
1- BM	3.86 ± 2.36	1.66 ± 1.66	1.57 ± 1.57	0.55 ± 0.55
2- BM KK	0.983 ± 0.983	145.9 ± 145.9	37.1 ± 19.5	2.53 ± 2.53
2- BM Kpi	0.106 ± 0.106	19.7 ± 19.7	6.73 ± 4.57	0.646 ± 0.646
2- BM	1.14 ± 1.14	165.6 ± 165.6	43.8 ± 20.02	3.17 ± 3.17
<i>Total Beam</i>	5.00 ± 2.62	167.3 ± 167.3	45.37 ± 20.08	$3.72 \pm$

Table 29: **Total Beam-Background.** Scaled to the 3/3 sample. k034 column is the result of e949-pnn1 analysis. e787 is the result of the e787-PNN2 analysis. The other columns are current results that are expanded upon throughout the rest of the tables. The errors are statistical. KB_{live} for k034 is 1.77×10^{12} and for e787 is 1.71×10^{12} . e787 background has been scaled up accordingly for comparison purposes.

12 Muon Background

Muon background was scaled to the 3/3 and scaled by the acceptance loss from the PV_{pnn2} . The acceptance values used are 0.95 for pnn1, 0.619 for loose pnn2, 0.330 for tight pnn2. The “All PV” and “PV ERbox” already has PV_{pnn2} applied, so PV acceptance scaling is not applied. As shown, the applying the pnn2 level PV is consistent with scaling by acceptance loss. However, in the ERbox there is not sufficient statistics when applying PV_{pnn2} .

Branches	muon loose	muon tight
Band All	65.10 ± 6.97	279.72 ± 65.81
Band ERbox	63.58 ± 18.21	348.00 ± 245.72
Band All PV	107.82 ± 32.36	517.00 ± 516.50
Band PV ERbox	49.00 ± 48.50	21.00 ± 20.49
Norm	1 ± 1.00	1 ± 1.00

Table 30: Rejection and Normalization Summary Table.

Branches	muon loose	muon tight
Band All	30.50 ± 30.50	3.74 ± 3.74
Band ERbox	31.23 ± 31.23	3.00 ± 3.00
Band All PV	28.08 ± 28.08	5.81 ± 5.81
Band PV ERbox	62.5 ± 62.5	150. ± 150.

Table 31: Summary Table. Scaled to the 3/3 ($\times 10^{-3}$).

13 Charge exchange background

The Charge EXchange (CEX) background is expected to come mainly from $K^+n \rightarrow K^0p$ followed by $K_L^0 \rightarrow \pi^+e^-\nu_e$ and $K_L^0 \rightarrow \pi^+\mu^-\nu_\mu$. The main K_S^0 decay products ($\pi^+\pi^-$ or $\pi^0\pi^0$) cannot constitute a background. In E787 this background is primarily determined by UMC. A more data-driven approach is tried for CEX background in E949 with a normalization sample is found in data containing clear CEX events. The number in normalization branch might be overestimated, but it can be well understood. Due the low statistic and difficulty to isolate this background, a reliable simulation is used to get the rejection of reversed cuts in normalization. Thus the systematic error can be easily controlled, since only a few cuts are involved in UMC.

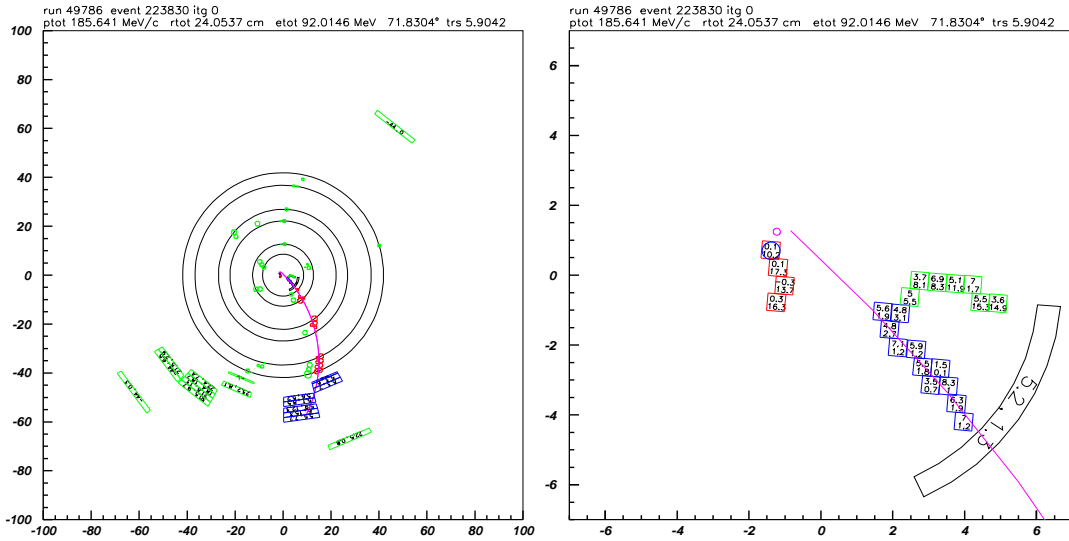


Figure 28: A CEX candidate. The x-y view and target view.

Three steps are taken to analyze CEX background. The first step is to find a normalization sample to be used for a visual scan. The probability for CEX process to happen is quite low, and many cuts are effective to this background. The observation of a clear CEX-like events will give strong confidence to this method.

The setup cuts is set to be very loose. TGPV, OPSVETO, DELCO, B4EKZ, EPITG, EPIMAX, EPIONK, DRP, TGB4, PHIVTX, CHI567, VERRNG, ANGLI, TGFITALLK and CCDPUL are turned off. KPIGAP is used to select events with the expected 'gap' between the kaon and pion fibers. (KPIGAP is a modified version of an inverted TARGF cut that takes into account target fibers identified as 'photon' fibers.) 27 candidates are left after all the criteria. All these events are scanned by eye. One CEX-like event is found there, while the others are not so easy to classify. The candidate is shown in Fig. 28

The second sample is built based on the first sample. The setup cuts are tightened with respect to previous set. The cuts which should be turned off are delicately selected. KPIGAP ($\approx \overline{\text{TARGF}}$) is used and DELCO is turned off as TARGF and DELCO have a large rejection for CEX background. These cuts basically exploit the lifetime of K_L^0 which is well-simulated, so their rejection can be measured with UMC. TGPV, OPSVETO and CCDPUL also can remove CEX background. The method used in $Ke4$ study is used here again to get their rejection and to estimate the uncertainty. For CEX events, the consistency between B4, the kaon target fiber energy and the z of the outgoing pion should be poor so B4EKZ will suppress CEX background. CHI567, CHI5MAX, VERRNG, ANGLI, TGFITALLK and CCDPUL are turned off. They do not have large rejection for background and it is almost impossible to get an appropriate simulation for them. Their rejection is taken to be the acceptance loss of signal. After these modifications, 1 event survives the tight cuts and 3 events for loose cuts in the normalization branch (Table 32).

For the simulation of CEX background the $K_S^0 \rightarrow \pi^+ \pi^-$ triggered events are studied. Information concerning the K_L^0 production points and momentum vector is thus obtained

Table 32: The pass2 cuts history of the normalization branch of the 1/3 data for the CEX study.

	Tight cuts	Loose cuts
skim567	12621399	12621399
delco2	7716700	7716700
KCUTS	206709	289592
CKTRS	182952(0.885)	256241(0.884)
CKTAIL	178646(0.976)	250182(0.976)
CPITRS	126363(0.707)	186280(0.744)
CPITAIL	126224(0.998)	186108(0.999)
BWTRS	119382(0.945)	176467(0.948)
B4DEDX	118158(0.989)	174641(0.989)
B4TRS	108812(0.920)	161046(0.922)
B4CCD	107089(0.984)	158536(0.984)
TIMCON	106186(0.991)	156924(0.989)
IPIFLG	105642(0.994)	156112(0.994)
ELVETO	98219(0.929)	145296(0.930)
TDFOOL	98051(0.998)	145025(0.998)
TDVARNN	67226(0.685)	133473(0.920)
PVCUT	188(0.002)	1395(0.010)
KPIGAP	12(0.063)	62(0.044)
TGZFOOL	8(0.666)	50(0.806)
EPITG	3(0.375)	29(0.580)
EPIMAXK	3(1.000)	29(1.000)
EPIONK	3(1.000)	29(1.000)
TIMKF	2(0.666)	18(0.620)
KIC	2(1.000)	14(0.777)
TGQUALT	2(1.000)	14(1.000)
NPITG	2(1.000)	14(1.000)
TGER	2(1.000)	14(1.000)
DTGTTP	2(1.000)	14(1.000)
RTDIF	2(1.000)	14(1.000)
DRP	2(1.000)	14(1.000)
TGKTIM	2(1.000)	14(1.000)
TGEDGE	2(1.000)	13(0.928)
TGDEDX	2(1.000)	13(1.000)
TGENR	2(1.000)	13(1.000)
PIGAP	2(1.000)	13(1.000)
TGLIKE	2(1.000)	9(0.692)
TGB4	2(1.000)	5(0.555)
PHIVTX	1(0.500)	5(1.000)
TPICS	1(1.000)	5(1.000)
TGTCON	1(1.000)	5(1.000)
B4ETCON	1(1.000)	5(1.000)
TGCEO	1(1.000)	3(0.600)

Table 33: CEX background number normalized to 3/3 data. The first error of N_{CEX} is statistical and the second error is the estimated systematic uncertainty due to TGPV, OPSVETO and CCDPUL.

	Tight cuts	Loose cuts
N_{norm}	1	3
$N_{targf, UMC}$	6_{-2}^{+6}	50_{-10}^{+33}
$N_{kpigap, UMC}$	3332	4136
N_{CEX}	$0.0046 \pm 0.0046_{-0.0015}^{+0.0046}$	$0.092 \pm 0.053_{-0.018}^{+0.070}$

from data. The corresponding B4 and K fiber information are also recorded from this $K_S^0 \rightarrow \pi^+\pi^-$ study. The rejection of TARGF, DELCO, TGPV, OPSVETO and CCDPUL are estimated by UMC. For TGPV and OPSVETO T_{xtg} (energy deposit in all photon veto fibers) is used. E_{hide} , the energy from the K_L^0 decay products in the kaon fibers, is extracted from UMC truth and used to estimate the CCDPUL rejection.

The CEX background is estimated as

$$N_{CEX} = N_{norm, data} \times \frac{N_{targf, UMC}}{N_{kpigap, UMC}} \times ACC_{unapplied},$$

where $N_{targf, UMC}$ is the number of events passing TARGF, DELCO, TGPV, OPSVETO and CCDPUL, $N_{kpigap, UMC}$ is the number of events passed KPIGAP which is equivalent to normalization branch in data, $ACC_{unapplied}$ is taken as 85% for CHI567 etc. Comparing with the uncertainty of the simulation of TARGF and DELCO, the systematic error associated with the mismatch of the energy scale in the target fibers between UMC and data is larger. The result of $T_{xtg} < 1.2MeV$ and $E_{hide} < 2.5MeV$ are taken as mean rejection and variations in the range of T_{xtg} $0.6 - 1.8MeV$ and E_{hide} $1.5 - 5MeV$ are considered as determining the systematic error of this background as summarized in Table 33

14 K_{e4} background

The K_{e4} decay ($K^+ \rightarrow \pi^+\pi^-e^+\nu_e$) with a branching ratio of $(4.09 \pm 0.09) \times 10^{-5}$ [10] and with the π^+ maximum momentum at 203 MeV could be a serious background in the pnn2 region because this decay contains no photon in the final state to veto on and the π^- and e^+ could be undetectable. Fig. 29 shows the total kinetic energy (T_2) of the π^- and e^+ versus the momentum of π^+ ($ptot$) for Monte Carlo events that passed the pnn2 trigger. When T_2 is very low, the π^- and the e^+ can not fly out of the target and they might escape detection if they deposit all their energy in some insensitive material or if their path overlaps with kaon fibers. For these low T_2 events the distribution of $ptot$ concentrates around 160 MeV which is in the range of the pnn2 signal box.

The low statistics of this background makes it hard to use bifurcated analysis here. Both data and UMC have to be used to evaluate the background. When T_2 is very low, the only effective cuts for this background are TGPV, OPSVETO and CCDPUL cut. A normalization sample is selected using data with $\overline{TGPV \cdot OPSVETO}$ and a Monte Carlo sample is used to estimate the rejection of TGPV·OPSVETO.

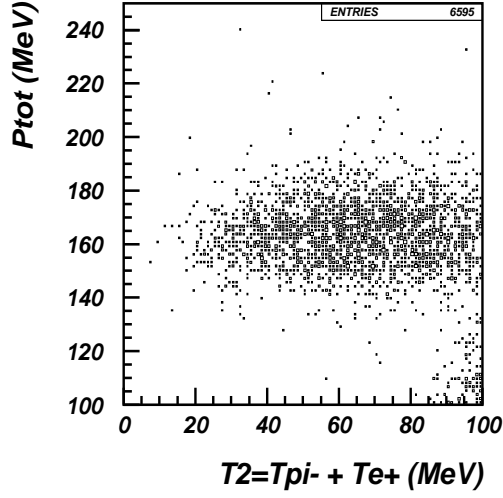


Figure 29: Total kinetic energy (T_2) of the π^- and the e^+ versus the momentum of the π^+ (P_{tot}) for Monte Carlo events that passed the trigger.

The pass2 cuts history of the normalization branch of the 1/3 data is tabulated in Table 34. For the loose box, 66 events remain at the end, before the final cut CCDPUL and EPIONK. To get further understanding of this sample, these events are scanned by eye. Obvious signatures of K_{e4} are found in most of them with some contamination by $K\pi 2$ events followed by Dalitz decay. Fig. 30 and Fig. 31 give two example events from this sample. This sample could be used as the normalization branch for a bifurcated analysis. However, it is not possible to get a clean data sample to estimate the rejection of TGPV·OPSVETO, so a Monte Carlo approach is used.

In order to understand the rejection of TGPV·OPSVETO and CCDPUL, Monte Carlo is used to simulate the energy deposit of charged tracks in the target. The main source of uncertainty in simulation comes from the absorption of π^- in the target. The π^- absorption is modeled with an experimental measurement of stopped π^- in the Range Stack [13]. Fig. 32 shows the distribution of the difference between the measured and expected energy of stopped π^- from experiment. In simulation the absorption energy is sampled according to this distribution. If the simulated absorption energy is negative, then it is assigned 0. In this model all the absorption energy is deposited in a single fiber promptly. Possible energy deposition in neighboring fibers is not simulated.

About 2×10^8 K_{e4} events are generated with this model with an additional cut at $T_2 < 50 MeV$ in order to enhance the phase space region most responsible for the background. To study the correlation between TGPV·OPSVETO and CCDPUL, two variables are used: the total energy deposit, T_{xtg} , in any fibers not identified as pion or kaon by the reconstruction, corresponding to the energy deposits available to TGPV·OPSVETO, and the total energy deposit, E_{hide} , of the negative pion and positron in kaon fibers, corresponding to the energy deposit that would be found by the CCDPUL. Because there is no simulation for CDD pulse, E_{hide} is taken directly from UMC truth.

UMC events are required to pass all possible cuts. Fig. 33 shows the correlation between T_{xtg} and E_{hide} of the remaining sample. In Tab. 35 and Tab. 36 for loose and tight

	Loose cuts	Tight cuts
skim567	12892189	12129662
KCUTS	764547	534649
PCUTS	179878	113377
TDCUTS	152873	71493
PVCUT	3011	489
DELC	1648 (0.547)	254 (0.519)
DELC3	1644 (0.997)	224 (0.881)
TGZFOOL	1579 (0.960)	213 (0.950)
R-cut	1554 (0.984)	211 (0.990)
PVICVC	1118 (0.719)	130 (0.616)
B4EKZ	933 (0.834)	113 (0.869)
EPITG	569 (0.609)	76 (0.672)
EPIMAXK	569 (1.000)	76 (1.000)
TIMKF	422 (0.741)	57 (0.750)
KIC	410 (0.971)	56 (0.982)
TGQUALT	374 (0.912)	54 (0.964)
NPITG	374 (1.000)	54 (1.000)
TGER	374 (1.000)	54 (1.000)
TARGF	359 (0.959)	51 (0.944)
DTGTP	359 (1.000)	51 (1.000)
RTDIF	356 (0.991)	51 (1.000)
DRP	327 (0.918)	46 (0.901)
TGKTIM	327 (1.000)	46 (1.000)
TGEDGE	312 (0.954)	44 (0.956)
TGDEDX	287 (0.919)	40 (0.909)
TGENR	282 (0.982)	39 (0.975)
PIGAP	277 (0.982)	37 (0.948)
TGLIKE	257 (0.927)	33 (0.891)
TGB4	250 (0.972)	33 (1.000)
PHIVTX	105 (0.420)	14 (0.424)
CHI567	93 (0.885)	13 (0.928)
CHI5MAX	93 (1.000)	13 (1.000)
VERRNG	81 (0.870)	10 (0.769)
ANGLI	81 (1.000)	10 (1.000)
TGFITALLK	80 (0.987)	10 (1.000)
TPICS	80 (1.000)	10 (1.000)
TGTCON	80 (1.000)	10 (1.000)
B4ETCON	80 (1.000)	10 (1.000)
CCDBADTIM	76 (0.950)	9 (0.900)
CCDBADFIT	66 (0.868)	6 (0.666)
CCD31FIB	66 (1.000)	6 (1.000)
CCDPUL	3 (0.045)	1 (0.166)
EPIONK	3 (1.000)	1 (1.000)

Table 34: The pass2 cuts history of the normalization branch of the 1/3 data for K_{e4} study. R-cut is $\overline{TGPV} \cdot \overline{OPSVETO}$.

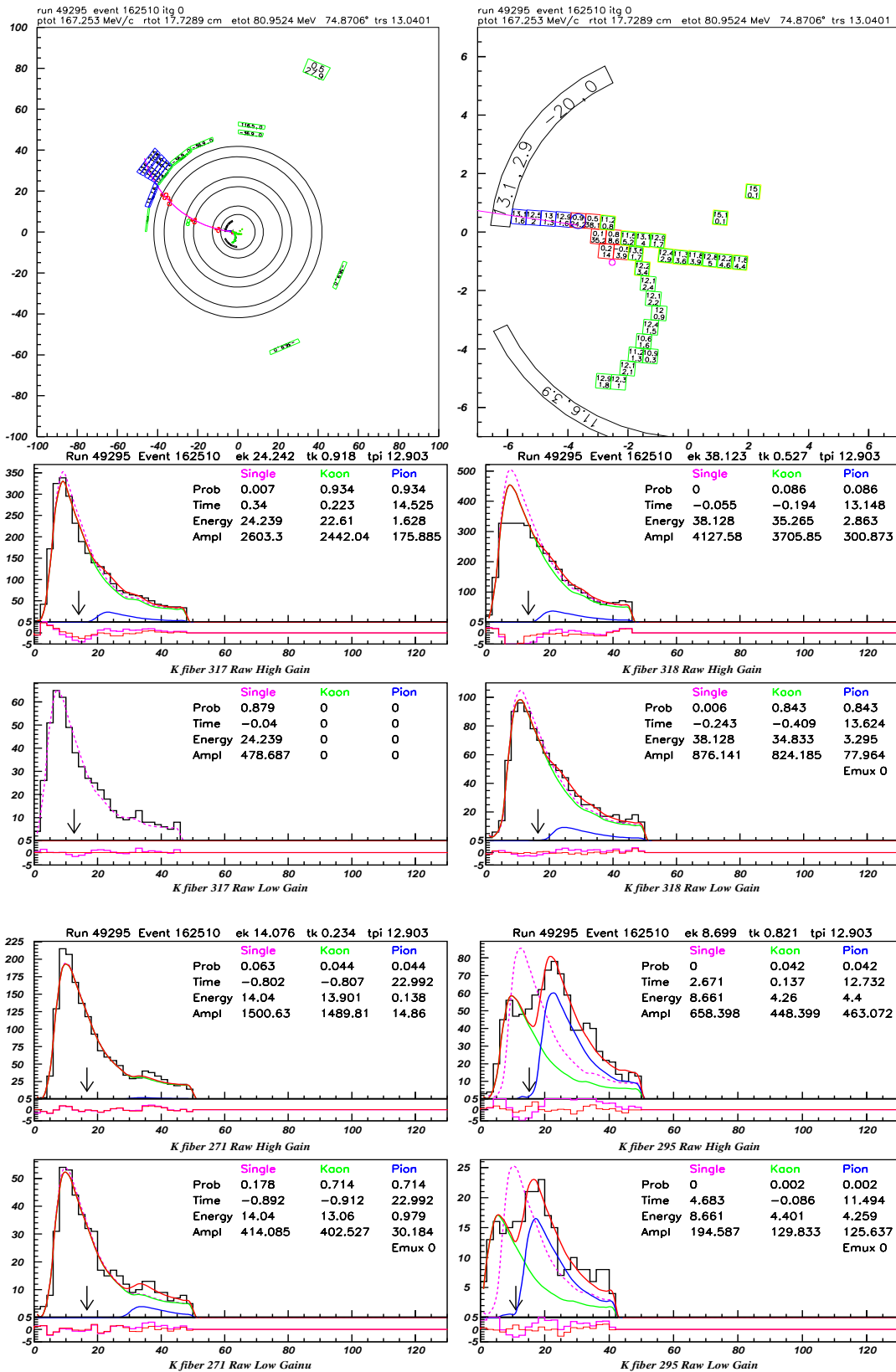


Figure 30: A possible K_{e4} candidate. The X-Y view, target and all double pulse hits in kaon fibers are plotted.

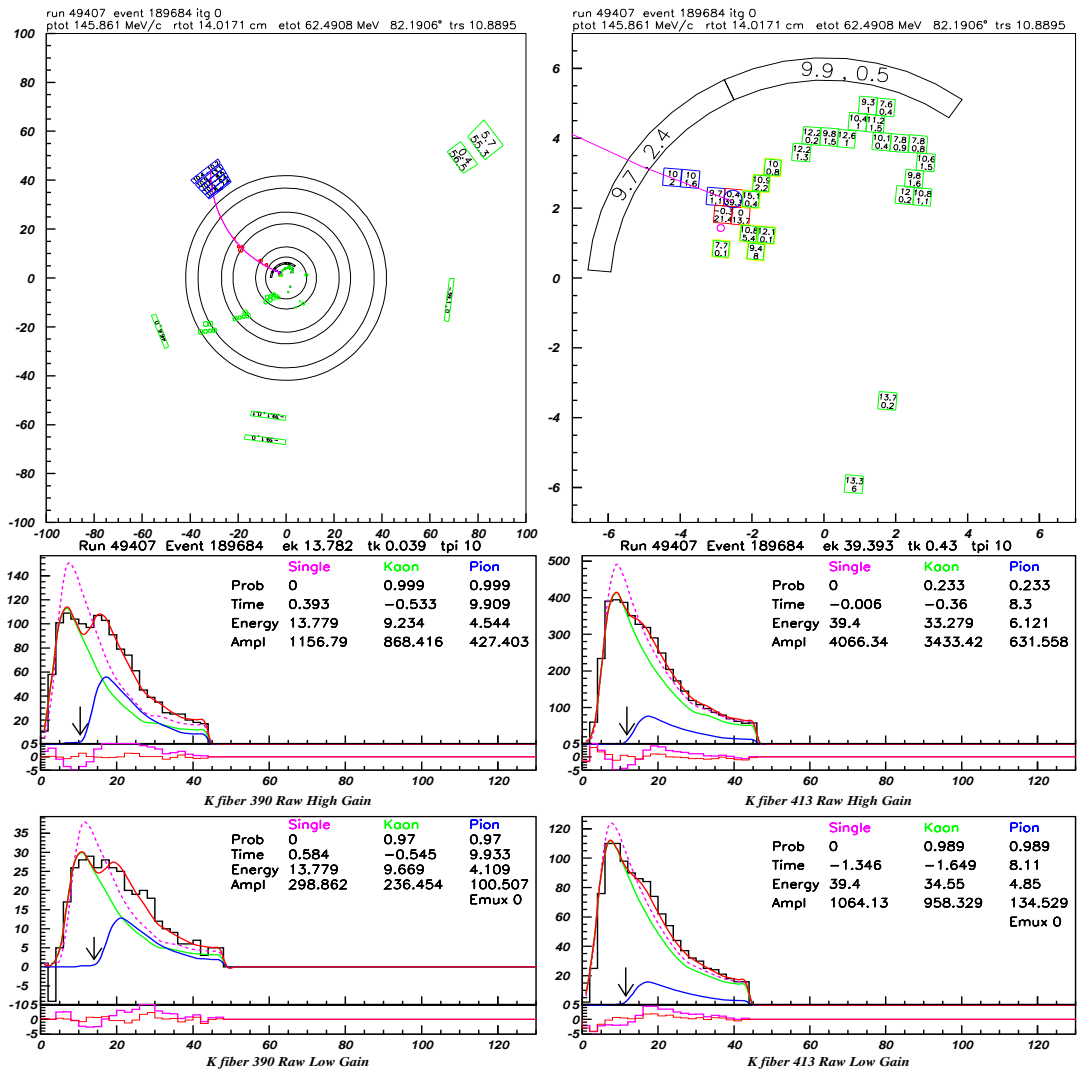


Figure 31: Another possible K_{e4} candidate. The X-Y view, target and all double pulse hits in kaon fibers are plotted.

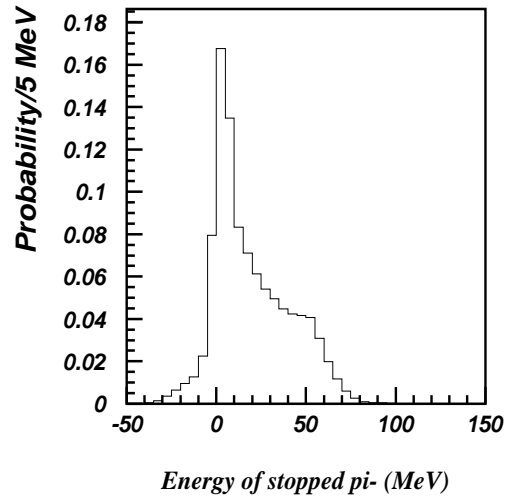


Figure 32: Observable absorption energy of π^- stopped in the RS.

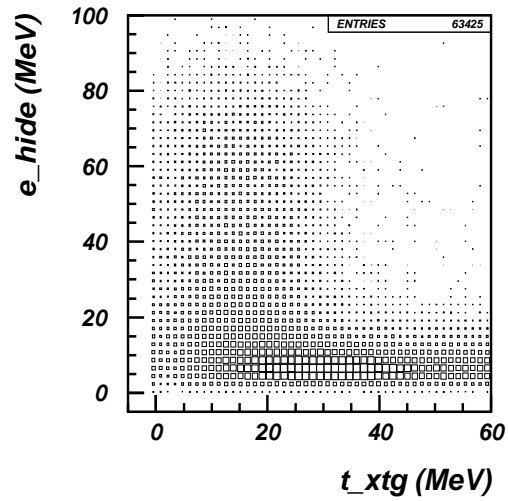


Figure 33: E_{hide} versus T_{xtg} .

Table 35: Rejection of $R_{TGPV.OPSVETO}$ as a function of E_{hide} for loose cuts.

	$T_{xtg} < 0.6$	$T_{xtg} < 1.2$	$T_{xtg} < 1.8$
$E_{hide} < 1.6$	2250/66 = 34	2250/86 = 26	2250/98 = 23
$E_{hide} < 2.5$	6769/100 = 68	6769/129 = 52	6769/149 = 45
$E_{hide} < 4.0$	34992/202 = 173	34992/288 = 122	34992/335 = 104
$E_{hide} < 10.0$	97100/627 = 155	97100/888 = 109	97100/1105 = 88

Table 36: Rejection of $R_{TGPV.OPSVETO}$ as a function of E_{hide} for tight cuts.

	$T_{xtg} < 0.6$	$T_{xtg} < 1.2$	$T_{xtg} < 1.8$
$E_{hide} < 1.6$	389/18 = 22	389/20 = 19	389/22 = 18
$E_{hide} < 2.5$	2282/23 = 99	2282/26 = 88	2282/31 = 74
$E_{hide} < 4.0$	15105/43 = 351	15105/53 = 285	15105/65 = 232
$E_{hide} < 10.0$	37174/160 = 232	37174/206 = 180	37174/269 = 138

cuts respectively the rejection of a T_{xtg} cut (corresponding to the TGPV·OPSVETO cuts) is calculated as a function of the cut on E_{hide} , which simulates the effect of CCDPUL cut.

Since the matching of the energy between UMC and data is uncertain, the cut on E_{hide} is varied from 1.6 to 10 MeV, and the cut on T_{xtg} between 0.6 and 1.8 MeV. The central value for the rejection $R_{TGPV.OPSVETO}$, 52 and 88, are used for background calculation for loose and tight cuts, and the variation with E_{hide} are introduced as the systematic error. The background numbers are summarized in Tab. 37.

15 Acceptance

15.1 Acceptance Factors from $K_{\mu 2}$ Events

$K_{\mu 2}$ events which have an incoming K^+ , one charged track entering the fiducial region, and no photons products are ideal in emulating signal event criteria for beam conditions, target reconstruction, tracking, and photons. To obtain appropriate samples for these aspects of the $K^+ \rightarrow \pi^+ \nu \bar{\nu}$ decay, setup cuts listed in Table 38 were employed.

To measure event reconstruction in the RS, see Table 39, the setup cuts chosen, $Setup_{Recon}$, created a sample with good tracks by requiring that the TG and UTC, which

Table 37: K_{e4} background number normalized to 3/3 data. The first error of $N_{K_{e4}}$ is statistical and the second error is from $R_{TGPV.OPSVETO}$.

	Loose cuts	Tight cuts
N_{norm}	3	1
$R_{TGPV.OPSVETO}$	52^{+121}_{-29}	88^{+263}_{-70}
$N_{K_{e4}}$	$0.18 \pm 0.10^{+0.23}_{-0.12}$	$0.03 \pm 0.03^{+0.14}_{-0.03}$

$K_{\mu 2}$ Setups	Component cuts
$Setup_{RS\ track}$	TRIGGER, ICBIT, $t_{IC} - t_{Ck} > 5$ ns, B4DEDX, UTC, UTC_QUAL
$Setup_{recon}$	TRIGGER, ICBIT, $t_{IC} - t_{Ck} > 5$ ns, B4DEDX, CPITRS, CPITAIL, CKTRS, CKTAIL, BWTRS, RDTRK, TRKTIM, $ t_{IC} - t_{RS} < 5$ ns, PVCUTPNN2(noBV+BVL)
$Setup_{beam}$	TRIGGER, ICBIT, RDTRK, TRKTIM, RDUTM, KM2PBOX, COS3D
$Setup_{PV}$	$Setup_{beam}$, A_{beam} cuts, stopping layer < 19

Table 38: Setup cuts used for the $K_{\mu 2}$ -based acceptance measurements. “ A_{beam} cuts” are the cuts whose acceptance is measured in “beam” category. ICBIT is the online-IC-trigger bit, KM2PBOX selects events with $226\text{ MeV}/c < p_{tot} < 246\text{ MeV}/c$.

are independent of the RS, have a valid reconstruction, a delayed-coincidence style cut using \check{C}_K and IC, K^+ entering the TG (B4DEDX). Measuring the reconstruction efficiency

Cut	Loose Box		Tight Box	
	Events	Acceptance	Events	Acceptance
$Setup_{RS\ track}$	2925784		2925784	
RD_TRK	2925784	1.0000	2925784	1.0000
TRKTIM	2925591	0.9999	2925591	0.9999
A_{RS}	0.99993 ± 0.000005		0.99993 ± 0.000005	

Table 39: RS reconstruction acceptance using $K_{\mu 2}(1)$ monitor events.

of the TG and UTC, see Table 40, requires a sample with a single K^+ (B4DEDX) and no beam π^+ ’s entering the detector (CPITRS, CPITAIL, CKTRS, CKTAIL, BWTRS). A requirement that insures a delayed coincidence using \check{C}_K and IC³ ($t_{IC} - t_{Ck} > 5$ ns), a good charged track traversing the UTC detector ($|t_{IC} - t_{RS}| < 5$ ns, RD_TRK, TRKTIM), and no photons (PVCUTPNN2(noBV+BVL)). BV and BVL photon-vetoing criteria is not used for the A_{RS} sample, so that the sample will not remove events with μ^+ ’s traversing the entire RS and entering the BVL and BV.

The acceptances associated with the beam and target-region cuts require a sample which is definitely a single K^+ decay with no photons. So the $K_{\mu 2}$ decay was chosen with requirements on the track momentum (KM2PBOX), on the quality of the track (RD_TRK, TRKTIM, RDUTM), and on the fiducial region (COS3D). The cuts in Table 41 were ordered in a way that would allow for a more meaningful acceptance value for each cut (e.g. TGQUALT was placed at the beginning because many of the following cuts require a successful TG reconstruction before they work properly.)

³DELCO could not be used in here because DELCO requires a TG reconstruction which in turn requires a reconstructed track from the UTC and RS.

Cut	Loose Box		Tight Box	
	Events	Acceptance	Events	Acceptance
<i>Setup_{recon}</i>	1520985		748449	
RDUTM	1520125	0.9994 ± 0.00002	748183	0.9996 ± 0.00002
TARGET	1520125	1.0000	748183	1.0000
<i>A_{recon}</i>	0.99943 ± 0.000019		0.99965 ± 0.000022	

Table 40: TG and UTC reconstruction acceptance using $K_{\mu 2}(1)$ monitor events.

Cut	Loose Box		Tight Box	
	Events	Acceptance	Events	Acceptance
$Setup_{beam}$	3771613		3771613	
TGCUT	3689137	0.9781 ± 0.00008	3689137	0.9781 ± 0.00008
TGQUALT	3560525	0.9651 ± 0.00010	3560525	0.9651 ± 0.00010
NPITG	3560525	1.0000	3560525	1.0000
TIMCON	3555328	0.9985 ± 0.00002	3555328	0.9985 ± 0.00002
TGTCON	3516829	0.9892 ± 0.00005	3516829	0.9892 ± 0.00005
B4ETCON	3481951	0.9901 ± 0.00005	3481951	0.9901 ± 0.00005
DCBIT	3067147	0.8809 ± 0.00017	3067147	0.8809 ± 0.00017
DELCO	2628388	0.8569 ± 0.00020	2160585	0.7044 ± 0.00026
PSCUT	2493148	0.9485 ± 0.00014	2045546	0.9468 ± 0.00015
B4DEDX	2479504	0.9945 ± 0.00005	2034267	0.9945 ± 0.00005
BWTRS	2275862	0.9179 ± 0.00017	1865809	0.9172 ± 0.00019
CPITRS	2272021	0.9983 ± 0.00003	1862726	0.9983 ± 0.00003
CPITAIL	2270965	0.9995 ± 0.00001	1861874	0.9995 ± 0.00002
CKTRS	2256478	0.9936 ± 0.00005	1852681	0.9951 ± 0.00005
CKTAIL	2220172	0.9839 ± 0.00008	1841678	0.9941 ± 0.00006
B4TRS	2163250	0.9744 ± 0.00011	1792894	0.9735 ± 0.00012
B4CCD	2134064	0.9865 ± 0.00008	1773887	0.9894 ± 0.00008
UPVTRS	2099003	0.9836 ± 0.00009	1745815	0.9842 ± 0.00009
RVTRS	2097001	0.9990 ± 0.00002	1744246	0.9991 ± 0.00002
TGCEO	2012822	0.9599 ± 0.00014	1672775	0.9590 ± 0.00015
B4EKZ	1834958	0.9116 ± 0.00020	1522582	0.9102 ± 0.00022
TGZFOOL	1812291	0.9876 ± 0.00008	1503775	0.9876 ± 0.00009
TARGF	1754010	0.9678 ± 0.00013	1455287	0.9678 ± 0.00014
DTGTTP	1754003	1.0000	1455280	1.0000
RTDIF	1737206	0.9904 ± 0.00007	1441269	0.9904 ± 0.00008
TGKTIM	1720074	0.9901 ± 0.00007	1436006	0.9963 ± 0.00005
EICCON	1673926	0.9732 ± 0.00012	1397533	0.9732 ± 0.00013
TICCON	1673922	1.0000	1397530	1.0000
PIGAP	1659315	0.9913 ± 0.00007	1385358	0.9913 ± 0.00008
TBDB4	1614464	0.9730 ± 0.00013	1347219	0.9725 ± 0.00014
TGDB4TIP	1606252	0.9949 ± 0.00006	1340136	0.9947 ± 0.00006
TGDVXTIP	1602025	0.9974 ± 0.00004	1336547	0.9973 ± 0.00004
TGDVXPI	1566607	0.9779 ± 0.00012	1309007	0.9794 ± 0.00012
PHIVTX	1519604	0.9700 ± 0.00014	1265387	0.9667 ± 0.00016
CCDPUL	687795	0.4526 ± 0.00040	627481	0.4959 ± 0.00044
EPIONK	684627	0.9954 ± 0.00008	624313	0.9950 ± 0.00009
CCDBADTIM	679562	0.9926 ± 0.00010	619649	0.9925 ± 0.00011
CCD31FIB	679553	1.0000	619640	1.0000
TIMKF	613292	0.9025 ± 0.00036	558769	0.9018 ± 0.00038
VERRNG	571441	0.9318 ± 0.00032	520584	0.9317 ± 0.00034
ANGLI	571092	0.9994 ± 0.00003	520260	0.9994 ± 0.00003
ALLKFIT	563903	0.9874 ± 0.00015	513528	0.9871 ± 0.00016
TPICS	563178	0.9987 ± 0.00005	512822	0.9986 ± 0.00005
KIC	563015	0.9997 ± 0.00002	512669	0.9997 ± 0.00002
A_{beam}	0.14928 ± 0.000183		0.13593 ± 0.000176	

Table 41 continued on next page

Table 41 continued from previous page				
Cut	Loose Box		Tight Box	
	Events	Acceptance	Events	Acceptance

Table 41: Target and Beam acceptance based on $K_{\mu 2}(1)$ events

Cut	Loose Box		Tight Box	
	Events	Acceptance	Events	Acceptance
<i>Setup_{PV}</i>	61031		54888	
LHEX	56983	0.9337 ± 0.00101	51233	0.9334 ± 0.00106
HEXAFTER	54888	0.9632 ± 0.00079	49374	0.9637 ± 0.00083
PVONLINE	52544	0.9573 ± 0.00086	47265	0.9573 ± 0.00091
LAY20or21	52129	0.9921 ± 0.00039	46891	0.9921 ± 0.00041
STLAY	51643	0.9907 ± 0.00042	46450	0.9906 ± 0.00045
RSHEX	49767	0.9637 ± 0.00082	44737	0.9631 ± 0.00087
PVCUT	47888	0.9622 ± 0.00085	43045	0.9622 ± 0.00090
TGPVCUT	47425	0.9903 ± 0.00045	42630	0.9904 ± 0.00047
TGPVTR	47425	1.0000	42630	1.0000
TGPV	45969	0.9693 ± 0.00079	39225	0.9201 ± 0.00131
ICPV	45923	0.9990 ± 0.00015	39108	0.9970 ± 0.00028
VCPV	45894	0.9994 ± 0.00012	39033	0.9981 ± 0.00022
COPV	45639	0.9944 ± 0.00035	38884	0.9962 ± 0.00031
MCPV	45634	0.9999 ± 0.00005	38873	0.9997 ± 0.00009
ECinner	42180	0.9243 ± 0.00124	30927	0.7956 ± 0.00205
ECouter	36778	0.8719 ± 0.00163	24669	0.7977 ± 0.00228
EC 2nd	36522	0.9930 ± 0.00043	22849	0.9262 ± 0.00166
RSPV	33844	0.9267 ± 0.00136	16253	0.7113 ± 0.00300
BVPV	31413	0.9282 ± 0.00140	14921	0.9180 ± 0.00215
BVLPV	30914	0.9841 ± 0.00071	14719	0.9865 ± 0.00095
ADPV	29410	0.9513 ± 0.00122	14069	0.9558 ± 0.00169
EARLY _{BV}	29385	0.9991 ± 0.00017	14063	0.9996 ± 0.00017
DSPV	29381	0.9999 ± 0.00007	14061	0.9999 ± 0.00010
EARLY _{BVL}	29381	1.0000	14061	1.0000
<i>PV_{PNN2}</i>	0.6391 ± 0.0022		0.3585 ± 0.0024	
<i>A_{PV}</i>	0.48141 ± 0.002023		0.25618 ± 0.001863	

Table 42: Online and offline photon-veto acceptance using $K_{\mu 2}(1)$ monitor events. PV_{PNN2} is the total acceptance of all offline PV cuts; it is composed of TGPV through EARLY_{BVL}. PV_{PNN2} is not an additional cut.

Measuring the photon-veto criteria required a valid decay and successfully reconstructed $K_{\mu 2}$ event without any additional secondary beam particles at decay time ($Setup_{beam}$, A_{beam}). Since a μ^+ from a $K_{\mu 2}$ decay could penetrate the whole RS and reach the BVL or BV photon detector, a requirement of *stopping layer* < 19 was imposed. Both the online and offline PV cuts are measured with $K_{\mu 2}(1)$ since there was no online PV requirement in the trigger.

15.2 Acceptance Factors from $\pi_{scatter}$ Events

Since the π^+ from $K^+ \rightarrow \pi^+\nu\bar{\nu}$ events has a spectrum of energy and range values, unlike π^+ 's from $K_{\pi 2}$, π_{scat} 's are ideal to measure acceptances dealing with RS kinematics. The π^+ from π_{scat} events have a continuous stopping-layer distribution, as is expected with $K^+ \rightarrow \pi^+\nu\bar{\nu}$ events, which is advantageous in considering possible layer dependences within the RS (such as the TD cuts). The setup cuts used to create these samples are listed in Table 43.

$\pi_{scatter}$ Setups	Component cuts
$Setup_{bad_stc}$	RD_TRK, TRKTIM, STLAY, UTC, RDUTM, PDC, ICBIT, $b4abm2 < 1.3MeV$, $ t_\pi - t_{RS} < 5$ ns, $ t_{IC} - t_{RS} < 5$ ns, TARGF, DTGTTP, RTDIF, TGQUALT, TGZFOOL, CKTRS, CKTAIL, PVCUTPNN2(only RS), COS3D, LAYV4, PNN2BOX
$Setup_{RSkin}$	$Setup_{bad_stc}$, BAD_STC, TDCUT02
$Setup_{\pi \rightarrow \mu \rightarrow e}$	$Setup_{bad_stc}$, BAD_STC, RNGMOM, ZFRF, ZUTOUT, LAYER14, UTC_QUAL, EIC

Table 43: Setup cuts used for the $\pi_{scatter}$ based acceptance measurements. $b4abm2$ is the energy of the B4 hit near beam time.

Creating a sample of single-beam π^+ 's which scatter in the TG required removing events with K^+ particles in the beam ($b4abm2 < 1.3MeV$, CKTRS, CKTAIL); the requirement $|t_\pi - t_{RS}| < 5$ ns requires a scattering of the incoming particle and $|t_{IC} - t_{RS}| < 5$ ns requires that the track in the RS and TG are from the same particle. The RS photon-vetoing requirements are applied so as to remove coincident activity within the RS that would otherwise artificially lower the acceptance. PVPNN2 was not applied due to the photon cuts removing events with additional activity at decay time; since a decay does not occur, timing used by the photon cuts are not as meaningful. The remaining cuts which make up $Setup_{bad_stc}$ require a nicely reconstructed track.

BADSTC, as discussed in Section 8, removes events when the TD in the determined stopping counter was not working properly.

Cut	Loose Box		Tight Box	
	Events	Acceptance	Events	Acceptance
$Setup_{bad_stc}$	153716		73145	
BADSTC	153474	0.9984 ± 0.00010	73089	0.9992 ± 0.00010
A_{badstc}		0.99843 ± 0.000101		0.99923 ± 0.000102

Table 44: BADSTC acceptance using $\pi_{scatter}$ monitor events.

15.3 Range-Stack-Kinematic Acceptance

Measuring the kinematic acceptance in the RS (A_{RSkin}) required further refinements to the sample employed by the A_{badstc} measurement. The particle-identification cuts TDCUT02 were utilized, requiring a stopped π^+ in the RS. Without the TDCUT02 requirement a π^+ , after entering the RS, could decay in flight yielding kinematics similar to a μ^+ or e^+ . A sample with decay-in-flight π^+ 's included would artificially lower A_{RSkin} .

Cut	Loose Box		Tight Box	
	Events	Acceptance	Events	Acceptance
$Setup_{RSkin}$	88719		31525	
UTCQUAL	84373	0.9510 ± 0.00072	30038	0.9528 ± 0.00119
RNGMOM	82845	0.9819 ± 0.00046	29506	0.9823 ± 0.00076
RSDEXMAX	80449	0.9711 ± 0.00058	28764	0.9749 ± 0.00091
RSDEXCL	76828	0.9550 ± 0.00073	27586	0.9590 ± 0.00117
RSLIKE	76828	1.0000	27586	1.0000
PRRF1	76196	0.9918 ± 0.00033	27433	0.9945 ± 0.00045
PRRFZ	73596	0.9659 ± 0.00066	26577	0.9688 ± 0.00105
A_{RSkin}	0.82954 ± 0.001262		0.84305 ± 0.002049	

Table 45: RS-kinematic acceptance using $\pi_{scatter}$ monitor events.

In order to account for the systematics associated with poor target reconstruction of the π_{scat} events, which is a function of the kinematics, the kinematic box cut was varied. The PNN2BOX was the nominal box cut. The size of the smaller and larger box cut was a shrunken or expanded PNN2BOX.

The difference in reconstruction quality for $\pi_{scatter}$ events and K_{π^2} events was evaluated from the resolution of the reconstructed π^+ mass, $m_{\pi} = \frac{ptot^2 - etot^2}{2 \cdot etot}$, of the two samples. The distributions from π_{scat} and $K_{\mu 2}$ samples, shown in Fig. 34, have resolutions of 13.8 and 8.4 respectively. The fractional uncertainty in $\pi_{scatter}$ -target-track reconstruction is therefore $\sqrt{13.8^2 - 8.4^2}/140.0 \simeq 7.8\%$.

Since $ptot$ and $etot$ contribute roughly equally to the resolution, their uncertainties are $7.8\%/\sqrt{2} = 5.5\%$. $rtot$ scales approximately linearly with $etot$, so its uncertainty is also 5.5%. The boundaries of the nominal PNN2 kinematic box were varied by 5.5% yielding

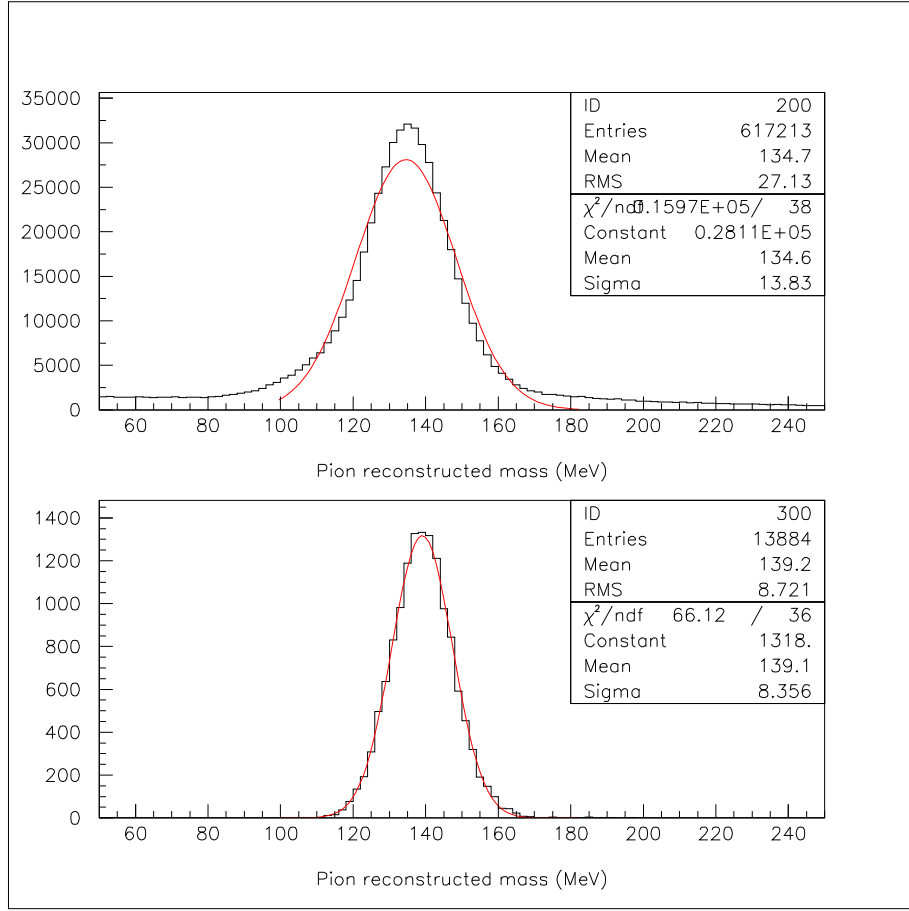


Figure 34: Distributions of the reconstructed π^+ mass from $\pi_{scatter}$ (top) and $K_{\pi 2}$ events (bottom).

the following small and large boxes:

Small box :

$$147.7 \text{ MeV}/c < p_{tot} < 188.1 \text{ MeV}/c$$

$$12.7 \text{ cm} < r_{tot} < 26.5 \text{ cm}$$

$$63.3 \text{ MeV} < e_{tot} < 95.0 \text{ MeV}$$

Large box :

$$132.3 \text{ MeV}/c < p_{tot} < 209.9 \text{ MeV}/c$$

$$11.3 \text{ cm} < r_{tot} < 29.5 \text{ cm}$$

$$56.7 \text{ MeV} < e_{tot} < 106.0 \text{ MeV}$$

The variation in the kinematic box determines the systemic error associated with the RS-kinematic cuts, as determined in Eq. (22).

$$A_{RSkin}^{sys} = \frac{A_{RSkin}^{large\ box} - A_{RSkin}^{small\ box}}{2} \quad (22)$$

Cut	Loose Box		Tight Box	
	Events	Acceptance	Events	Acceptance
$Setup_{RSkin}^{small}$	63400		29195	
UTCQUAL	60350	0.9519 ± 0.00085	27906	0.9558 ± 0.00120
RNGMOM	59251	0.9818 ± 0.00054	27396	0.9817 ± 0.00080
RSDEXMAX	57778	0.9751 ± 0.00064	26746	0.9763 ± 0.00092
RSDEXCL	55375	0.9584 ± 0.00083	25685	0.9603 ± 0.00119
RSLIKE	55375	1.0000	25685	1.0000
PRRF1	55017	0.9935 ± 0.00034	25548	0.9947 ± 0.00045
PRRFZ	53324	0.9692 ± 0.00074	24778	0.9699 ± 0.00107
LAYER14	53324	1.0000	24778	1.0000
$A_{RSkin}^{small\ box}$	0.84107 ± 0.001452		0.84871 ± 0.002097	

Table 46: RS kinematic acceptance using $\pi_{scatter}$ monitor events.

Cut	Loose Box		Tight Box	
	Events	Acceptance	Events	Acceptance
$Setup_{RSkin}^{large}$	110317		51078	
UTCQUAL	104830	0.9503 ± 0.00065	48730	0.9540 ± 0.00093
RNGMOM	102909	0.9817 ± 0.00041	47846	0.9819 ± 0.00060
RSDEXMAX	99517	0.9670 ± 0.00056	46347	0.9687 ± 0.00080
RSDEXCL	94726	0.9519 ± 0.00068	44201	0.9537 ± 0.00098
RSLIKE	94726	1.0000	44201	1.0000
PRRF1	93737	0.9896 ± 0.00033	43806	0.9911 ± 0.00045
PRRFZ	90176	0.9620 ± 0.00062	42205	0.9635 ± 0.00090
LAYER14	90176	1.0000	42205	1.0000
$A_{RSkin}^{large\ box}$	0.81743 ± 0.001163		0.82629 ± 0.001676	

Table 47: RS kinematic acceptance using $\pi_{scatter}$ monitor events.

Eq. (22) is valid when the systematic error is symmetric; this was not the case for the tight signal region. Therefore, the systemic error for the tight region was determined by the difference in the small and large box compared to the nominal box.

Hence, the RS-kinematic acceptance is

$$(23)$$

$$(24)$$

15.4 $\pi^+ \rightarrow \mu^+ \rightarrow e^+$ Identification Acceptance

In an analogous way as the RS-kinematic-acceptance sample was created, the $\pi^+ \rightarrow \mu^+ \rightarrow e^+$ acceptance ($A_{\pi \rightarrow \mu \rightarrow e}$) requires the sample to be purified via cuts which are uncorrelated to the $\pi \rightarrow \mu \rightarrow e$ criteria (or simply TD cuts) being measured. RS-kinematic requirements were used to insure that the track was from a π^+ . Since the $\pi_{scatter}$ did not include the online LEV1.1 and LEV1.2, the acceptances of these online requirements on the $\pi\nu\bar{\nu}(1)$ and $\pi\nu\bar{\nu}(2)$ could also be measured.

RSDEDX is correlated with EV5 due to μ^+ accidentals along the track causing EV5 to reject the event along with RSDEDX rejecting the event due to incorrect dE/dX value. PRRF1's dependence on the stopping-counter energy correlates it to the TD-pulse fitting utilized by TDNN. Tables 48 and 49 show the measured acceptances without and with RSDEDX and PRRF1, PRRFZ included in the setup cuts (A_{TD1} , A_{TD2}), respectively.

$A_{\pi \rightarrow \mu \rightarrow e}$ will be determined by the average of A_{TD1} and A_{TD2} and the systematic error is calculated from the difference. A 1.014% correction for π^+ decay-in-flight and π^+ absorption in the stopping counter, estimated from Monte Carlo, was applied to A_{TD2} .

Cut	Loose Box		Tight Box	
	Events	Acceptance	Events	Acceptance
$Setup_{\pi \rightarrow \mu \rightarrow e}$	126239		60258	
PIFLG	104055	0.8243 ± 0.00107	49850	0.8273 ± 0.00154
RSHEX2	102123	0.9814 ± 0.00042	48999	0.9829 ± 0.00058
LEV1.1	82659	0.8094 ± 0.00123	39953	0.8154 ± 0.00175
LEV1.2	69374	0.8393 ± 0.00128	35850	0.8973 ± 0.00152
TDCUT	65186	0.9396 ± 0.00090	33754	0.9415 ± 0.00124
ELVETO	62425	0.9576 ± 0.00079	32471	0.9620 ± 0.00104
TDFOOL	62208	0.9965 ± 0.00024	32365	0.9967 ± 0.00032
TDNN	58607	0.9421 ± 0.00094	27401	0.8466 ± 0.00200
EV5	58607	1.0000	22794	0.8319 ± 0.00226
A_{TD1}	0.46425 ± 0.001404		0.37827 ± 0.001976	

Table 48: $\pi^+ \rightarrow \mu^+ \rightarrow e^+$ acceptance using $\pi_{scatter}$ monitor events.

Hence, the RS kinematic acceptance is

$$A_{\pi \rightarrow \mu \rightarrow e} = 0.4805 \pm 0.0015 \pm 0.016 \quad (25)$$

Cut	Loose Box		Tight Box	
	Events	Acceptance	Events	Acceptance
<i>Setup</i> $_{\pi \rightarrow \mu \rightarrow e}$	126239		60258	
RSDEDXMAX				
RSDEDXCL				
RSLIKE				
PRRF1				
PRRFZ	107124		51828	
PIFLG	90161	0.8417 ± 0.00112	43749	0.8441 ± 0.00159
RSHEX2	88616	0.9829 ± 0.00043	43045	0.9839 ± 0.00060
LEV1.1	72545	0.8186 ± 0.00129	35471	0.8240 ± 0.00184
LEV1.2	61913	0.8534 ± 0.00131	32333	0.9115 ± 0.00151
TDCUT	58288	0.9415 ± 0.00094	30492	0.9431 ± 0.00129
ELVETO	55833	0.9579 ± 0.00083	29339	0.9622 ± 0.00109
TDFOOL	55655	0.9968 ± 0.00024	29255	0.9971 ± 0.00031
TDNN	52472	0.9428 ± 0.00098	24807	0.8480 ± 0.00210
EV5	52472	1.0000	20673	0.8334 ± 0.00237
$A_{uncorr\ TD2}$	0.48983 ± 0.001527		0.39888 ± 0.002151	
π^+ DIF/abs	$\times 1.014$			
A_{TD2}	0.4967 ± 0.0015		0.4045 ± 0.0022	

Table 49: $\pi^+ \rightarrow \mu^+ \rightarrow e^+$ acceptance using $\pi_{scatter}$ monitor events. $A_{uncorr\ TD2}$ is the acceptance before the correction factor for decay-in-flight (DIF) and π^+ absorption (abs) in the stopping counter (π^+ DIF/abs).

15.5 Acceptance Factors from $K_{\pi 2}$ Events

Within the E949 analysis, events from $K_{\pi 2}(1)$ monitors are similar to $K^+ \rightarrow \pi^+ \nu \bar{\nu}$ events in a few aspects: (1) They both have a single π^+ track emerging from a single incoming K^+ . (2) The π^+ within the TG is minimum ionizing. Condition (1) allows for a valid target reconstruction with a good decay-vertex determination. These properties allow acceptances to be measured for target kinematics.

$K_{\pi 2}$ Setups	Component cuts
$Setup_{utc}$	TRIGGER, RD_TRK, TRKTIM, STLAY, BAD_STC
$Setup_{ops}$	$Setup_{utc}$, UTC, RDUTM, PDC, PSCUT06, KCUTS, TGCUT06 without the ones measured, TDCUT02, KP2BOX
$Setup_{TGkin}$	$Setup_{ops}$, OPSVETO, TGPVCUT

Table 50: Setup cuts used for the $K_{\pi 2}$ -based acceptance measurements.

To obtain a sample of PNN2 signal-like events, setup cut in Table 50 were utilized on $K_{\pi 2}(1)$ triggers. Measuring the acceptance of the PASS1 UTC cuts required reconstructing the TG and RS.

Cut	Events	Acceptance
$Setup_{utc}$	1502895	
UTC	1417906	0.9435 ± 0.00019
A_{utc}		0.94345 ± 0.000188

Table 51: UTC acceptance using $K_{\pi 2}(1)$ monitor events.

The acceptance measurement of OPSVETO, Table 52, requires a sample with valid reconstruction within the TG and RS along with the requirement that there are no secondary beam particles (PSCUT06). Applying KP2BOX and TDCUT02 further purifies the sample to be valid $K_{\pi 2}$ decays.

Cut	Events	Acceptance
$Setup_{ops}$	62989	
OPSVETO	61365	0.9742 ± 0.00063
A_{tgkin}		0.97422 ± 0.000631

Table 52: OPSVETO acceptance using $K_{\pi 2}(1)$ monitor events.

Obtaining the best sample to measure acceptance of target kinematics is a combination of (1) good TG reconstruction, which is not available in a $\pi_{scatter}$ sample due to poor

reconstruction of the TG at very small delayed-coincidence, and (2) π^+ 's with kinetic energies spread throughout the PNN2 signal region ($60.0\text{MeV} \leq E_{\pi^+} \leq 100.5\text{MeV}$), which is not available in a $K_{\pi_2}(1)$ sample. That is, E949 monitor samples do not satisfy both (1) and (2). In the $\pi_{scatter}$ sample, TG fiber hits may be identified as a π^+ -fiber near the scattering point (ideally reconstructed as the decay vertex) could have energy much greater than a normal π^+ from a $K^+ \rightarrow \pi^+\nu\bar{\nu}$ decay. Thus, using a $\pi_{scatter}$ sample would yield a TG kinematic acceptance systematically lower than the true value.

Measuring the acceptance of TGDEDX with the sample used for calibration, $\pi_{scatter}$, would bias the acceptance measurement (see Section 7.3). Therefore, the clean K_{π_2} sample obtained by applying $Setup_{TGkin}$ is employed. The rest of the cuts in Table 53 employed the K_{π_2} sample due to their dependence on good determination of the decay vertex and assuming no π^+ energy dependence.

Cut	Loose Box		Tight Box	
	Events	Acceptance	Events	Acceptance
$Setup_{TGkin}$	60696		36719	
TGDEDX	60044	0.9893 ± 0.00042	36319	0.9891 ± 0.00054
TGER	60029	0.9998 ± 0.00006	36310	0.9998 ± 0.00008
TGENR	58065	0.9673 ± 0.00073	35058	0.9655 ± 0.00096
TGLIKE1	57014	0.9819 ± 0.00055	34413	0.9816 ± 0.00072
TGLIKE2	56103	0.9840 ± 0.00053	33858	0.9839 ± 0.00068
EPITG	50297	0.8965 ± 0.00129	30427	0.8987 ± 0.00164
EPIMAXK	50297	1.0000	30427	1.0000
TGEDGE	50018	0.9945 ± 0.00033	30271	0.9949 ± 0.00041
DRP	49932	0.9983 ± 0.00019	30214	0.9981 ± 0.00025
CHI567	43649	0.8742 ± 0.00148	26432	0.8748 ± 0.00190
CHI5MAX	43648	1.0000 ± 0.00002	26431	1.0000 ± 0.00004
A_{tgkin}	0.71913 ± 0.001824		0.71982 ± 0.002344	

Table 53: TG kinematic acceptance using $K_{\pi_2}(1)$ monitor events.

15.6 UMC based acceptance

The acceptance of the online trigger and the phase space and solid angle cuts and the acceptance loss due to pion decay-in-flight and pion nuclear interactions (“NIDIF”) are calculated with $K^+ \rightarrow \pi^+\nu\bar{\nu}$ Monte Carlo simulated events. About 10^5 signal events were generated with NIDIF on and another 10^5 with NIDIF off. The trigger A_{tr} and phase space A_{ps} acceptance are measured with NIDIF-off sample, and then are corrected for NIDIF by comparing with the NIDIF-on sample (A_{NIDIF}). The results are shown in Tab. 54. UFATE, USTMED and USTOP_HEX cuts are based on UMC truth variables. UFATE requires that the pion stopped without decay or interaction. USTMED requires that the pion stopped in the RS scintillator, and USTOP_HEX requires that the offline

reconstructed stopping counter agrees with the real one. The SETUP cut is $ptot < 300 \text{ MeV}$.

	NIDIF on	NIDIF off
	99999	100000
T•2	39227	41036
$3_{ct} \cdot 4_{ct} \cdot 5_{ct} \cdot 6_{ct}$	27575	33742
pnn1 or pnn2	26288	32914
A_{tr}	0.2629 ± 0.0014	0.3291 ± 0.0015
SETUP	25793	32887
UFATE	22688	32887
USTMED	22517	32620
USTOP_HEX	21743	32500
COS3D	20870	31294
LAYER14	20838	31282
ZFRF	20175	30083
ZUTOUT	20148	30063
Ke4 BOX	7758	10812
A_{Ke4}	0.3008 ± 0.0029	0.3288 ± 0.0026
Loose BOX	9552	13334
A_{loose}	0.3703 ± 0.0030	0.4054 ± 0.0027

Table 54: UMC based acceptance.

15.7 Acceptance Summary

The total acceptance is summarized in Table 55.

	Loose Box	Tight Box
$A_{K\mu 2}$	0.07183 ± 0.001981	0.0348 ± 0.0074
$A_{\pi_{scat}}$	$0.3980 \pm 0.0014 \pm 0.014$	$0.3297 \pm 0.0020^{+0.011}_{-0.013}$
$A_{K\pi 2}$	0.6610 ± 0.0017	0.6612 ± 0.0022
A_{UMC}	$0.0974 \pm 0.0021 \pm 0.0097$	$0.0791 \pm 0.016 \pm 0.0079$
A_{tot}	$(1.778 \pm 0.063) \times 10^{-3}$	$(0.600 \pm 0.176 \pm 0.0600) \times 10^{-3}$

Table 55: Total acceptance for PNN2.

16 Kaon exposure

17 Single Cut Failure Study

Group	skim	new
Box	37	36
Photon	192	190
ADPV	1	
Delco		
B4EKZ		
TGZ		
TGE	1	1
EKAON	3	3
IC	1	1
TD		
Kinematics	2	2
Beam		
Other	3	3
Total	240	236

Table 56: 1-cut failures. Skim column is the results of the study done in June 2007 for the data processed from the skimmed sample from disk (and before creation of safety cuts). *new* column is the new data processed from tape.

All events from the 'skim' (June 2007) and the 'new' (Oct 2007) studies have been verified that they are the same events (barring the events that are now 2-cut failures).

The numbers are consistent. We have changed a few cuts and included some safety cuts. The change of 2 PV was expected from the *EARLY_{BVL}* safety cut. The change of 1 in the ADPV was due to a change in the CCDPUL-cuts (I believe CCDBADTIM was created to remove events such as this). However, further investigation to determine if there is a one-to-one correspondence of the single-cut failures in each group and determine the fate of the events that no longer in the single-cut sample.

17.1 Events Removed by Safety Cuts

17.1.1 Change in Box Group

Event 255066 Run 49069 is no longer in the single-cut failures. The event is now a 2-cut failure by also failing the Photon-Veto Group. This was expected as π^0 photons were completely contained in this event leading to *EARLY_{BVL}* cut failing.

17.1.2 Change in PV Group

- Event 87966 Run 50179 is no longer in the single-cut failure list. It now fails the EKaon group as well as the PV. CCDBADTIM was created to remove this event.

- Event 24636 Run 50086 now also fails Ekaon. CCDBADTIM was created to remove this event.

17.1.3 Change in ADPV Group

Event 19149 Run 49905 now also fails the Ekaon group. CCDBADTIM was created to remove this event.

18 Sensitivity

18.1 Single event sensitivity

18.2 E949 pnn2 Cell definition

Nine cells are defined for E949 pnn2 analysis. They are based on the combinations of the following four cuts.

- KIN: Ke4 phobic box,
- PV: Tight PV, at 30% offline acceptance,
- DELCO: DELCO6,
- TD: E949 PNN1-level TDCUTS: include ev5 and tight tdvarnn.

Ke4 phobic box can effectively suppress K_{e4} and $K_{\pi 2}$ background. The rejection of Ke4 phobic box on K_{e4} background is estimated with UMC sample like in Sec. 5.2, while the rejection on $K_{\pi 2}$ background is estimated with its normalization branch. The rejection of TGPV·OPSVETO for K_{e4} background and the rejection of PVCUT for $k_{\pi 2}$ are not sensitive for this change of kinematic range. When tightening the upper bound of kinematic cut, the possible momentum of π^+ from $k_{\pi 2\gamma}$ decay will decrease. Correspondingly the minimum energy of the inner bremsstrahlung increases. The higher the energy of the gamma is, the higher rejection of PVCUT. So besides shrinking the effect phase space of $k_{\pi 2\gamma}$ background, tightening kinematic cut also contributes more rejection. However its rejection is almost the same with acceptance loss. Muon, beam and CEX background are thought to be not dramatically affected by this cut. Acceptance loss are taken into account for the decrease of these background.

Only muon background situation is significantly improved by tightening TDCUTS. Acceptance loss are used to explain the decrease of the others background.

DELCO will suppress single beam and CEX background. However single beam background is only several percents of total beam background. Attention is only put onto CEX background.

Tight PV cut also suppress $k_{\pi 2}$ and $k_{\pi 2\gamma}$ background. Acceptance loss are calculated for the other background.

The rejections of these cuts and the acceptance losses of them are summarized in 57.

	KIN	TD	DELCO	PV
Acc loss	81.2%	81.5%	91.1%	54.7%
Rej for specific bkg	2.0 (Kp2) 2.7 (Ke4) 1.2 (Kp2g)	4.2 (Muon)	6.7 (CEX)	2.5 (kp2,kp2g)

Table 57: Acceptance loss and rejection for each background.

The low statistics in pnn2 background study does not allow a more intensive analysis for these four cuts and does not allow to have too more cells. And from the metarial

shown in the following sections one can find that more cells also does not provide more useful information for signal search and final BR measurement. Tab. 58 gives a summary for the acceptance and background. Tab. 59 is a breakdown of each kind of backgrounds in each cells. Loose is for entire E949 pnn2 search region. Shorthand KIN means KIN is applied in addition to the loose cuts. And KIN* means the counterpart of KIN is applied in addition to the loose cuts. (KIN* = Loose kinematic box - tight kinematic box) The same definitions is also used to TD, TD*, DC, DC*, PV and PV*. The 9th cell is defined to the cell with KIN* since it has low acceptance and poor Acc/Bkg. No separation is done for that cell. $Kp2$ RS background is assumed zero here.

Cell No.	Cuts	Acc	Total bkg	Acc/Bkg
	Loose	1.000	$0.973 \pm 0.219^{+0.307}_{-0.244}$	1.028
9	KIN*	0.188	$0.441 \pm 0.112^{+0.161}_{-0.128}$	0.427
	KIN	0.812	$0.532 \pm 0.112^{+0.146}_{-0.117}$	1.526
1	KIN +TD +DC +PV	0.330	$0.152 \pm 0.032^{+0.040}_{-0.035}$	2.166
2	KIN +TD +DC +PV*	0.273	$0.184 \pm 0.043^{+0.035}_{-0.048}$	1.489
3	KIN +TD +DC*+PV	0.032	$0.043 \pm 0.017^{+0.025}_{-0.008}$	0.754
4	KIN +TD +DC*+PV*	0.027	$0.041 \pm 0.014^{+0.021}_{-0.008}$	0.651
5	KIN +TD*+DC +PV	0.075	$0.043 \pm 0.012^{+0.009}_{-0.008}$	1.729
6	KIN +TD*+DC +PV*	0.062	$0.049 \pm 0.013^{+0.008}_{-0.011}$	1.268
7	KIN +TD*+DC*+PV	0.007	$0.011 \pm 0.004^{+0.006}_{-0.002}$	0.693
8	KIN +TD*+DC*+PV*	0.006	$0.010 \pm 0.003^{+0.005}_{-0.002}$	0.605

Table 58: Acceptance and background summary of each cell. All the acceptance is normalized to that in loose cuts.

18.3 Junk method

Junk method is used for computing approximate confidence levels for searches for new particles where the expected signal and background levels are small enough to require the use of Poisson statistics. The results of many independent searches for the same particle may be combined easily, regardless of the discriminating variables which may be measured for the candidate events. The effects of systematic uncertainty in the signal and background models are incorporated in the confidence levels. The original paper is presented by Thomas Junk ([16]). Some effective tools can also be found in this website [18]. And more recent effort on this subject can be found in another web [19]. An intensive study on this method and its tools have been done since pnn1 analysis, like [17]. Here only the sketch of this method is explained.

For the case of n independent counting search analyses, one may define a test statistic X which discriminates signal-like outcomes from background-like ones. A choice for the test statistic is the likelihood ratio. If the estimated signal in the i th channel is s_i , the estimated background is b_i , and the number of observed candidates is d_i , then the

cuts	kp2 TG	kp2 RS	Beam	Muon	Ke4	Kp2g	CEX
Loose	$0.575 \pm 0.184^{+0.063}_{-0.201}$	0.0 ± 0.0	0.045 ± 0.020	0.031 ± 0.031	$0.180 \pm 0.100^{+0.230}_{-0.120}$	$0.050 \pm 0.008 \pm 0.003$	$0.092 \pm 0.053^{+0.070}_{-0.018}$
KIN*	$0.288 \pm 0.092^{+0.032}_{-0.101}$	0.0 ± 0.0	0.009 ± 0.004	0.006 ± 0.006	$0.113 \pm 0.063^{+0.145}_{-0.076}$	$0.008 \pm 0.001 \pm 0.001$	$0.017 \pm 0.010^{+0.013}_{-0.003}$
KIN	$0.288 \pm 0.092^{+0.032}_{-0.101}$	0.0 ± 0.0	0.037 ± 0.016	0.025 ± 0.025	$0.067 \pm 0.037^{+0.085}_{-0.044}$	$0.042 \pm 0.007 \pm 0.003$	$0.075 \pm 0.043^{+0.057}_{-0.015}$
KIN+TD +DC +PV	$0.085 \pm 0.027^{+0.009}_{-0.030}$	0.0 ± 0.0	0.015 ± 0.007	0.003 ± 0.003	$0.027 \pm 0.015^{+0.035}_{-0.018}$	$0.017 \pm 0.003 \pm 0.001$	$0.005 \pm 0.003^{+0.004}_{-0.001}$
KIN+TD +DC +PV*	$0.128 \pm 0.041^{+0.014}_{-0.045}$	0.0 ± 0.0	0.012 ± 0.006	0.002 ± 0.002	$0.022 \pm 0.013^{+0.029}_{-0.015}$	$0.014 \pm 0.002 \pm 0.001$	$0.004 \pm 0.002^{+0.003}_{-0.001}$
KIN+TD +DC*+PV	$0.008 \pm 0.003^{+0.001}_{-0.003}$	0.0 ± 0.0	0.002 ± 0.001	0.000 ± 0.000	$0.003 \pm 0.002^{+0.003}_{-0.002}$	$0.002 \pm 0.000 \pm 0.000$	$0.028 \pm 0.016^{+0.022}_{-0.006}$
KIN+TD +DC*+PV*	$0.013 \pm 0.004^{+0.001}_{-0.004}$	0.0 ± 0.0	0.001 ± 0.001	0.000 ± 0.000	$0.002 \pm 0.001^{+0.003}_{-0.002}$	$0.001 \pm 0.000 \pm 0.000$	$0.024 \pm 0.014^{+0.018}_{-0.005}$
KIN+TD*+DC +PV	$0.019 \pm 0.006^{+0.002}_{-0.007}$	0.0 ± 0.0	0.003 ± 0.002	0.009 ± 0.009	$0.006 \pm 0.003^{+0.008}_{-0.004}$	$0.004 \pm 0.001 \pm 0.000$	$0.001 \pm 0.001^{+0.001}_{-0.000}$
KIN+TD*+DC +PV*	$0.029 \pm 0.009^{+0.003}_{-0.010}$	0.0 ± 0.0	0.003 ± 0.001	0.008 ± 0.008	$0.005 \pm 0.003^{+0.007}_{-0.004}$	$0.003 \pm 0.001 \pm 0.000$	$0.001 \pm 0.001^{+0.001}_{-0.000}$
KIN+TD*+DC*+PV	$0.002 \pm 0.001^{+0.000}_{-0.001}$	0.0 ± 0.0	0.000 ± 0.000	0.001 ± 0.001	$0.001 \pm 0.003^{+0.001}_{-0.000}$	$0.000 \pm 0.000 \pm 0.000$	$0.006 \pm 0.004^{+0.005}_{-0.001}$
KIN+TD*+DC*+PV*	$0.003 \pm 0.001^{+0.000}_{-0.001}$	0.0 ± 0.0	0.000 ± 0.000	0.001 ± 0.001	$0.001 \pm 0.000^{+0.001}_{-0.000}$	$0.000 \pm 0.000 \pm 0.000$	$0.005 \pm 0.003^{+0.004}_{-0.001}$

Table 59: Detailed background information of each cell.

likelihood ratio is:

$$X = \prod_{i=1}^n X_i$$

with

$$X_i = \frac{e^{-(s_i+b_i)}(s_i + b_i)^{d_i}}{d_i!} / \frac{e^{-b_i}b_i^{d_i}}{d_i!}$$

The confidence level for excluding the possibility of simultaneous presence of new particle production and background (the $s + b$ hypothesis) is

$$CL_{s+b} = P_{s+b}(X \leq X_{obs})$$

i.e., the probability, assuming the presence of both signal and background at their hypothesized levels, that the test statistic would be less than or equal to that observed in the data. This probability is the sum of Poisson probabilities

$$P_{s+b}(X \leq X_{obs}) = \sum_{X(d'_i) \leq X(d_i)} \prod_{i=1}^n \frac{e^{-(s_i+b_i)}(s_i + b_i)^{d'_i}}{d'_i!}$$

where $X(d_i)$ is the test statistic computed for the observed set of candidates in each channel d_i , and the sum runs over all possible configurations d'_i which have test statistics less than or equal to the observed one.

Another confidence level is for background alone,

$$CL_b = P_b(X \leq X_{obs})$$

where the probability sum assumes the presence only of the background. i.e.

$$P_b(X \leq X_{obs}) = \sum_{X(d'_i) \leq X(d_i)} \prod_{i=1}^n \frac{e^{-b_i}b_i^{d'_i}}{d'_i!}$$

The modified confidence level CL_s is defined as:

$$CL_s = CL_{s+b}/CL_b$$

And CL is introduced:

$$CL = 1 - CL_s$$

This CL is an extension of the common single channel confidence level calculation [20]. It doesn't have the traditional probability explanation of confidence level. (Classic Bayesian description: given s_i and d_i , the probability of finding more than or equal to d_i events is CL .) However the CL of Junk method shows the same trend with Bayesian's result. And they are totally the same for single channel case.

18.4 BR measurement

18.4.1 Repeat the result of E949 pnn1 publication

18.4.2 E949 pnn2 only

18.4.3 E787 and E949 pnn2 only

18.4.4 All E787 and E949 result

18.4.5 Correlated and Uncorrelated uncertainties

19 Measurement of the $K_{\pi 2}$ branching fraction

19.1 Introduction and experimental data

The purpose of $K_{\pi 2}$ branching fraction measurement using the $K_{\pi 2}(1)$ monitor sample is to check the validity of the f_s calculation and provide a consistency check of the pnn2 acceptance.

The $K_{\pi 2}(1)$ monitor data set of the 2002 data taking run has been used in this analysis. Data have been taking by following trigger conditions:

$$(ONLINE\ TRIGGER)_{K_{\pi 2}} = KB \times T \cdot 2 \times (6_{ct} + 7_{ct}) \times \overline{19}_{ct} \quad (26)$$

and with prescale factors of 163840 (runs 47737-48045) and 131072 after run 48045. The number of $K_{\pi 2}$ events, number of beam K^+ -mesons, and prescale factor versus run are shown on Fig. 35. It should be noted that a small fraction of $K_{\pi 2}(1)$ monitor data was not used in analysis because of the absence end-of-spill information. Also note that no offline prescaling was applied to the $K_{\pi 2}(1)$ monitor data for this analysis. For some runs (about 50) the prescaler factor in the prescaler file was not defined and have been taken equal to prescaler of previous run.

The $K_{\pi 2}$ branching fraction is calculated according to following equation:

$$BR(K_{\pi 2}) = \frac{N_{K_{\pi 2}}}{\epsilon_{T \cdot 2 \cdot IC} \cdot (KB_{live})_{K_{\pi 2}} \cdot A_{K_{\pi 2}, Br} \cdot A_{K_{\pi 2}, kin}^{UMC} \cdot f_s \cdot A_{K_{\pi 2}, trig}^{UMC}} \quad (27)$$

where:

$$A_{K_{\pi 2}, Br} = A_{RD, Br} \times A_{RECO, Br} \times A_{REST, Br} \times A_{IPIFLG} \times A_{\mu}^{acc} \quad (28)$$

The values of f_s , $\epsilon_{T \cdot 2 \cdot IC}$, A_{μ}^{acc} (acceptance loss due to the $\overline{19}_{ct}$ requirement), and A_{IPIFLG} are taken from the 2002 PNN1 analyses [21]. The values of $A_{RD, Br}$, $A_{RECO, Br}$ and $A_{REST, Br}$ are given in Table 62. The values of $A_{K_{\pi 2}, kin}^{UMC}$ and $A_{K_{\pi 2}, trig}^{UMC}$ are given in Table 60. The value of $N_{K_{\pi 2}}$ is given in Table 61.

19.2 Monte Carlo kinematic and trigger acceptances

The kinematic and trigger acceptances for $K_{\pi 2}$ events have been defined by Monte Carlo simulation and are presented in Table 60 along with the result of 2002 PNN1 analyses [17] for comparison. The following additional cuts to remove muons, duplicate events and

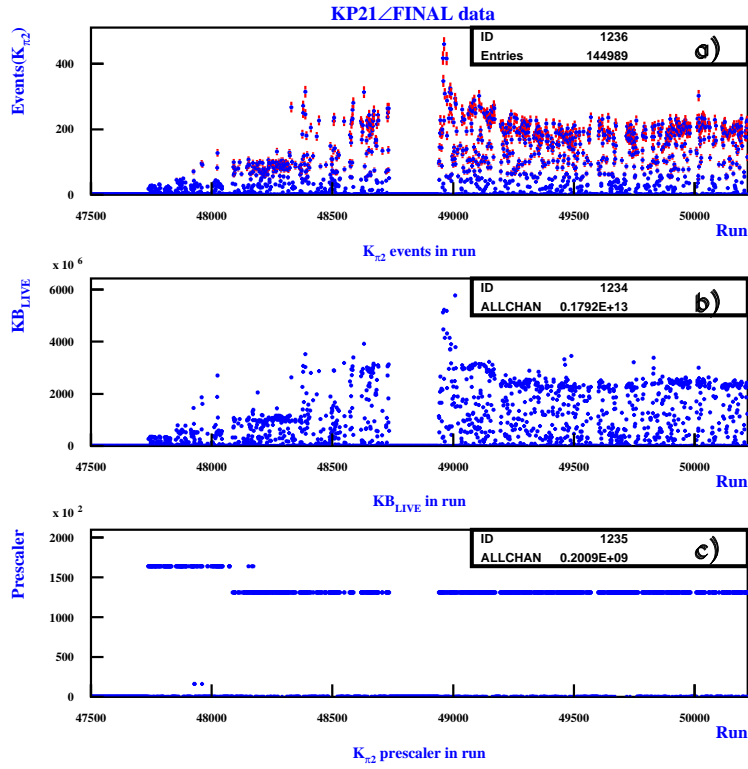


Figure 35: The $K_{\pi 2}$ a) events, b) beam K^+ -mesons and c) prescale factor versus run number.

poorly reconstructed tracks are applied as setup or at the TRIGGER level in Tables 60, 61 and 62:

1. Remove $K_{\mu 2}$ and duplicate events $(rngmom_new3(0.) \leq 3) \cdot \overline{cut(6)}$
2. $tlay \leq 21$
3. $PTOT \neq 0 \cdot PTOT \neq 300$

It should be noted that these cuts do not affect the UMC data sample. Also note that the KP2BOX cut in the PNN1 analysis,

$$KP2BOX = |RDEV| < 3 \cdot |EDEV| < 3 \cdot |PDEV| < 3 \quad (29)$$

differs from the KP2BOX cut in this analysis. The description of the KP2BOX cut and the UMC cuts are in Sec. 19.6. Note that $A_{K_{\pi 2}, trig}^{UMC}$ is consistent with the 2002 measurement and that $A_{K_{\pi 2}, recon}^{UMC}$ and $A_{K_{\pi 2}, kin}^{UMC}$ differ due to changes in the UTCQUAL and TARGET cuts, and the KP2BOX cuts, respectively.

Cut	2002 (acc.)	2007 (acc.)
KT	49997	99993
T•A	22697(0.45397)	44891(0.44894)
Reach Layer B	19090(0.84108)	37605(0.83769)
$\overline{T9_{ct}}$	18797(0.98465)	36986(0.98354)
UFATE	15910(0.84641)	31222(0.84416)
USTMED	15568(0.97850)	30518(0.97745)
USTOP_HEX	13909(0.89344)	27426(0.89868)
$A_{K_{\pi 2}, trig}^{UMC}$	0.27820 ± 0.00200	0.27428 ± 0.00141
UTC/RANGE	13909(1.00000)	—————
RDUTM	—————	27426(1.00000)
UTCQUAL	12660 (0.91020)	26910(0.98119)
TARGET	12532 (0.98989)	—————
TARGET+TGQUALT	—————	25659(0.95351)
$A_{K_{\pi 2}, recon}^{UMC}$	0.90100 ± 0.00253	0.93557 ± 0.00148
KPI2STOP	12072 (0.96329)	24639(0.96025)
COS3D	11878 (0.98393)	23671(0.96071)
KP2BOX(PNN1)	10840 (0.91261)	—————
KP2BOX(PNN2)	—————	20213(0.85391)
$A_{K_{\pi 2}, kin}^{UMC}$	0.86499 ± 0.00305	0.78775 ± 0.00255
$A_{K_{\pi 2}}^{UMC}$	0.2168 ± 0.0018	0.20214 ± 0.00127

Table 60: UMC $K_{\pi 2}$ acceptance of cuts applied in the $K_{\pi 2}$ branching fraction analysis. NIDIF is on.

19.3 K_{π_2} event selection

The cuts applied to $K_{\pi_2}(1)$ monitor data to select the K_{π_2} events are shown in table 61 and compared to the results of the 2002 PNN1 analysis in K-038 [17]. There are differences in the relative acceptance of some cuts due to changes to the cut definition for the PNN2 analysis (UTCQUAL, TGQUALT, B4EKZ, and KP2BOX) and the application of cuts at the TRIGGER level as described in Sec. 19.2.

19.4 Acceptance factors for the K_{π_2} branching fraction

The values of the acceptance factors $A_{RD,Br}$, $A_{RECO,Br}$ and $A_{REST,Br}$ are given in Table 62 along with a comparison to that for the PNN1 analysis taken from Table 23 of Ref. [17].

Cut & discrepancy	$N_{K_{\pi 21}}$ 2002	$N_{K_{\pi 21}}$ 2007	$N_{K_{\pi 21}} \times PS \times 10^{-10}$
ALL 0.000%	84844(0.000)	1938973(0.000)	25.4999(0.000)
BAD_RUN 1.254%	84803(0.99952)	1913712(0.98697)	25.3029(0.99227)
TRIGGER 54.108%	84803(1.00000)	878246(0.45892)	11.6109(0.45888)
BAD_STR 0.009%	84388(0.99511)	873864(0.99501)	11.5521(0.99494)
RD_TRK 0.000%	84388(1.00000)	873864(1.00000)	11.5521(1.00000)
TRKTIM 0.000%	84388(1.00000)	873864(1.00000)	11.5521(1.00000)
RDUTM 0.000%	84388(1.00000)	873864(1.00000)	11.5521(1.00000)
UTCQUAL -7.029%	67194(0.79625)	757238(0.86654)	10.0093(0.86645)
TARGET+TGQUALT 5.639%	65495(0.97471)	695393(0.91833)	9.19259(0.91841)
COS3D 3.695%	64425(0.98366)	658341(0.94672)	8.70245(0.94668)
B4DEDX 0.538%	62832(0.97527)	638520(0.96989)	8.43952(0.96979)
CPITRS 0.407%	61933(0.98569)	626788(0.98163)	8.28465(0.98165)
CPITAIL 0.007%	61882(0.99918)	626228(0.99911)	8.27728(0.99911)
ICBIT 0.001%	61857(0.99960)	625970(0.99959)	8.27389(0.99959)
TIC -0.429%	61352(0.99184)	623545(0.99613)	8.24150(0.99608)
TIMCON 0.193%	60882(0.99234)	617564(0.99041)	8.16218(0.99038)
TGTCON 0.332%	60212(0.98899)	608715(0.98567)	8.04531(0.98568)
DCBIT -0.542%	51016(0.84727)	519045(0.85269)	6.86302(0.85305)
DELC -0.236%	44193(0.86626)	450851(0.86862)	5.96163(0.86866)
CKTRS 0.082%	42835(0.96927)	436628(0.96845)	5.77414(0.96855)
CKTAIL -0.042%	41570(0.97047)	423918(0.97089)	5.60547(0.97079)
BWTRS 0.088%	39270(0.94467)	400092(0.94380)	5.28988(0.94370)
RVUPV -0.090%	38354(0.97667)	391120(0.97757)	5.17075(0.97748)
TARGF 0.324%	36430(0.94984)	370232(0.94659)	4.89491(0.94665)
DTGTTP -0.018%	36422(0.99978)	370219(0.99996)	4.89474(0.99996)
RTDIF -0.031%	36039(0.98948)	366439(0.98979)	4.84457(0.98975)
TGQUALT 0.000%	36039(1.00000)	366439(1.00000)	4.84457(1.00000)
PIGAP 0.175%	35657(0.98940)	361912(0.98765)	4.78419(0.98754)
TGB4 1.362%	33611(0.94262)	336217(0.92900)	4.44510(0.92912)
KIC -0.084%	33118(0.98533)	331568(0.98617)	4.38364(0.98617)
TGCEO 0.528%	27505(0.83052)	273622(0.82524)	3.61775(0.82528)
B4EKZ 4.915%	26657(0.96917)	251738(0.92002)	3.32839(0.92002)
B4ETCON -0.064%	26523(0.99497)	250633(0.99561)	3.31343(0.99550)
TGZFOOL 1.266%	26523(1.00000)	247461(0.98734)	3.27153(0.98735)
PV_noBV 0.000%	26523(1.00000)	247461(1.00000)	3.27153(1.00000)
IPIFLG 0.181%	18688(0.70460)	173913(0.70279)	2.29944(0.70286)
KPI2BOXM 4.515%	16469(0.88126)	145410(0.83611)	1.92215(0.83592)
KP2STOP -0.099%	16405(0.99611)	144989(0.99711)	1.91660(0.99711)
RTOT40 0.000%	16405(1.00000)	144989(1.00000)	1.91660(1.00000)
$N_{K_{\pi 2}}$ 2.836%	16405(0.193)	144989(0.165)	1.91660(0.165)

Table 61: The number of selected $K_{\pi 2}$ candidate events with a comparison to the 2002 PNN1 results.

Cut Acc2002-Acc2007%	$N_{K_{\pi 21}}$ (Acc) 2002	$N_{K_{\pi 21}}$ (Acc) 2007
SETUP_{RD}	51416	490579
RD_TRK 0.000%	51416(1.00000)	490579(1.00000)
TRKTIM 0.000%	51416(1.00000)	490579(1.00000)
A_RD,Br 0.000%	1.00000 \pm 0.00000	1.00000 \pm 0.00000
SETUP_{RECON}	32980	449621
RDUTM 0.000%	32980(1.00000)	449621(1.00000)
UTCQUAL -5.355%	28117(0.85255)	407402(0.90610)
TARGET+TGQUALT 4.116%	27831(0.98983)	386491(0.94867)
A_RECO,Br -1.572%	0.84388 \pm 0.00200	0.85959 \pm 0.00052
SETUP_{REST}	32055	336407
TIC 0.070%	32055(1.00000)	336173(0.99930)
TIMCON 0.124%	31970(0.99735)	334866(0.99611)
TGTCON 0.757%	31847(0.99615)	331041(0.98858)
DCBIT 10.327%	31542(0.99042)	293685(0.88716)
DELC 0.883%	27898(0.88447)	257163(0.87564)
CKTRS -9.986%	24368(0.87347)	250305(0.97333)
CKTAIL 0.125%	23710(0.97300)	243233(0.97175)
B4DEDX -1.279%	23032(0.97140)	239389(0.98420)
CPITRS -0.636%	22657(0.98372)	237015(0.99008)
CPITAIL -0.872%	22442(0.99051)	236833(0.99923)
TARGF 4.115%	22431(0.99951)	226972(0.95836)
DTGTPP -4.295%	21467(0.95702)	226965(0.99997)
RTDIF 0.935%	21462(0.99977)	224789(0.99041)
TGQUALT -0.862%	21277(0.99138)	224789(1.00000)
PIGAP 1.024%	21277(1.00000)	222488(0.98976)
TGB4 5.875%	21098(0.99159)	207545(0.93284)
KIC -3.865%	20002(0.94805)	204785(0.98670)
TGCEO 16.326%	19855(0.99265)	169847(0.82939)
B4EKZ -10.248%	16358(0.82387)	157338(0.92635)
B4ETCON -2.463%	15886(0.97115)	156673(0.99577)
TGZFOOL 0.754%	15806(0.99496)	154703(0.98743)
BWTRS 4.324%	15806(1.00000)	148013(0.95676)
RVUPV -2.685%	14817(0.93743)	145339(0.98193)
A_REST,Br 3.891%	0.46224 \pm 0.00278	0.43203 \pm 0.00085
A_IPIFLG 1.100%	0.8350 \pm 0.0054	0.8350 \pm 0.0054
loss due to $\overline{19}_{ct} A_{\mu}^{acc}$ 0.000%	0.9931 \pm 0.0002	0.9931 \pm 0.0002
$A_{K_{\pi 2}, Br}$ 4.140%	0.3235 \pm 0.0030	0.3080 \pm 0.0021

Table 62: $K_{\pi 2}$ -based acceptances of cuts applied in the $K_{\pi 2}$ BR analysis. A_IPIFLG and A_{μ}^{acc} are taken from the 2002 PNN1 analysis [17]. The SETUP cuts are defined in Table 66.

Name of value	All runs	Prescale 163840	Prescale 131072
$K_{\pi 2}$ Events	144989	2973	141926
$\langle Prescale \rangle$	131926	163840	131072
$KB_{LIVE} \times 10^{-12}$	1.79229	0.052475671	1.737988
$A_{K_{\pi 2}, Br}$	0.3080 ± 0.0021	0.3136 ± 0.0049	0.3078 ± 0.0021
$Br(K_{\pi 2})$	0.2213 ± 0.0022	0.1905 ± 0.0051	0.2216 ± 0.0016

Table 63: $K_{\pi 2}$ branching fraction results for all runs and broken down by prescale factor.

19.5 The measured $K_{\pi 2}$ branching fraction

The value of $K_{\pi 2}$ branching fraction has been calculated using Equation 27,

$$BR(K_{\pi 2}) = \frac{191660 \times 10^5}{0.9383 \cdot 1.792 \times 10^{12} \cdot 0.3080 \cdot 0.78775 \cdot 0.774 \cdot 0.27428} \quad (30)$$

$$= 0.2213 \pm 0.0022 \quad (31)$$

and is within 6% of the PDG2007 [22] value 0.2092 ± 0.0012 . The values of $f_s = 0.7740 \pm 0.0011$ (Eqn.21 of Ref. [17]) and of $\epsilon_{T \cdot 2 \cdot IC} = 0.9383 \pm 0.0027$ (derived from Table 17 of Ref. [17]) have been taken from the 2002 PNN1 analysis. Investigation of run-, prescale-factor- and rate-dependence of this modest discrepancy with the nominal branching fraction has been done.

The run dependence of $K_{\pi 2}$ branching fraction is shown in Fig.36 along with the run dependence of f_S determined from the $K_{\mu 2}$ monitor data for comparison ⁴. Some indication of a modest run-dependence of the branching fraction and f_S is observed.

The calculation of $K_{\pi 2}$ branching fraction for runs with different prescale factors has been done using $A_{K_{\pi 2}, Br}$ calculated for the runs with the given prescale factor. The results are shown on Table 63. There is a significant difference in the branching fraction determined for the two sets of prescale factors.

The rate-dependence is shown in Fig. 37 and Table 64. Rate is measured in millions of kaons per second. There is a clear-rate dependence in the branching fraction measurement.

Figure 38 plots the results from Table 64. The rate-dependence of the entire data sample is clear. The rate-dependence of the subset of data with prescaler 163840 is not consistent with the rate-dependence of the entire sample.

Table 65 shows the $K_{\pi 2}$ candidate event selection broken down by the two prescale factors. There are no glaring difference in event selection. Figure 39 shows the branching fraction versus run for the two prescale factors.

There is a clear rate dependence of the measured $K_{\pi 2}$ branching fraction. The range of variation in the measured branching fraction of $\sim 4.4\%$ as a function of rate quantified in Table 64 does not account for the $\sim 5.8\%$ overestimate of the average branching fraction in Eqn. 31. In addition there are some inconsistencies in the measured branching fraction for the two different prescale factors used in this analysis as well as indications of run-dependence. All these concerns lead us to assign a systematic uncertainty of $\pm 10\%$ in the PNN2 acceptance.

⁴Thanks to Shaomin Chen for providing the f_S data from the 2002 PNN1 analysis.

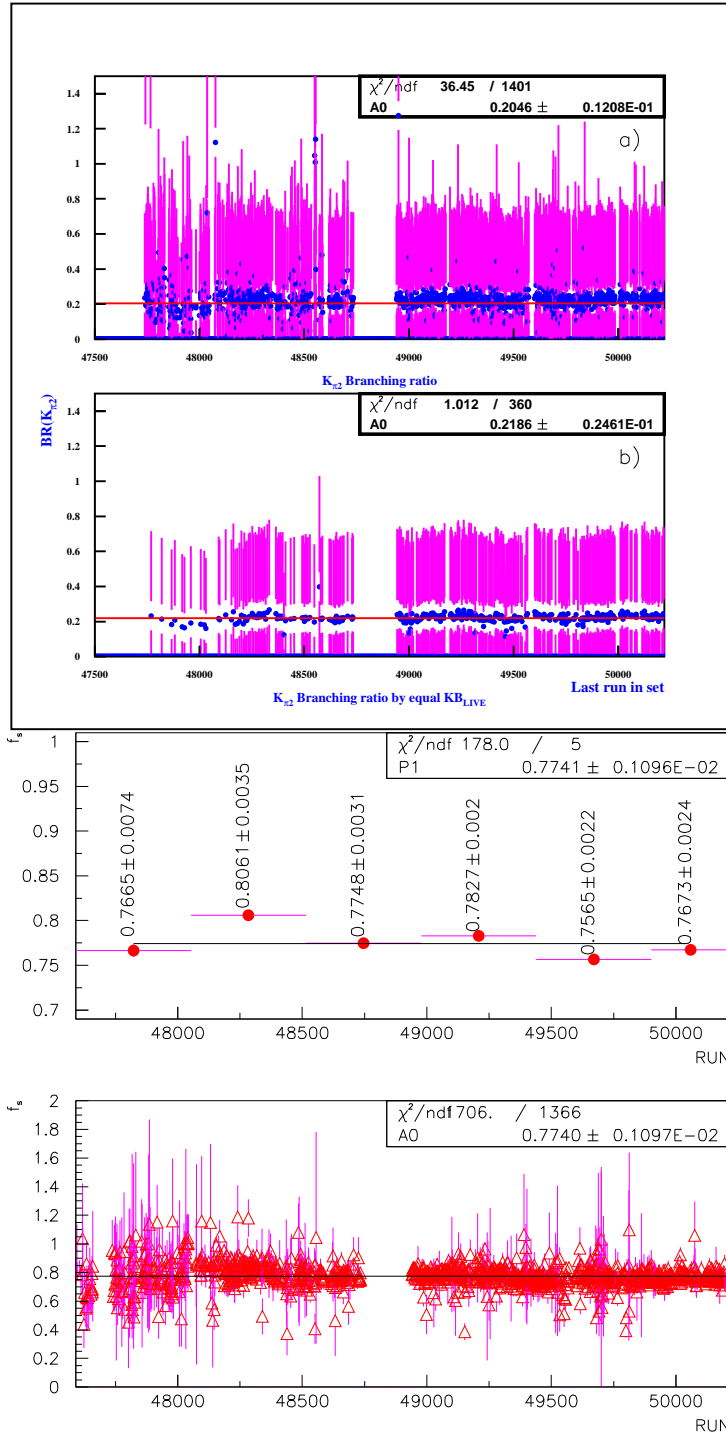


Figure 36: Top: The $K_{\pi 2}$ branching fraction a) versus run number and b) versus last run in a block of runs defined by $\sum_{i=1}^{N_{\text{Spill}}} \frac{K_{\text{BLIVE}_i}}{\text{Prescale}_i} \geq 3000$. Bottom: The f_S value versus run. The first point at upper plot corresponding to runs of $K_{\pi 2}(1)$ monitor data with a prescale factor of 163840.

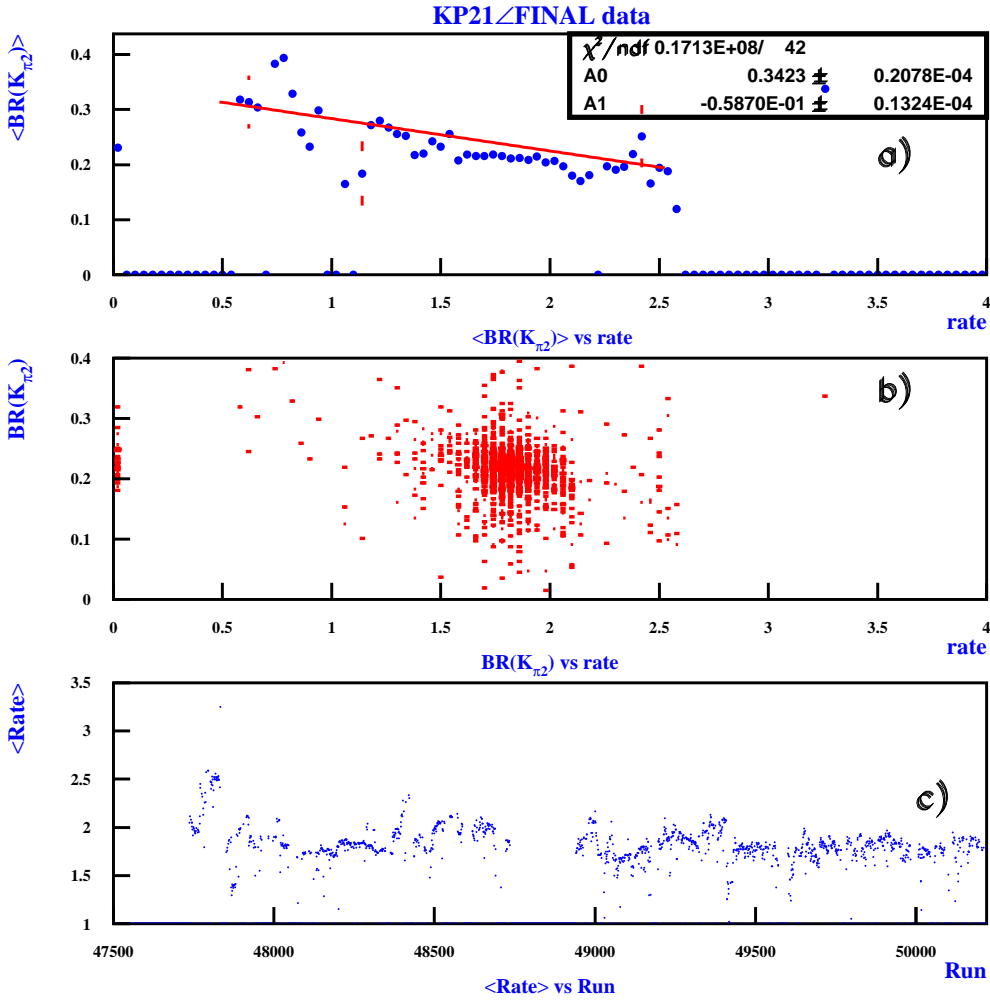


Figure 37: The K_{π_2} branching fraction a) versus average rate and b) versus rate (scatter plot). c) shows the average rate versus run. Rate is measured in $K_{B,live}/T_{eff}$ ($10^6/s$).

All prescale factors Quantity	Rate $K_{B,live}/T_{eff}$ ($10^6/s$)				
	All	0.00-1.70	1.70-1.85	1.85-2.00	> 2.0
K_{π_2} BR	0.2212 ± 0.0022	0.2284 ± 0.0025	0.2208 ± 0.0023	0.2194 ± 0.0023	0.2187 ± 0.0024
$A_{K_{\pi_2},BR}$	0.3081 ± 0.0021	0.3248 ± 0.0026	0.3088 ± 0.0023	0.3034 ± 0.0023	0.2989 ± 0.0025
$A_{RECO,BR}$	0.8597 ± 0.0005	0.8709 ± 0.0012	0.8608 ± 0.0009	0.8564 ± 0.0009	0.8524 ± 0.0014
$A_{REST,BR}$	0.4321 ± 0.0009	0.4497 ± 0.0021	0.4326 ± 0.0014	0.4273 ± 0.0015	0.4228 ± 0.0022
$KB_{LIVE} \times 10^{-12}$	1.792	0.280	0.639	0.594	0.279
Selected events	144989.	24716.	52010.	47141.	21116.
Selected events $\times PS \times 10^{-5}$	191660.	32602.	68366.	62050.	28635.
Trigger	878246.	138934.	312610.	290840.	135834.
Trigger $\times PS \times 10^{-5}$	1161090.	183250.	410936.	383023.	183845.
Events/Trigger	0.1651	0.1779	0.1664	0.1621	0.1555
Events $\times PS$ /Trigger $\times PS$	0.1651	0.1779	0.1664	0.1620	0.1558
PS factor=163840 Quantity	Rate $K_{B,live}/T_{eff}$ ($10^6/s$)				
	All	0.00-1.70	1.70-1.85	1.85-2.00	> 2.0
K_{π_2} BR	0.1905 ± 0.0051	0.2115 ± 0.0077	0.1765 ± 0.0065	0.1812 ± 0.0058	0.2003 ± 0.0068
$A_{K_{\pi_2},BR}$	0.3136 ± 0.0049	0.3462 ± 0.0105	0.3140 ± 0.0099	0.3126 ± 0.0082	0.2915 ± 0.0084
$A_{RECO,BR}$	0.8538 ± 0.0037	0.8733 ± 0.0076	0.8484 ± 0.0081	0.8590 ± 0.0064	0.8375 ± 0.0073
$A_{REST,BR}$	0.4429 ± 0.0060	0.4780 ± 0.0135	0.4464 ± 0.0131	0.4389 ± 0.0107	0.4198 ± 0.0113
$KB_{LIVE} \times 10^{-12}$	0.052	0.009	0.012	0.017	0.014
Selected events	2973.	635.	621.	926.	791.
Selected events $\times PS \times 10^{-5}$	4871.	1040.	1017.	1517.	1296.
Trigger	18535.	3547.	3793.	5749.	5445.
Trigger $\times PS \times 10^{-5}$	30368.	5811.	6214.	9419.	8921.
Events/Trigger	0.1604	0.1790	0.1637	0.1611	0.1453
Events $\times PS$ /Trigger $\times PS$	0.1604	0.1790	0.1637	0.1611	0.1453

Table 64: Measured rate-dependence of the K_{π_2} branching fraction and factors entering in the branching fraction calculation for all data (top) and runs with the prescale factor 163840.

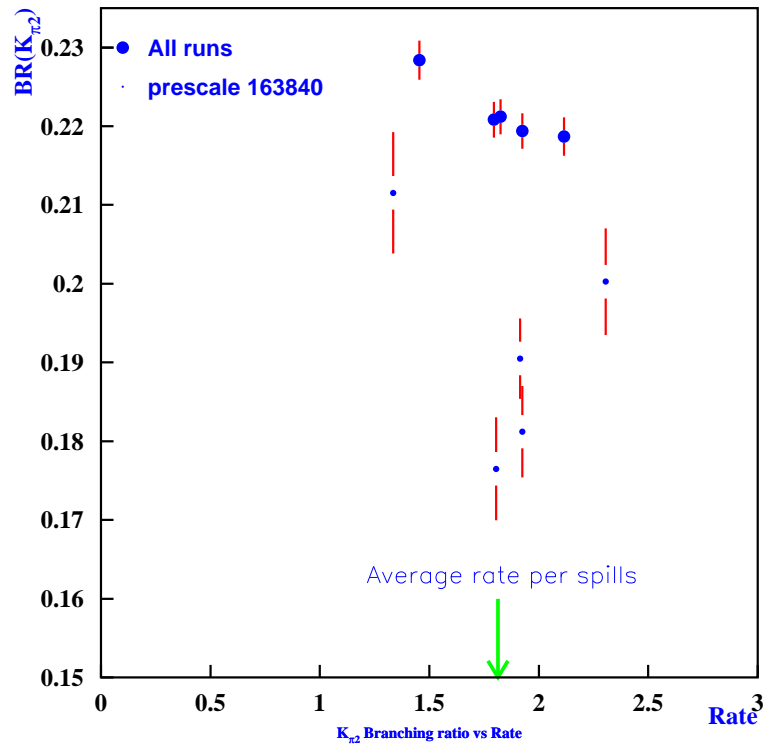


Figure 38: The K_{π_2} branching fraction versus rate for all runs (large points) and for runs with prescaler 163840 (small points). The arrow shows the average rate.

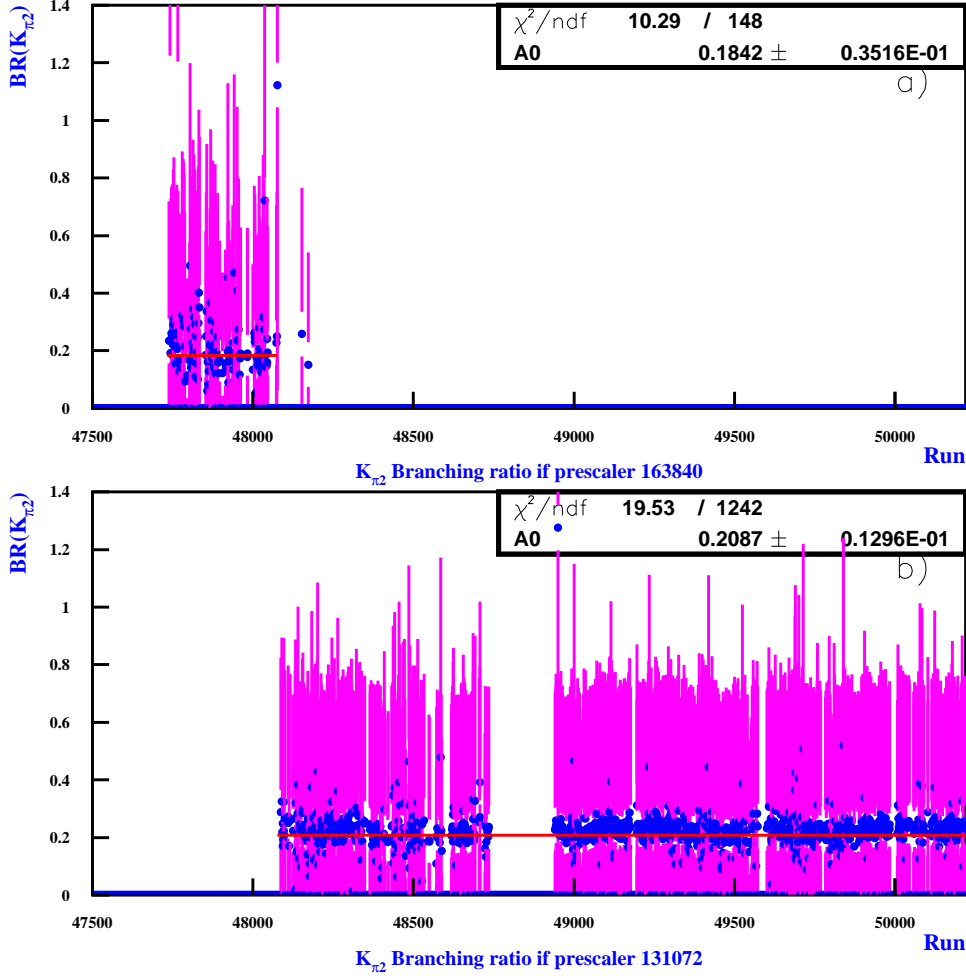


Figure 39: The $K_{\pi 2}$ branching fraction versus run number a) for runs with prescaler 163840 and b) for runs with prescaler 131072

19.6 UMC cut definitions

The following cuts have been used in the calculation of Monte Carlo kinematic and trigger acceptances for $K_{\pi 2}$ branching fraction measurement.

- $T \bullet A \equiv T \bullet 2$
- Reach layer $B = 1ayv4 \geq 6$.
- $\overline{19_{ct}}$ μ -veto (described on p.207 of Ref. [21]).
- **UFATE**⁵ requires that the pion stopped without decaying or interacting.

⁵UFATE, USTMED and USTOP_HEX are cuts based on UMC truth variables.

- **USTMED** requires that the pion stopped in the RS scintillator.
- **USTOP_HEX** The offline reconstructed and true stopping counters agree.
- **UTC/RANGE** The track reconstructed in UTC matches the track reconstructed in the Range Stack and Target [23]. For the PNN2 analysis, the **RDUTM** cut is used.
- **UTCQUAL** The UTCQUAL cut is described in Sec. 5.
- **TARGET** is SWATH CCD reconstruction cut. $\text{TARGET} \equiv \text{ITGQUAL} \geq 2$ in PNN1 and $\text{ITGQUAL} \geq 9$ in PNN2.
- **KP2STOP** requires the stopping layer to be between layers 8 and 15 inclusive.
- **COS3D** Cut any event with a dip angle outside the effective detection region $|\cos 3d| < 0.5$.
- **KP2BOX** is a fixed cut corresponding to $\sim 3\sigma$ cuts in range, energy and momentum.

$$(199. < \text{PTOT} < 215.) \cdot (28. < \text{RTOT} < 35.) \cdot (100.5 < \text{ETOT} < 115.) \quad (32)$$

Cut & discrepancy	$N_{K_{\pi 21}}$	
	163840	131072
TRIGGER+Prescaler	18535	859195
BAD_STR -1.839%	18109(0.97702)	855246(0.99540)
RD_TRK 0.000%	18109(1.00000)	855246(1.00000)
TRKTIM 0.000%	18109(1.00000)	855246(1.00000)
RDUTM 0.000%	18109(1.00000)	855246(1.00000)
UTCQUAL -0.729%	15563(0.85941)	741238(0.86670)
TARGET+TGQUALT 0.643%	14390(0.92463)	680603(0.91820)
COS3D -0.804%	13510(0.93885)	644454(0.94689)
B4DEDX 0.247%	13136(0.97232)	625022(0.96985)
CPITRS 0.562%	12967(0.98713)	613466(0.98151)
CPITAIL 0.028%	12959(0.99938)	612914(0.99910)
ICBIT 0.011%	12955(0.99969)	612660(0.99959)
TIC -0.117%	12890(0.99498)	610302(0.99615)
TIMCON 0.068%	12775(0.99108)	604443(0.99040)
TGTCON 0.184%	12615(0.98748)	595759(0.98563)
DCBIT 3.939%	11243(0.89124)	507499(0.85185)
DELC -3.480%	9383(0.83456)	441201(0.86936)
CKTRS 0.076%	9094(0.96920)	427275(0.96844)
CKTAIL -0.284%	8804(0.96811)	414865(0.97096)
BWTRS -0.026%	8307(0.94355)	391554(0.94381)
RVUPV -0.624%	8070(0.97147)	382826(0.97771)
TARGF 0.431%	7673(0.95081)	362341(0.94649)
DTGTTP 0.004%	7673(1.00000)	362328(0.99996)
RTDIF 0.004%	7595(0.98983)	358630(0.98979)
TGQUALT 0.000%	7595(1.00000)	358630(1.00000)
PIGAP 0.239%	7519(0.98999)	354183(0.98760)
TGB4 1.425%	7090(0.94295)	328929(0.92870)
KIC -0.042%	6989(0.98576)	324383(0.98618)
TGGEO 0.635%	5811(0.83145)	267649(0.82510)
B4EKZ 0.488%	5374(0.92480)	246216(0.91992)
B4ETCON -0.027%	5349(0.99535)	245138(0.99562)
TGZFOOL -0.751%	5242(0.98000)	242075(0.98750)
PV_noBV 0.000%	5242(1.00000)	242075(1.00000)
IPIFLG -0.642%	3651(0.69649)	170158(0.70291)
KP2BOX -1.890%	2985(0.81758)	142334(0.83648)
KP2STOP -0.115%	2973(0.99598)	141926(0.99713)
RTOT40 0.000%	2973(1.00000)	141926(1.00000)
$N_{K_{\pi 2}}$ -0.479%	2973	141926

Table 65: $K_{\pi 2}$ candidate selection for runs with prescale 131072 and 163840.

$K_{\pi 2}$ SETUP	component cuts
$SETUP_{RD}$	TRIGGER, ICBIT, $t_{IC} - t_{Ck} > 5$ ns ⁶ , B4DEDX, UTC, TARGET
$SETUP_{recon}$	TRIGGER, ICBIT, $t_{IC} - t_{Ck} > 5$ ns, B4DEDX, CPITRS, CPITAIL, CKTRS, CKTAIL, BWTRS, RVUPV, A_{RD} cuts,
$SETUP_{rest}$	TRIGGER, ICBIT, A_{RD} cuts, A_{recon} cuts, KP2BOX, KP2STOP, IPIFLG, COS3D.

Table 66: Setup cuts used for the $K_{\pi 2}$ acceptance measurements and event selection.

References

- [1] M. Diwan, et. al. “PNN2 1/3 Analysis”, “PNN2 2/3 Analysis”, E787 Technical Notes **tn385**, **tn386**, 2001.
- [2] E949, note K-034 (2003).
- [3] Tetsuro Sekiguchi, Ph. D thesis (2004).
- [4] I. Christidi, “Search for the rare decay $K^+ \rightarrow \pi^+ \nu \bar{\nu}$ with $p_{\pi^+} < 199$ MeV/c”, Ph.D. thesis, 2006.
- [5] K.Mizouchi, “Experimental Search for the Decay $\pi^0 \rightarrow \nu \bar{\nu}$ ”, Ph.D. Thesis, January 2006.
- [6] B.Bassalleck *et al.*, “Beam Instrumentation III What Was Built”, E949 Technical Note K-021, 1 August 2001.
- [7] Ilektra A. Christidi, “The Downstream Photon Veto”, E949 Technical Note K-067, 1 February 2007.
- [8] Victorov, “Downstream Photon Veto Counter”, E949 Technical Note K-015, 29 November 2000.
- [9] B. Lewis, “PNN2 1/3 Beam Background”, E949 Technical Note **K-061**, 2006. Unpublished.
- [10] W. M. Yao *et al.* [Particle Data Group], J. Phys. G **33**, 1 (2006).
- [11] Bipul Bhuyan, Ph. D thesis (2003).
- [12] Correspondence with Kentarou
- [13] E787, note 278 (1994).
- [14] E949, note K-042 (2004).
- [15] E949, note K-055 (2006).
- [16] T. Junk, Nucl. Instrum. Meth. A **434**, 435 (1999).
- [17] E949, note K-038 (2004).
- [18] <http://thomasj.web.cern.ch/thomasj/searchlimits/ecl.html>.
- [19] http://www.hep.uiuc.edu/home/trj/cdfstats/mclimit_csm1/.
- [20] R.M. Barnett *et al.* [Particle Data Group], Phys. Rev. D54 (1996) and earlier editions.
- [21] E949, Technical Note K-034 (2004).

[22] The 2007 off-year update of [10].

[23] E787 Technical note 391 (some year).